NACA TN 2608

NATIONAL ADVISORY COMMITTEE FOR AERONAUTICS

TECHNICAL NOTE 2608

CHARTS AND APPROXIMATE FORMULAS FOR THE ESTIMATION OF AEROELASTIC EFFECTS ON THE LOADING OF SWEPT AND UNSWEPT WINGS

By Franklin W. Diederich and Kenneth A. Foss

Langley Aeronautical Laboratory
Langley Field, Va.

NACA
Washington
February 1952

CONTENTS

NATIONAL ADVISORY COMMITTEE FOR AERONAUTICS

TECHNICAL NOTE 2608

CHARTS AND APPROXIMATE FORMULAS FOR THE ESTIMATION OF AEROELASTIC EFFECTS ON THE LOADING OF SWEPT AND UNSWEPT WINGS

By Franklin W. Diederich and Kenneth A. Foss

SUMMARY

Charts and approximate formulas are presented for the estimation of aeroelastic effects on the spanwise lift distribution, lift-curve slope, aerodynamic center, and damping in roll of swept and unswept wings at subsonic and supersonic speeds. Two types of stiffness distributions are considered, one which consists of a variation of the stiffness with the fourth power of the chord and one which is based on an idealized constant-stress structure. Some design considerations brought out by the results of this paper are discussed.

INTRODUCTION

A knowledge of the spanwise lift distribution and of some of the aerodynamic parameters associated with it is required for the design of a wing structure. Under certain conditions, such as high dynamic pressures, thin wings, swept wings, or wings designed for low wing loadings, the spanwise lift distribution may be affected to a significant extent by aeroelastic effects in somewhat the following manner.

A wing which carries a certain lift necessarily deforms under that lift. If the angles of attack along the span are changed as a result of this deformation, the lift carried by the wing is changed as well; in turn, this change in lift causes a change in the deformation of the wing and hence another change in lift, and so on, until an equilibrium condition is reached. The changes in the magnitude and the distribution of the lift are reflected in changes of the wing lift-curve slope, the wing bending and rolling moments, the spanwise center of pressure of the lift, and, on a swept wing, the longitudinal center of pressure. Since the lift produced by a given change in angle of attack is proportional to the dynamic pressure, the various aeroelastic effects tend to increase with dynamic pressure. In fact, for certain wings a sufficiently large dynamic

pressure may produce a condition of instability in which the change in lift caused by deformation is greater than the amount of lift required to produce the deformation, so that a given deformation will tend to increase until the structure fails. This phenomenon is aeroelastic divergence; since it involves only torsional deformations in the case of unswept wings, it is often referred to as torsional divergence.

Several methods are available for calculating these effects (reference 1, for instance), but since these effects depend on the structural characteristics of the wing, which are not accurately known in advance of its design, the relatively large amount of time required for even the most efficient of these methods militates against their use in connection with preliminary design calculations. A need exists, therefore, for means of estimating some of the more important aeroelastic effects on the spanwise lift distribution quickly and with an accuracy that is sufficient for preliminary design purposes.

Charts and approximate formulas are presented in this paper for estimating the changes in spanwise lift distribution, lift-curve slope, wing rolling-moment coefficient, spanwise center of pressure, and aerodynamic center occasioned by aeroelastic action of swept and unswept wings at subsonic and supersonic speeds. Also included are summary charts which indicate whether the various aeroelastic phenomena considered are likely to affect any given design. By means of these charts the conventional procedure of designing a wing on the basis of certain strength criteria, checking it for aeroelastic phenomena, and then reinforcing it, when necessary, to meet the stiffness requirements imposed by these phenomena can often be simplified greatly, inasmuch as the effect of some of these phenomena can be estimated in advance of design.

The use of the charts is described in the section headed "Calculation of the Various Aeroelastic Phenomena," and some considerations involved in the selection of the aerodynamic, structural, and geometric parameters are discussed in some detail in the section headed "Selection of Parameters." These two sections, as well as the sections headed "Illustrative Example" and "Preliminary Survey of Aeroelastic Behavior," are likely to prove of greatest interest at a first reading of this paper. The various parts of the section headed "Discussion" are concerned with the limitations of the charts, with the light they shed on such practical design problems as the relative significance of strength and stiffness as design criteria, with efficient ways of stiffening a wing that is strong but not stiff enough, and with the achievement of aeroisoclinic conditions. A brief description of the calculations (based on references 1 and 2) used in preparing the charts is contained in the appendixes.

SYMBOLS

A	aspect ratio (b^2/S)
A_Λ	swept-span aspect ratio $(A/\cos^2 \Lambda)$
$\bar{A}$	cross-sectional area of the (assumed) single torsion cell, square inches
a	distance from leading edge to section aerodynamic center, fraction of chord
$\bar{a}$	distance from leading edge of mean aerodynamic chord to wing aerodynamic center, fraction of mean aerodynamic chord
b	wing span, inches
b'	wing span less width of fuselage, inches $(b - w)$
C_B	wing-root bending-moment coefficient $\left(4M_r/qSb\right)$
C_{L_w}	lift coefficient of wings alone, exclusive of fuselage $\left(L_w/qS\right)$
C_{L_α}	wing lift-curve slope, per radian
C_{l_w}	rolling-moment coefficient on both wings alone, exclusive of fuselage (Rolling moment/qSb)
C_T	wing-root twisting-moment coefficient $\left(2T_r/qSc_r\right)$
c	chord (measured perpendicular to elastic axis), inches
$\bar{c}$	average chord, inches $\left(\frac{c_r + c_t}{2}\right)$
c_{l_α}	section lift-curve slope, per radian
c_{MAC}	mean aerodynamic chord (parallel to plane of symmetry), inches
E	Young's modulus of elasticity, pounds per square inch

e	distance from leading edge to elastic axis, fraction of chord
e_1	dimensionless moment arm of the section lift about the elastic axis $(e - a)$
$\bar{e}_1$	effective or average dimensionless moment arm
F_B	allowable bending stress, pounds per square inch
F_r	root-stiffness function
F_T	allowable shear stress, pounds per square inch
F_w	structural weight function
F_1, F_2	dimensionless parameters used in approximate formulas for angle of attack due to aeroelastic deformation
f_1, f_2	dimensionless functions of the distance along the span used in approximate formulas for angle of attack due to aeroelastic deformation
G	modulus of rigidity, pounds per square inch
h	wing thickness, inches
I	section bending moment of inertia, inches^4
J	section moment of inertia in torsion, inches^4
K_1, K_2	dimensionless parameters used in approximate formulas for dimensionless dynamic pressures at divergence
k	dimensionless sweep parameter $\left(\frac{s_t}{e_1 c_r} \frac{(GJ)_r}{(EI)_r} \tan \Lambda\right)$
L_w	lift of both wings alone, exclusive of fuselage, pounds
l	lift per unit distance along span, pounds per inch
M	bending moment about an axis perpendicular to elastic axis, inch-pounds
M_o	free-stream Mach number

n	design load factor
p	rolling angular velocity, radians per second
q	dynamic pressure, pounds per square foot
q^*	dimensionless dynamic pressure $\left(\frac{q}{144}\frac{C_{l_{\alpha_e}} e_1 c_r^2 s_t^2 \cos \Lambda}{(GJ)_r}\right)$
$\bar{q}$	dimensionless dynamic pressure $\left(\frac{q}{144}\frac{C_{l_{\alpha_e}} c_r s_t^3 \sin \Lambda}{(EI)_r}\right)$
S	total wing area, square inches
s	distance along elastic axis measured from wing root, inches
s^*	dimensionless distance along elastic axis (s/s_t)
$\bar{s}$	distance from root to center of pressure of lift along elastic axis, inches
$\bar{s}^*$	dimensionless distance from root to center of pressure of lift $(\bar{s}/s_t)$
T	accumulated torque about elastic axis, inch-pounds
t	thickness of most highly stressed element of skin, inches
t_e	thickness of equivalent skin which includes the material in stringers and spar flanges, inches
t_i	distributed torque due to inertia loading, inch-pounds per inch
V	free-stream velocity, feet per second
W	design gross weight of airplane, pounds
W_s	weight of primary structure of both wings, pounds
W_w	weight of both wings exclusive of fuselage, pounds
w	width of fuselage, inches
w_s	weight of primary load-carrying structure per unit distance along span, pounds per inch

y	lateral coordinate, inches
y^*	dimensionless lateral coordinate $\left(\frac{y}{b/2}\right)$
$\bar{y}$	lateral distance to center of pressure
α	angle of attack in a plane parallel to plane of symmetry, radians
Γ	angle of local dihedral, radians, or spanwise slope of normal displacement of elastic axis
γ_s	density of the material of the primary structure (or an equivalent density in the case of sandwich construction), pounds per cubic inch
η	lateral distance measured from wing root, inches $\left(y - \frac{w}{2}\right)$
η^*	dimensionless lateral distance $\left(\frac{\eta}{b'/2}\right)$
$\eta_{1,2,\ldots 21}$	factors defined in table 1
κ	ratio of lift-curve slopes $\left(C_{L_{\alpha_e}}/C_{L_\alpha}\right)$
Λ	angle of sweepback at elastic axis
λ	wing taper ratio $\left(c_t/c_r\right)$
ρ	free-air density, slugs per cubic foot
φ	angle of structural twist in planes perpendicular to elastic axis, radians
ω	tip stiffness ratio $\left((EI)_t/(EI)_{t_{cs}}\right)$
μ,ν,τ	dimensionless parameters used in approximate formulas for lift, root bending moment, and root twisting moment

Subscripts:

cs	constant-stress
D	at divergence
e	effective

g	geometric (due to airplane attitude or built-in twist)
i	inertia
0	rigid wing (for $q = 0$)
r	at wing root
s	structural (due to structural or aeroelastic deformation)
t	at wing tip

Superscripts:

M	due to bending moment
T	due to torque
Γ	due to root bending
φ	due to root twist

USE OF THE CHARTS AND APPROXIMATE FORMULAS

Summary of Method and Scope of Calculations on Which Charts and Approximate Formulas Are Based

Although a detailed understanding of the method and scope of the calculations on which the charts of this paper are based is not essential to the use of the charts, a brief account of these matters is given, primarily to aid in the appreciation of the limitations of the charts. The method is described more fully in appendix A.

Most of the calculations on which the charts are based were made by the method of reference 1, which consists in solving the differential equations descriptive of an elastically deformed wing under aerodynamic loading by numerical methods employing matrix techniques. Treated by this method were wings with four taper ratios λ (1.0, 0.5, 0.2, and 0), two types of stiffness distributions (one proportional to the fourth power of the chord and one dictated by constant-stress considerations), and four values of a sweep parameter k, at several values of the dynamic-pressure ratio $\frac{q}{q_D}$. Calculated for each case were the dynamic pressure at divergence and the changes in spanwise lift distribution,

total wing lift, root bending moment, rolling moment, and spanwise center of pressure of the lift. For the wings of constant chord and constant stiffness, calculations were also performed for six values of k by a method which is an extension of that of reference 2 and consists in solving the differential equations exactly for these relatively simple cases.

Two important approximations that have been made in all calculations are:

(1) Aerodynamic induction effects at subsonic speeds are taken into account by an over-all reduction of the strip-theory loading and, in the matrix calculations, by rounding off the strip-theory loading at the tip (see references 1 and 2); at supersonic speeds strip theory is used, with a small reduction at the tip for the matrix calculations.

(2) The rigid-body rotations imparted to a swept wing by its triangular root portion are taken into account by a suitable choice of an effective root.

These assumptions were made not so much to simplify the problem as to make the results more generally applicable. The most severe limitation on the use of the charts is probably imposed by the fact that calculations have been made for only two types of spanwise distributions of bending and torsional stiffnesses:

(1) Stiffness distributions which vary as the fourth power of the chord, such as those of solid wings

(2) Stiffness distributions associated with structures designed for a constant level of combined bending and torsion stress at every point on the span, as described in appendix B

Except for solid wings and those with geometrically similar cross sections, for which the stiffnesses vary as the fourth power of the chord, the stiffness distributions of any given wing depend on the detailed design of the wing and cannot be generalized easily. Consequently, the constant-stress concept outlined in appendix B has been used to estimate stiffness distributions for some of the calculations; it constitutes an effort to relate the stiffness of a wing to its strength on the basis of the following assumptions:

(1) The combined bending and torsional stresses are constant along the span.

(2) The structure is designed for combined bending and torsional stresses in such a manner that the sum of the ratio of the actual to the allowable bending stress and the ratio of the actual to the allowable torsion stress is equal to unity when the margin of safety is zero.

(3) The structure is of the thin-skin, stringer-reinforced shell type and its main features do not vary along the span; for instance, the number of spars and their chordwise locations are constant along the span.

(4) At the design condition the spanwise distribution of the applied loading is proportional to the chord.

Although root rotations of swept wings have not been taken into account explicitly in the calculations because they vary among different designs in a largely unpredictable manner, means for taking these rotations into account approximately are discussed in a subsequent section.

Selection of Parameters

Geometric parameters.- The geometric parameters used in the analysis are defined in figure 1. The location of the effective root indicated in figure 1 is discussed in the section concerned with the structural parameters.

Aerodynamic parameters.- The aerodynamic parameters which enter the analysis are the wing lift-curve slope and the location of the aerodynamic center. Two lift-curve slopes are used at subsonic speeds: The wing lift-curve slope C_{L_α} is used only in conjunction with additional lift distributions; for all other lift distributions, that is, those due to built-in twist, due to roll, or due to aeroelastic twist, an effective lift-curve slope $C_{L_{\alpha_e}}$ is used. Approximate values of these parameters are given for subcritical speeds by the relations

$$C_{L_\alpha} = c_{l_\alpha} \frac{A \cos \Lambda}{A + 2 \frac{c_{l_\alpha}}{2\pi} \cos \Lambda} \tag{1}$$

$$C_{L_{\alpha_e}} = c_{l_\alpha} \frac{A \cos \Lambda}{A + 4 \frac{c_{l_\alpha}}{2\pi} \cos \Lambda} \tag{2}$$

where c_{l_α} is the lift-curve slope of the section perpendicular to the quarter-chord line at a Mach number equal to $M_o \cos \Lambda$. An approximate value is given by

$$c_{l_\alpha} = \frac{2\pi}{\sqrt{1 - M_o^2 \cos^2 \Lambda}} \tag{3}$$

Equation (1) is given in reference 3 and shown to be applicable both to incompressible and to subcritical compressible flow. Equation (2) is given in references 1 and 2 but without the term $c_{l_\alpha}/2\pi$ in the denominator. This term is introduced into equation (2) in order to extend its applicability to compressible flows in the same manner as that employed for the coefficient of damping in roll in reference 3.

At supersonic speeds both lift-curve slopes are approximately equal to the effective section lift-curve slope

$$c_{l_{\alpha_e}} = \frac{4 \cos \Lambda}{\sqrt{M_o^2 \cos^2 \Lambda - 1}} \tag{4}$$

The ratio of the lift-curve slopes C_{L_α} and $C_{L_{\alpha_e}}$ is defined by

$$\kappa = \frac{C_{L_{\alpha_e}}}{C_{L_\alpha}} \tag{5}$$

so that for supersonic speeds κ is equal to 1.

The local aerodynamic centers are assumed to be at a constant fraction of the chord from the leading edge, so that their distances from the leading edge (as fractions of the local chords) are all equal to the distance of the wing aerodynamic center from the leading edge of the mean aerodynamic chord (as a fraction of the mean aerodynamic chord). The moment arm e_1 is then given by the relation

$$e_1 = e - a \tag{6}$$

The lift-curve slopes and the locations of the aerodynamic center vary with the free-stream Mach number; hence the appropriate values must be used at each flight condition for which aeroelastic calculations are made. For airplanes designed to operate at subsonic speeds, only the highest Mach number attainable at the highest dynamic pressure is likely to be critical from aeroelastic considerations. For airplanes designed to operate at supersonic speeds no such general statement can be made; however, at a given altitude either the region of Mach numbers near the

transition from the subsonic to the transonic regime or the highest attainable Mach number is likely to be critical as far as the aeroelastic phenomena considered in this paper are concerned. (See figure 4 of reference 1 and figure 5 of reference 2, for instance.)

The airspeeds at which the various aeroelastic phenomena are of interest enter the calculations in the form of the corresponding dynamic pressures. These dynamic pressures, in turn, are expressed in dimensionless form as

$$q^* = \frac{q}{144} \frac{C_{L_{\alpha_e}} e_1 c_r^2 s_t^2 \cos \Lambda}{(GJ)_r} \tag{7}$$

or

$$\bar{q} = \frac{q}{144} \frac{C_{L_{\alpha_e}} c_r s_t^3 \sin \Lambda}{(EI)_r} \tag{8}$$

The parameter q^* is useful in the analysis of unswept wings, for which torsional deformations are predominant; the parameter $\bar{q}$ is useful for highly swept wings, for which bending deformations are predominant. In general, the parameter q^* is used in this paper unless e_1 is zero. The ratio of these parameters

$$k = \frac{\bar{q}}{q^*} = \frac{s_t}{e_1 c_r} \frac{(GJ)_r}{(EI)_r} \tan \Lambda \tag{9}$$

is independent of the dynamic pressure and depends only on geometric and structural parameters. This ratio is very useful for analyzing the aeroelastic behavior of swept wings.

Structural parameters.- For the purposes of an aeroelastic analysis, the wing structure is characterized by the location of the elastic axis and the magnitude and distribution of the bending and torsional stiffnesses (EI and GJ), as well as by the magnitude of the rigid-body rotations imparted to the wing by its root.

The elastic axis is usually defined as the locus of points at which normal loads can be applied without causing the wings to twist. Such a locus does not generally exist for practical wings; however, for unswept wings without cut-outs an axis can be determined which approximately satisfies this condition. Similarly, for swept wings without cut-outs

an elastic axis can be defined for the outboard part of the wing if the wing is considered to be clamped along some such line as the effective root shown in figure 1. In most aeroelastic calculations the locus of shear centers for both swept and unswept wings is assumed to be the elastic axis. If the structure has large cut-outs which result in sudden changes in the stiffnesses and in the shear center along the span, the charts of this paper cannot be used except in a qualitative sense.

The magnitude and the spanwise distributions of the bending and torsional stiffnesses enter aeroelastic calculations by means of the charts and approximate formulas in different ways. The magnitudes, as characterized by the values of the stiffnesses at the effective root, have to be known in order to perform any calculations; the distributions are implicit in the charts. The root stiffnesses, if not known otherwise, can be estimated either from experience with similar designs, from the results of the constant-stress concept outlined in appendix B, or from a combination of the two.

The required bending stiffness at the root $(EI)_r$ is proportional to the design load factor, the wing loading, the wing thickness ratio, the fourth power of the root chord, the square of the swept-span aspect ratio $(A/\cos^2\Lambda)$, and the ratio of the modulus of elasticity to the allowable bending stress, and depends on the taper ratio and on the detailed design of the wing (see appendix B). By means of this relation the bending stiffness of one wing can be estimated from that of a reasonably similar wing. Or, with the constants of proportionality η_{20} and F_w given in table 1 and appendix B, respectively, which take into account some of the detailed design parameters as well as the taper ratio, the stiffness can be estimated directly. However, in view of the fact that these constants have been derived on the basis of a highly idealized structure and loading condition they must be used with caution. The ratio of the root bending stiffness to the root torsional stiffness can be estimated by means of equations given in appendix B or, preferably, from experience with structures similar to that under consideration.

The spanwise stiffness distributions need not be known in detail in order to use the charts and approximate formulas. If the wing is solid or nearly solid, or if its cross sections are geometrically similar at all points, the charts for stiffness distributions proportional to the fourth power of the chord are used. If the wing does not have large cut-outs and is designed for a constant stress level, the charts for the stiffness distributions associated with constant stress are used. The use of these charts tends to overestimate aeroelastic effects to some extent because, although actual wings are designed for constant stress over most of the span, the portions near their tips are designed on the basis of other considerations, such as handling loads or minimum standard

sheet thicknesses; therefore, wings tend to be stiffer near the tip than they would be if designed on the basis of constant stress throughout. This difference in stiffness is particularly large if the taper ratio is zero.

If the wing contains large cut-outs or if, for any other reason, the wing stiffness distribution is known to be substantially different from a constant-stress type, the charts can be used to furnish semi-qualitative results for the various aeroelastic phenomena by using fictitious stiffnesses, provided the actual stiffness distribution is known at least approximately. The root stiffnesses of these fictitious distributions may be assumed to be the ones that give rise to twist or bending angles at the tip which are the same as those of the actual wing if the bending moments or torques vary as the square of the distance from the tip. For convenience, the spanwise distribution of these fictitious stiffnesses may then be assumed to be proportional to the fourth power of the chord. On the basis of these assumptions,

$$\frac{1}{(EI)_{r_e}} = 3\lambda \int_0^1 \frac{1}{EI}(1 - s^*)^2 ds^* \tag{10}$$

where the subscript e refers to the fictitious stiffness, and where the integral represents the moment of inertia of the area under the function $\frac{1}{EI}$ plotted against s^* about the point $s^* = 1$.

The fictitious torsional stiffness at the root can be obtained in the same manner. The aeroelastic phenomena can then be estimated by use of these fictitious root stiffnesses and the charts for stiffness distributions proportional to the fourth power of the chord.

In the derivation of the charts the wing is considered to be clamped at the effective root perpendicular to the elastic axis. From the data and analyses presented in references 1, 2, 4, and 5 a satisfactory location of the effective root appears to be at the intersection of the elastic axis and the side of the fuselage.

If the rotations at this effective root are known as a result of deflection tests or a detailed analysis such as that of reference 5, the root twist due to torque and the root bending due to bending moment may be taken into account by moving the effective root inboard by the distance

$$\Delta s^{\varphi} = \frac{\varphi_r}{T_r}^{T}(GJ)_r \tag{11}$$

or

$$\Delta s^{\Gamma} = \frac{\Gamma_r^M}{M_r}(EI)_r \tag{12}$$

where φ_r^T is the angle of twist at the root due to a root torque T_r, and where Γ_r^M is the deflection slope at the effective root due to a bending moment M_r. Since the distances Δs^{φ} and Δs^{Γ} may differ from each other, some compromise between the two must be made; for unswept wings the use of Δs^{φ} appears to be indicated, whereas for highly swept wings the use of Δs^{Γ} is more appropriate.

Preliminary Survey of Aeroelastic Behavior

The information contained in some of the subsequent sections has been summarized in figure 2 for the purpose of ascertaining in advance of more detailed estimates, if desired, whether the aeroelastic phenomena considered herein are likely to affect the design of the wing structure. This preliminary survey is not essential to any of the further calculations but may show them to be unnecessary in some cases.

The charts of figures 2(a) to 2(d) pertain to wings of taper ratios 0, 0.2, 0.5, and 1.0 and constitute plots of the dynamic-pressure parameter q^* defined by equation (7) against the sweep parameter k defined by equation (9). These parameters contain the root stiffnesses $(GJ)_r$ and $(EI)_r$; if, when a preliminary survey of aeroelastic effects is to be made, no information whatever concerning the wing stiffness is available, the following relations for q^* and k may be used:

$$q^* = \frac{q}{18432} \frac{C_{L_{\alpha_e}} e_1 (1 + \lambda)^2 \cos \Lambda}{\frac{G}{E_B} \frac{nW}{S} \frac{h_r}{c_r} \eta_a F_r} \tag{13}$$

$$k = \frac{1 + \lambda}{2} \frac{G}{E} \frac{A_\Lambda}{\eta_{19} e_1} \eta_b \tan \Lambda \tag{14}$$

where F_r is a root-stiffness parameter defined in appendix B and plotted in figure 3, and where η_a and η_b are defined by

$$\eta_a = \frac{\eta_3\eta_5\eta_6\eta_7^2}{\eta_4\eta_8\eta_9\eta_{15}\eta_{17}} \tag{15a}$$

and

$$\eta_b = \frac{\eta_7}{\eta_5\eta_8\eta_9\eta_{16}} \tag{15b}$$

in terms of some of the factors defined in table 1.

Figure 2(e) pertains to wings for which the moment arm e_1 is zero and, hence, k is infinite; with the degree of approximation involved in the use of figures 2(a) to 2(d), figure 2(e) can be used for wings with $|k| > 25$. This figure consists in a plot of the dynamic-pressure parameter $\bar{q}$, defined by equation (8), against the taper ratio λ. If no information is available concerning the root bending stiffness $(EI)_r$ contained in $\bar{q}$, the following relation may be used:

$$\bar{q} = \frac{C_{L_{\alpha_e}}(1+\lambda)^3 A_\Lambda \sin\Lambda}{\frac{E}{F_B}\frac{nW}{S}\frac{h_r}{c_r}\frac{\eta_a}{\eta_b}\eta_{19}F_r}\frac{q}{36864} \tag{16}$$

The various lines of the charts of figure 2 designate the conditions at which a wing designed on the basis of strength considerations alone is likely to encounter divergence or spanwise shifts of the center of pressure by various amounts; positive shifts are those toward the tip. These spanwise shifts furnish an estimate of the increase in root bending moment due to aeroelastic action and an estimate of the shift in wing aerodynamic center, since

$$\Delta\bar{a} = \sin\Lambda\,\frac{\Delta\bar{s}}{c_{MAC}} \tag{17}$$

Inasmuch as the parameters q^* and $\bar{q}$ contain the dynamic pressure, the negative values of q^* shown in figure 2 may require some explanation. The four quadrants of each of the charts of figures 2(a) to 2(d) may be characterized for practical purposes as follows:

Quadrant	Sweep	e_1	Divergence	Shift in $\bar{y}$
1	Back	Positive	Impossible beyond a certain sweep	Inboard beyond a certain sweep
2	Forward	Positive	Likely	Outboard
3	Back	Negative	Impossible	Inboard
4	Forward	Negative	Possible beyond a certain sweep	Outboard beyond a certain sweep

For unswept wings k is approximately equal to zero, and the aeroelastic phenomena referred to in the charts of figure 2 are similar to those of swept wings defined by points in quadrant 2 if q^* is positive and by points in quadrant 3 if q^* is negative. In other words, the aeroelastic phenomena of unswept wings are similar to those of swept-forward wings if e_1 is positive and to those of sweptback wings if e_1 is negative. The aerodynamic-center shift associated with the shift in the lateral center of pressure $\bar{y}$ or in the spanwise center of pressure $\bar{s}$ is always forward, except for small positive values of k (associated with sweep angles smaller than a certain value), in both quadrants 1 and 4.

The significance of negative values of q^* is that e_1 is negative, rather than that q is negative. A negative value of e_1 may be obtained at supersonic speeds, but under most conditions e_1 is likely to be positive. Similarly, a negative value of $\bar{q}$ implies that Λ is negative (that is, that the wing is swept forward).

In using figures 2(a) to 2(d), estimates must be made of either the root stiffnesses (in conjunction with equations (7) and (9)) or of the effectiveness factors η_a and η_b (for use in equations (13) and (14)). The factor F_r is obtained from figure 3 for the largest value of e_1 likely to be encountered at the design load factor and for the given taper ratio λ. The parameter q^* is calculated for the combination of dynamic pressure q, lift-curve slope $C_{L_{\alpha_e}}$, and moment arm e_1 which is likely to be critical from an aeroelastic point of view. For an unswept wing the combination for which the product $qC_{L_{\alpha_e}}e_1$ is a maximum is likely to be critical; for a swept wing the combination for which $qC_{L_{\alpha_e}}$ is a maximum is likely to be critical. The parameter k is then calculated for the same value of e_1.

The values of q^* and k define a point on one of the charts of figures 2(a) to 2(d) (whichever is closest to the actual taper ratio). If the shift in spanwise center of pressure (and any associated shift in the aerodynamic center) at that point is small and, in the case of an unswept or a sweptforward wing, if the absolute value of the ratio of the value of q^* at that point to the value of q^* at divergence for the value of k at that point is small, the static aeroelastic phenomena discussed in this paper probably need not be taken into account in designing the wing structure. On the other hand, if the point on the chart indicates the likelihood of significant aeroelastic effects on the spanwise center of pressure or the possibility of an approach to the divergence condition, further calculations are desirable. The charts of this paper may be used for the preliminary calculations; once the structure has been designed, more refined methods such as that of reference 1 may be used.

If the moment arm e_1 is so small or the angle of sweep so large that the parameter k exceeds the range covered by figures 2(a) to 2(d), the chart of figure 2(e) may be used for the purpose of a preliminary aeroelastic appraisal of the given wing. In this figure only the parameter $\bar{q}$ is required, since k is considered to be infinite. The parameter $\bar{q}$ can be obtained from equation (16). The analysis then proceeds in the same manner as for figures 2(a) to 2(d).

Calculation of the Various Aeroelastic Phenomena

Dynamic pressure at divergence.- The solutions for the divergence speed obtained by the direct method in reference 2 and those obtained by the numerical matrix method given in appendix A can be summarized by approximate formulas which give the dimensionless parameters q^*_D and $\bar{q}_D$ (the values of the parameters defined in equations (7) and (8) that correspond to the value of the dynamic pressure q at divergence) in terms of their ratio k defined by equation (9).

These approximate formulas are

$$q^*_D = \frac{K_1}{1 - K_2 k} \tag{18}$$

and

$$\bar{q}_D = -\frac{K_1}{K_2 - \frac{1}{k}} \tag{19}$$

When the angle of sweep is zero, equation (18) reduces to $q^*_D = K_1$, and when the moment arm e_1 is zero, as it may be in supersonic flow, equation (19) reduces to $\bar{q}_D = -\frac{K_1}{K_2}$. The constants K_1 and K_2 are given in table 2 for wings with taper ratios of 0, 0.2, 0.5, and 1.0, for both types of stiffness distributions; the parameter q^*_D for unswept wings and the parameter $\bar{q}_D$ for swept wings with $e_1 = 0$ are plotted in figures 4(a) and 4(b), respectively, against the taper ratio λ.

With the values of q^*_D or $\bar{q}_D$ given by equations (18) and (19) and the definitions of these two parameters given by equations (7) and (8), the values of q required for divergence may be determined. If desired, the corresponding airspeed may be determined from the relation

$$V_D = \sqrt{\frac{q_D}{\rho/2}}$$

The value of q_D is often negative for sweptback wings, and since a negative dynamic pressure does not correspond to any real speed, these wings cannot diverge. These negative values of q_D, nonetheless, are useful as reference values in other aeroelastic phenomena.

The values of the constants K_1 and K_2 given in reference 2 differ somewhat from the corresponding values resulting from the matrix solution in appendix A. The matrix results are probably more significant because they are based upon more realistic aerodynamic assumptions; the K_1 and K_2 values in reference 2 tend to give conservative results.

The value of q_D calculated for any given value of q^*_D or $\bar{q}_D$ depends on the value of the effective lift-curve slope $C_{L_{\alpha_e}}$ or $c_{l_{\alpha_e}}$ and, hence, on the Mach number. As suggested in references 1 and 2, the value of q_D calculated at various Mach numbers may be plotted against Mach number. If lines of the actual dynamic pressure at several altitudes as a function of Mach number are drawn on the same plot, an intersection of the divergence line with one of the lines of actual dynamic pressure designates possible divergence at that value of dynamic pressure, Mach number, and altitude. If this plot is on log-log coordinates, the lines of actual dynamic pressure are straight and the ratio of the dynamic pressure at divergence to the actual dynamic pressure at a given Mach number and altitude can be scaled off directly. (See references 1 and 2.)

Spanwise angle-of-attack distribution.- In appendix A, an approximate expression is determined for the change in angle of attack due to wing flexibility. For the additional-type angle-of-attack distribution (α_g is constant) the angle of attack due to structural deformation α_s is given by

$$\frac{\alpha_s}{\alpha_g} = \frac{1}{\kappa} \frac{q/q_D}{1 - \frac{q}{q_D}} \left(f_1 + F_1 \Delta f_1\right) \tag{20}$$

The functions f_1 and Δf_1, which depend on the spanwise coordinate s^*, and the function F_1, which depends on the parameter k, are given in figure 5 for swept wings with taper ratios of 0.2, 0.5, and 1.0 and with the two different types of stiffness distributions. For wings with zero taper ratio the structural deformation cannot be obtained from equation (20), as is pointed out in appendix A. However, the ratio $\kappa\frac{\alpha_s}{\alpha_g}$ as a function of the spanwise coordinate s^* is shown in figure 6 for the two different stiffness distributions, several values of q/q_D, and several values of the parameter k.

The spanwise distribution of α_s due to a linear twist $\left(\alpha_g = s^*\alpha_{g_t}\right)$, which may be either symmetric or antisymmetric, is approximately

$$\frac{\alpha_s}{\alpha_{g_t}} = \frac{q/q_D}{1 - \frac{q}{q_D}} \left(f_2 + F_2 \Delta f_2\right) \tag{21}$$

where the functions f_2, Δf_2, and F_2 are given in figure 7 for wings of taper ratios 0.2, 0.5, and 1.0. The angle-of-attack ratio is shown in figure 8 as a function of s^*, q/q_D, and k for wings of zero taper ratio.

The results of equations (20) and (21) may be superimposed. For example, if the spanwise distribution of α_s due to rolling is to be found, these equations must be added in such proportion that

$$\alpha_g = y^* \frac{pb}{2V}$$

But

$$y^* = \frac{w}{b} + \frac{b'}{b} s^*$$

so that

$$\alpha_g = \left(1 - \frac{b'}{b} + \frac{b'}{b}\, s^*\right)\frac{pb}{2V} \tag{22}$$

where $pb/2V$ is the angle of attack at the tip due to roll. The distribution of α_s due to roll is then

$$\frac{\alpha_s}{\frac{pb}{2V}} = \frac{q/q_D}{1 - \frac{q}{q_D}}\left[\frac{1}{\kappa}\left(1 - \frac{b'}{b}\right)\left(f_1 + F_1\,\Delta f_1\right) + \frac{b'}{b}\left(f_2 + F_2\,\Delta f_2\right)\right] \tag{23}$$

Spanwise lift distributions.- If desired, the lift distributions can be obtained for the angle-of-attack distributions given in the preceding section by one of the commonly used methods of calculating spanwise lift distributions, such as that of reference 6. However, the following method is simpler.

Within the framework of the assumptions made in the analysis the lift per inch of span is proportional to the local angle of attack, so that

$$\frac{l}{l_0} = 1 + \kappa\,\frac{\alpha_s}{\alpha_g} \tag{24a}$$

for geometrical angles of attack which are constant along the span, and

$$\frac{l}{l_0} = 1 + \frac{\alpha_{g_t}}{\alpha_g}\,\frac{\alpha_s}{\alpha_{g_t}} \tag{24b}$$

for geometrical angles of attack due to linear twist, where $\kappa\,\frac{\alpha_s}{\alpha_g}$ and α_s/α_{g_t} are obtained as indicated in the preceding section. If no better approximation is available for the rigid-wing ($q = 0$) loading l_0, it may be estimated from the relation

$$l_0 \approx C_{L_\alpha} c q \alpha_g \tag{25a}$$

for geometric angles of attack which are constant along the span, and from

$$l_0 \approx C_{L_{\alpha_e}} c q \alpha_g \tag{25b}$$

for all other geometric angles of attack.

Lift and moment coefficients.- The wing lift coefficient C_{L_w}, the wing-root bending-moment coefficient C_B, and the wing-root twisting-moment coefficient C_T may be obtained in terms of their respective rigid-wing values by means of the following approximate expressions:

$$\frac{C_{L_w}}{C_{L_{w_0}}} = \frac{1 - \frac{q}{q_D}(1 - \nu)}{1 - \frac{q}{q_D}} \tag{26}$$

$$\frac{C_B}{C_{B_0}} = \frac{1 - \frac{q}{q_D}(1 - \mu\nu)}{1 - \frac{q}{q_D}} \tag{27}$$

$$\frac{C_T}{C_{T_0}} = \frac{1 - \frac{q}{q_D}(1 - \tau\nu)}{1 - \frac{q}{q_D}} \tag{28}$$

where the coefficients ν, μ, and τ depend on the type of loading. The subscript 1 is used for additional-type angle-of-attack distributions and the subscript 2 for linear-twist-type angle-of-attack distributions. The coefficients ν_1, μ_1, and τ_1 are given in figure 9 as functions of the parameter k for wings of taper ratios 0.2, 0.5, and 1.0. The ratios of the lift, bending-moment, and twisting-moment coefficients to their respective rigid-wing values are given in figure 10 as a function of q/q_D for several values of the parameter k when the taper ratio is zero. The values of ν_2, μ_2, and τ_2 are given in figure 11 for wings of taper ratios 0.2, 0.5, and 1.0, and ratios of the lift, bending-moment, and twisting-moment coefficients are given in figure 12 for wings of zero taper ratio. The additional-twist and linear-twist results of equations (26) to (28) may be superimposed in the same way as those of equations (20) and (21).

The wing rolling-moment coefficient C_{l_w} is defined as the rolling moment of the loads on both wings about the fuselage center line divided by qSb. Therefore,

$$C_{l_w} = \frac{2M_r \cos\Lambda + 2T_r \sin\Lambda + \frac{w}{2} L_w}{qSb} \tag{29}$$

The angle-of-attack distribution due to rolling given in equation (22) must be used in finding the values of M_r, T_r, and L_w in equation (29).

Spanwise centers of pressure and aerodynamic center.- The spanwise location of the center of pressure is given by the distance

$$\bar{s} = \frac{b}{2} \frac{C_B}{C_{L_w}} \tag{30}$$

or the dimensionless distance

$$\bar{s}^* = \frac{C_B}{C_{L_w}} \tag{31}$$

(Inasmuch as η^* is equal to s^* by virtue of the definitions of those dimensionless quantities (see also fig. 1), equation (31) can be considered to be an expression for $\bar{\eta}^*$ rather than $\bar{s}^*$, if desired.) With the values of the bending-moment and lift coefficients given in the preceding section, the ratio of $\bar{s}$ to its value for the rigid wing may be calculated from either of the equations

$$\left.\begin{aligned} \frac{\bar{s}}{\bar{s}_0} &= \frac{1 - \frac{q}{q_D}(1 - \mu\nu)}{1 - \frac{q}{q_D}(1 - \nu)} \\ \text{and} \\ \frac{\Delta\bar{s}}{\bar{s}_0} &= \frac{\nu\frac{q}{q_D}(\mu - 1)}{1 - \frac{q}{q_D}(1 - \nu)} \end{aligned}\right\} \tag{32}$$

where μ_1 and ν_1 are used for constant geometrical angles of attack and μ_2 and ν_2, for linearly varying geometrical angles of attack.

The shift due to aeroelastic action of the longitudinal position of the center of pressure associated with a given shift of the spanwise center of pressure, $\Delta\bar{s} \equiv \bar{s} - \bar{s}_0$, is equal to $\sin \Lambda \, \Delta\bar{s}$. The shift in aerodynamic center (positive when rearward, or stabilizing) can consequently be calculated by substituting into equation (17) the values of $\Delta\bar{s}$ obtained from equation (32) with values of μ_1 and ν_1.

Inertia effects.- No charts are presented in this paper for the effects of inertia on quasi-static aeroelastic phenomena, that is, aeroelastic phenomena associated with flight at constant acceleration; the manner in which mass is distributed varies so widely among different wings that preparation of a generally applicable set of charts for inertia effects appears to be impractical at present. Furthermore, except for flying wings, the wing deformations due to inertia loads are small compared with those due to aerodynamic loads, the two types of loads being in about the same ratio as the wing weight to the weight of the entire airplane. If desired, however, inertia effects and the aeroelastic increment in these effects can be calculated in the manner described in the following paragraphs.

From the known or estimated mass distribution of the wing the inertia load l_i per inch of span and the inertia torque t_i per inch of span can be calculated for any given normal, pitching, or rolling acceleration. Substitution of these loads and torques for the terms l and le_1c in equations (A3) or (A36) and equations (A2) or (A35), respectively, yields the values of the accumulated bending moment and torque due to the distributed inertia loads and torques. In turn, substitution of these accumulated bending moments and torques in equations (A4), (A5), and (A6), or in equations (A37) and (A38) and the matrix equivalent of equation (A6), yields the angle-of-attack distribution due to the deformations caused by the inertia effects associated with the given acceleration.

This angle-of-attack distribution can be considered as a geometrical angle-of-attack distribution. For the purpose of calculating the increment caused by aeroelastic action, this distribution can be approximated by a linear-twist angle-of-attack distribution with a value at the wing tip which is such that the moment about the effective wing root of the area under the linear-twist distribution equals the moment of the area under the calculated angle-of-attack distribution due to inertia effects. (The moment, rather than the area, is suggested as a basis of correlation because the angles of attack near the wing tip are more important in aeroelastic phenomena than those at the wing root.) The justification for this rather arbitrary approximation to the angle-of-attack distribution is as follows: As previously mentioned, the wing deformations due to inertia loads are likely to be small compared with those due to aerodynamic loads; furthermore, the correction to be applied to these deformations as a result of aeroelastic action is usually small compared with these deformations and, hence, is very small in comparison with the total wing load, so that the correction need not be calculated as accurately as the correction for aeroelastic effects to the rigid-wing lift distribution.

The angle of attack due to structural deformation α_s associated with the linear-twist distribution can then be obtained from equation (21) and

figure 7 or, if $\lambda = 0$, from figure 8. The lift distribution associated with the total angle-of-attack distribution due to the deformations caused by the inertia effects, including the increment in this angle-of-attack distribution produced by aeroelastic action, can then be found from equation (24b), in which α_g, α_{g_t}, and l_0 pertain to the calculated angle-of-attack distribution due to the inertia effects (not the linear approximation to this distribution). This lift distribution can be integrated to obtain the lift, bending moment, rolling moment, and aerodynamic-center position due to inertia effects, as modified by aeroelastic action.

The lift and rolling moment calculated in this manner may then be combined with the lift and rolling moment for steady level or rolling flight calculated by the method outlined in the preceding sections. For instance, if the contributions of the tail and the fuselage to the airplane lift can be neglected, the wing lift can be written as

$$n(W - W_w) = \frac{1}{144} C_{L_{\alpha_s}} \alpha q S + \left(\frac{\partial L_w}{\partial n}\right)_s n$$

where $\left(\frac{\partial L_w}{\partial n}\right)_s$ is the total normal force per unit load factor due to inertia effects, including aeroelastic effects; it is equal to $-W_w$ plus the lift on both wings due to inertia effects, as modified by aeroelastic action, per unit load factor and is almost always negative. In the preceding equation $C_{L_{\alpha_s}}$ is a wing lift-curve slope which includes static aeroelastic effects and is equal to C_{L_α} multiplied by the factor on the right side of equation (26). Then

$$n = \frac{1}{144} \frac{1}{1 - \frac{1}{W - W_w}\left(\frac{\partial L_w}{\partial n}\right)_s} \frac{C_{L_{\alpha_s}} \alpha q S}{W - W_w}$$

$$= \frac{1}{144} \frac{C_{L_{\alpha_{s,i}}} \alpha q S}{W - W_w}$$

where

$$C_{L_{\alpha_{s,i}}} \equiv \frac{1}{1 - \frac{1}{W - W_w}\left(\frac{\partial L_w}{\partial n}\right)_s} C_{L_{\alpha_s}}$$

is a wing lift-curve slope which includes static aeroelastic effects, inertia effects, and aeroelastic modification of the inertia effects.

Illustrative Example

The parameters of a swept wing, which differs from the wing of the illustrative example of reference 1 only in the width of the fuselage to which it is attached, are given in table 3. The values of Δs^{φ} and Δs^{Γ} were calculated from the dimensionless root-rotation constants used in the example of reference 1, $Q_{\varphi_T} = 0$ and $Q_{\Gamma_M} = -0.25$, by means of the relations

$$\Delta s^{\varphi} = Q_{\varphi_T} w_e$$

$$\Delta s^{\Gamma} = Q_{\Gamma_M} w_e$$

where w_e, as defined in reference 1, is the distance along the span between the effective root and the innermost complete section of the torsion box perpendicular to the elastic axis. In the wing of the illustrative examples of the present paper and of reference 1, w_e is 22.4 inches. These relations for Δs^{φ} and Δs^{Γ} can be obtained from equations (11) and (12) of the present paper in conjunction with the definitions of the root-rotation constants given in equations (15a) and (15d) of reference 1; in the notation of the present paper the definitions are:

$$Q_{\varphi_T} = \frac{\varphi_r^T / T_r}{w_e/(GJ)_r}$$

$$Q_{\Gamma_M} = \frac{\Gamma_r^M / M_r}{w_e/(EI)_r}$$

The stiffness is assumed to vary as the fourth power of the chord in the example of the present paper.

The subsonic and supersonic values of the parameter k were calculated from equation (9). By means of appropriate values of the constants K_1 and K_2 taken from table 3, the values of q^*_D were calculated from equation (18) and included in table 3. From these values of q^*_D, the subsonic and supersonic dynamic pressures at divergence were found through the use of equation (7) and are given in table 3. These values of q_D vary as the reciprocal of the effective lift-curve slope, the corresponding values of e_1 being assumed to remain constant.

In order to find the angle-of-attack distribution for additional-type loadings from equation (20), the values of F_1 and of the functions f_1 and Δf_1 were taken from figure 5(c). The spanwise change in angle of attack is shown in figure 13 for different values of the dynamic-pressure ratio.

The values of ν_1, τ_1, and μ_1 were obtained from figure 9(c) and substituted into equations (26), (27), and (28). The wing lift coefficient, wing rolling-moment coefficient, and spanwise center-of-pressure ratios, as well as the shift in aerodynamic center, were calculated by use of these approximate equations in conjunction with equations (17) and (29) and are shown in figure 13 as functions of the dynamic-pressure ratio $\frac{q}{-q_D}$.

DISCUSSION

Limitations of the Charts and Approximate Formulas

The charts and the approximate formulas presented in this paper are subject to certain limitations as a result of the approximations made in the calculations on which they are based. These limitations take the form of restrictions on the plan form, on the speed regime, and on the wing structure. The results obtainable by the use of the charts are likely to be unsatisfactory for wings of very low aspect ratio or very large sweep and relatively unsatisfactory for wings of zero taper ratio.

Wings of low aspect ratio are ruled out on three counts: (1) the extent to which aerodynamic forces are overestimated in replacing the wing by one with an effective root and tip is larger for wings of low aspect ratio than for wings of high aspect ratio, (2) elementary beam theory is unsatisfactory for calculating the deformations of wings of very low aspect ratio (because the effects of end constraint, shear lag, shear deformation, and bending-torsion interaction are more important when the aspect ratio is low), and (3) the assumptions made concerning the lift distribution of the wing are more nearly true for wings of high than for those of low aspect ratio.

For wings with very large angles of sweep, also, the use of an effective root and tip introduces relatively large errors in the aerodynamic forces. Furthermore, the root rotations neglected in the calculations (bending rotation due to torsion and twist due to bending) are likely to be important for wings with large angles of sweep.

The aeroelastic analysis of wings with zero taper ratio entails certain mathematical difficulties which do not arise in the case of wings with nonzero taper ratio. The stiffness of such wings is zero at the tip and very low near the tip, so that the boundary conditions for φ and Γ given by equations (A10a) to (A10c) in appendix A are indeterminate. As a result of the relatively large values of the reciprocal of the stiffness near the tip, the numerical-integration methods used in the matrix calculations are less accurate. These difficulties also occur in other methods of solving the aeroelastic equations, such as energy methods. Furthermore, the structural behavior near the wing tip is not represented adequately by elementary beam theory. Finally, that the aeroelastic results calculated for wings of zero taper ratio are not as reliable as those for other wings is evidenced also by the fact that they do not lend themselves to systematization by means of approximate formulas, as do the aeroelastic results calculated for other wings.

As a result of these considerations one type of plan form of recent interest, the delta wing, is seen to be unsuitable for aeroelastic analysis by means of these charts because it has a low aspect ratio, a large angle of sweep, and zero taper ratio.

In order to use the charts two aerodynamic parameters must be known for any given case, the effective wing lift-curve slope and the section aerodynamic center. From an aerodynamic point of view the charts of this paper may be used in almost all cases for which these quantities are known. The exceptions stem from the fact that the spanwise distribution of the lift is assumed to be proportional to the chord, and the distance from the section aerodynamic center to the elastic axis (as a fraction of the chord) is assumed to be constant along the span. These assumptions are not valid for wings with large angles of sweep and wings of low aspect ratio, as implied previously. They are also invalid to a greater or lesser extent for most wings in the transonic region. Consequently, even when the lift-curve slope and the section aerodynamic center are known, any results calculated for transonic speeds must be used with caution.

Another aerodynamic assumption implied in the charts is that no concentrated aerodynamic forces, such as those due to a tip tank or nacelle, act on the wing. Relatively small nacelles in the inboard half of the span can probably be ignored for the purpose of an aeroelastic analysis at the preliminary design stage. However, large tip tanks cannot usually be ignored even in a preliminary aeroelastic analysis; the aeroelastic phenomena may in such cases be greatly underestimated by calculations made with the charts of this paper.

The assumption concerning the applicability of elementary beam theory to the calculation of wing deformations due to aeroelastic action serves to restrict the wings that can be analyzed by means of the charts

to those of moderate or high aspect ratio, as stated previously. Neglect of chordwise bending (elastic camber) effects in the calculations on which the charts are based serves to impose a lower limit on the thickness of the wings for which the charts may be used. Whether this limit is within the region of practical thicknesses is questionable, however. The divergence tests of reference 2, which were performed on flat plates of moderately high aspect ratio and with a thickness of 2.5 percent, showed no obvious chordwise-bending effects, although the relatively small differences between the measured and calculated divergence speeds may have been due in part to such effects.

As mentioned previously, for wings with taper ratios between 0 and 0.2 the results of aeroelastic calculations are likely to be relatively unreliable. For taper ratios greater than 0.2, the stiffness of actual wings tends to be greater near the tip than that given by the constant-stress criterion; consequently, any given aeroelastic effect is likely to be somewhat less than that calculated on the basis of a constant-stress stiffness distribution, but much larger than that calculated on the basis of a c^4 distribution.

If a given structure contains large cut-outs which give rise to discontinuities in the stiffness distributions, equation (10) can be used to calculate a fictitious root stiffness to be used in conjunction with charts for c^4-type stiffness distributions, provided the magnitudes of the discontinuities are known or estimable.

Use of the charts of this paper is premised on the assumption that the elastic axis is at an approximately constant fraction of the chord. If the location of the elastic axis varies somewhat along the span, the use of an average value tends to give satisfactory results for the aeroelastic phenomena of swept wings; for unswept wings, however, the results obtained on the basis of this approximation have to be used with caution. If the elastic axis exhibits abrupt shifts along the span as a result of large cut-outs or for other reasons, the charts should not be used, except possibly for moderately or highly swept wings. This restriction is mitigated to a certain extent by the fact that an abrupt shift in the locus of shear centers does not necessarily imply an equally large or equally abrupt shift in the elastic axis.

Relation between Strength and Stiffness as Design Criteria

The strength of a structure is its ability to withstand applied loads without failure; the stiffness of a structure is its ability to deform relatively little under the applied loads. The two terms are related (a fact which forms the basis of the constant-stress type of stiffness distributions used in this paper) but are not synonymous.

The problem of when to design for strength and when to design for stiffness and the related problem of how to design a wing for stiffness when required to do so have been recognized for a long time. Because of the complexity of these problems no generally satisfactory solution exists at present, but the charts presented herein shed a certain amount of light on the problem insofar as stiffness requirements occasioned by the aeroelastic phenomena considered in this paper are concerned.

The charts of figure 2 indicate the extent to which a wing is likely to be affected by aeroelastic phenomena; that is, how far it is from divergence and how much its spanwise center of pressure is likely to shift as a result of aeroelastic action, provided the wing is designed on the basis of strength considerations alone. If the margin against divergence is too small, or if the spanwise center of pressure and the associated shift in the aerodynamic center are deemed excessive, the wing has to be stiffened beyond the amount associated with the required strength. The charts of figure 2 therefore serve to delimit the regions in which a wing can be designed on the basis of strength considerations alone and those in which stiffness considerations predominate, at least to the extent of satisfying the stiffness requirements associated with the aeroelastic phenomena considered herein.

The bending moment of inertia required by considerations of strength alone for the root section of a wing is directly proportional to the design load $n(W - W_w)$, to the spanwise coordinate of the center of pressure, and to the wing thickness at the root and is inversely proportional to the allowable bending stress F_B. Alternatively, this bending moment of inertia may be considered to be proportional to the design wing loading $\frac{n(W - W_w)}{S}$, to the square of the wing area, to the wing thickness ratio at the root, and to a function of the taper ratio $\left(\text{which is } \frac{1 + 2\lambda}{(1 + \lambda)^2}\right.$ if strip theory is assumed to apply$\left.\right)$; this bending moment of inertia is inversely proportional to F_B and independent of the aspect ratio. These relations for the bending moment of inertia required by considerations of strength alone must be kept in mind in the following discussion of the bending moment of inertia required by considerations of stiffness.

In general, a wing with a high value of q^* (see equations (7) and (13)) is most likely to be affected by aeroelasticity (see fig. 2) and, for a given value of q^*, swept wings are much more likely to be affected by aeroelasticity than unswept ones. (See fig. 2 and equations (9) and (14).) Consequently, the following wings are most likely to be subject to aeroelastic phenomena, provided they are designed on the basis of strength considerations alone:

(1) Wings designed for a high flying speed or high dynamic pressure

(2) Swept wings

(3) Thin wings

(4) Wings designed for a low wing loading

(5) Unswept and moderately swept wings with an elastic axis relatively far back on the chord or likely to fly in a condition in which the section aerodynamic centers are relatively far forward on the chord

(6) Wings operating at a Mach number at which the lift-curve slope is relatively high.

For given wing loadings and given wing areas, some aeroelastic phenomena of wings designed on the basis of strength considerations alone appear to be substantially unaffected by changes in the taper ratio - for instance, the spanwise shift of the center of pressure and the dynamic pressure required for divergence. (In the case of the dynamic pressure required for divergence, the parameter q^*_D (fig. 4), the root stiffness, and the root chord decrease with increasing taper ratio, and the net effect of taper is small.) On the other hand, the change in the lift due to aeroelastic action is more sensitive to the taper ratio; it is more significant for wings with high taper ratio than for wings with low taper ratio.

The effect of aspect ratio on aeroelastic phenomena tends to be small for unswept wings of a given wing area, because these phenomena are determined largely by the magnitude of the parameter q^*, which is independent of the aspect ratio for a given wing area. For the aeroelastic phenomena of highly swept wings, however, the parameter $\bar{q}$ is more significant. This parameter is proportional to the swept-span aspect ratio for wings of a given area. Consequently, with a given wing area, taper ratio, and design wing loading, the aeroelastic effects of swept wings tend to be more pronounced for wings with high aspect ratio than for those with low aspect ratio. This statement is particularly true for the shift of the aerodynamic center, because a given spanwise shift of the center of pressure results in a much greater chordwise shift in the case of a swept wing of high aspect ratio than in the case of a swept wing with low aspect ratio.

Structural Weight Associated with the Required Stiffness

When a given wing has been shown to be subject to undesirably large aeroelastic effects (by means of the charts of this paper or by any other method), the problem arises how to distribute the additional required

stiffness. If, for instance, the pressure on an unswept wing is within 10 percent of the dynamic pressure required for divergence and a margin of 20 percent is desired, an increase of 10 percent in the torsional stiffness along the entire span will produce the desired result. The question remains, however, whether structural weight can be saved by increasing the stiffness more than 10 percent in some places and less in others.

Some insight into this problem may be gained, at least insofar as the aeroelastic phenomena considered herein are concerned, from aeroelastic and weight calculations that have been made for a family of somewhat arbitrarily selected stiffness distributions which differ from the distribution required by the constant-stress criterion. The ratios of the local stiffnesses to those associated with constant stress are shown at the top of figure 14. The structural-weight factor F_W is shown for two of these stiffness distributions as a function of the taper ratio. The function F_W is proportional to the weight W_s of the primary load-carrying structure and depends on the manner in which the wing stiffness and thickness are distributed along the span. (See appendix B.)

The results of the aeroelastic calculations for wings with taper ratio 0.5, constant wing thickness ratio h/c along the span, and these two stiffness distributions are included in table 2 and figures 5(b), 7(b), 9(b), and 11(b). The designation "excess strength" in these figures refers to the stiffness distributions increased over the constant-stress requirement, as shown in figure 14, with a value of $\omega = 2.0$. The results of the aeroelastic calculations for the stiffness distributions decreased below the constant-stress requirement to a value of $\omega = 0.5$ are the same as those for the constant-stress stiffness distributions for wings with varying wing thickness ratio; that is, $\frac{(h/c)_t}{(h/c)_r} = 0.5$.

The results of the weight calculations and the aeroelastic calculations may be combined in several ways. The dynamic pressure at divergence, for instance, can be varied by changing the bending and torsional stiffnesses uniformly along the span, by leaving the stiffnesses at the root unchanged and varying the stiffness distribution in a manner similar to that indicated at the top of figure 14, or by a combination of the processes. A specified dynamic pressure at divergence can therefore be obtained as the result of several combinations of root stiffnesses and stiffness distributions. Figure 15(a) consists in essence of a plot of the structural weights associated with various combinations of this type against the tip stiffness ratio ω for a specified dynamic pressure at divergence. This figure indicates that the least weight is associated with values of the tip stiffness ratio greater than 1.

Similarly, figures 15(b) and 15(c) consist in essence of plots of the structural weights associated with various combinations of root stiffnesses and stiffness distributions required for shifts of ±10 percent in the spanwise center of pressure at a specified dynamic pressure. Figures 15(b) and 15(c) also indicate that the structural weight is least for values of the stiffness ratio ω greater than 1.

The significance of figure 15 is that, if a given wing designed on the basis of strength alone needs to be stiffened for aeroelastic reasons, most of the stiffening material should be added in the outboard regions, provided the weight of the material other than that of the primary load-carrying structure is unaffected by the stiffening process. In fact, on the basis of aeroelastic considerations alone, weight might be saved in some cases by removing material from the root and adding material at the tip; needless to say, however, strength requirements would be violated by this procedure. Just where the material should be added in the outboard regions cannot be said on the basis of the calculations made for figure 15, since these calculations assume any modifications to the constant-stress stiffness distributions to be made as indicated at the top of figure 14. However, it appears unlikely that great weight savings can be had by using modifications which differ substantially from those of figure 14.

The Aeroisoclinic Wing

The term "aeroisoclinic" refers to wings which deform under an aerodynamic load in such a fashion that the angles of attack of all sections relative to the free stream remain unchanged. Such a wing has the advantage that its aerodynamic loads do not change under aeroelastic action either in magnitude or in distribution; its aerodynamic center, for instance, is unchanged, and the wing cannot diverge. The achievement of such "section aeroisoclinicism" is very difficult and can be realized only by separate variation of the bending and torsion stiffnesses; even so, the aeroisoclinic condition obtains for only one type of aerodynamic loading condition at one Mach number. However, an over-all type of aeroisoclinicism in which bending and torsion action tend to cancel for the wing as a whole is relatively easy to achieve. This over-all type has, for practical purposes, the same advantages as section aeroisoclinicism, in that the aeroelastic phenomena considered in this paper tend to be negligibly small for such a wing.

As may be seen from figure 2, at a small positive value of the parameter k the values of the parameter q^* for divergence as well as those for given shifts in the spanwise center of pressure tend to infinity. This particular value of k represents aeroisoclinic wings in the over-all sense; from equations (18) and (19) it may be seen to be the reciprocal of the value of K_2 given in table 2. Hence, from the definition of k

(equation (9)),

$$\frac{s_t}{e_1 c_r} \frac{(GJ)_r}{(EI)_r} \tan \Lambda = \frac{1}{K_2} \tag{33}$$

with the implication that the distributions of the stiffness are of either the c^4 or the constant-stress type and that K_2 pertains to either of these types and to the appropriate taper ratio. Equation (33) indicates that, for a given plan form with assigned values of s_t, c_r, and Λ, the disposable parameters for the achievement of aeroisoclinicism are the elastic-axis location e, which enters into the parameter e_1, and the root-stiffness ratio $\frac{(GJ)_r}{(EI)_r}$; the aerodynamic center is not under the control of the designer.

A decrease in the torsional stiffness can sometimes be effected without decrease in the bending stiffness or impairment of the strength characteristics of the wing, and over-all aeroisoclinicism may be achieved in this manner for sweptback wings. Or, if aeroisoclinic conditions are considered at the outset, a wing can be designed with the elastic-axis location relatively far back (in the case of a sweptback wing) or forward (in front of the aerodynamic center, in the case of a sweptforward wing) in order to achieve aeroisoclinicism. However, the fact that only certain types of aeroelastic phenomena are considered in this paper must be kept in mind. Locating the elastic axis far back or decreasing the torsional stiffness, for instance, may lead to flutter difficulties, the solution of which may require excessive mass balancing of the wing as a whole.

Relation of Charts to Design Procedure

The first step in the design of a wing structure, once the wing geometry and the over-all airplane characteristics have been decided upon, usually consists of a rough apportioning of structural material along the span in a manner intended to satisfy strength requirements approximately. At a later stage in the design procedure the structure is checked for aeroelastic effects and modified, if necessary. The modifications are then checked again, and so on, until both stiffness and strength requirements are met with what is believed to be a near-optimum structure from weight considerations. The charts of this paper may be used to facilitate the procedure at several stages.

At the very outset, the preliminary-survey charts can be used to establish some over-all aeroelastic characteristics of the wing structure that would be obtained by designing the wing for strength alone. If

these characteristics are satisfactory, the design of the wing structure can proceed on the basis of strength requirements alone. The final design can then be checked for the aeroelastic effects considered in this paper by means of the charts contained herein, and for other aeroelastic effects, such as flutter and loss of lateral control, by equally approximate methods. However, if the preliminary survey indicates that a wing designed on the basis of strength alone would be unsatisfactory from consideration of aeroelasticity, sufficient additional stiffness may be incorporated in the preliminary design stage, provided the taper ratio does not differ greatly from 0.5 and the wing thickness ratio is constant along the span. For instance, the preliminary-survey charts may indicate a shift in the spanwise center of pressure which gives rise to a shift of 4 percent in the aerodynamic center, whereas the desired maximum shift is 2 percent, so that the spanwise shift must be reduced to 50 percent of that indicated on the preliminary-survey chart. The shifts in the spanwise center of pressure for a wing with increased stiffness at the tip (the "excess strength" case, for which $\omega = 2.0$) and for a wing with decreased stiffness at the tip (the wing with $\omega = 0.5$, for which the results of the case of $\frac{(h/c)_t}{(h/c)_r} = 0.5$ may be used) can then be obtained from figure 9(b) and equation (32), in conjunction with the value of the dynamic pressure at divergence estimated from equation (18) or (19). The fact that the wings with $\omega = 2.0$ and $\omega = 0.5$ have different dynamic pressures at divergence than does the constant-stress wing must be kept in mind.

From the shifts of the spanwise center of pressure calculated in this manner the value of ω for the desired spanwise shift can be obtained by interpolation and, hence, the approximate magnification factors to be applied to the stiffness distribution for constant stress can be obtained from the chart at the top of figure 14. Estimates for the other aeroelastic characteristics considered in this paper can then be obtained for the wing with this modified stiffness distribution by interpolating between the results given for these characteristics for wings with $\omega = 0.5$, 1.0, and 2.0; that is, for the cases referred to, respectively, as

$$\frac{(h/c)_t}{(h/c)_r} = 0.5$$

$$\frac{(h/c)_t}{(h/c)_r} = 1.0$$

and

$$\frac{(h/c)_t}{(h/c)_r} = 1.0 \quad \text{(excess strength)}$$

in table 2 and figures 5(b), 7(b), 9(b), and 11(b). Once the structure of such a wing has been designed, the various aeroelastic effects considered herein should be checked by a more accurate method, such as that of reference 1, and the loss of lateral control and the flutter characteristics should be calculated.

CONCLUDING REMARKS

Charts have been presented for the estimation of aeroelastic effects on the spanwise lift distribution, lift-curve slope, aerodynamic center, and damping in roll of swept and unswept wings at subsonic and supersonic speeds. Two types of stiffness distributions have been considered, one which consists of a variation of the stiffness with the fourth power of the chord and is appropriate for solid wings, and one which is based on an idealized constant-stress structure and is believed to be more nearly representative of actual structures.

The limitations of these charts are that they do not apply to wings with very low aspect ratio or very large angles of sweep, nor to wings with large sources of concentrated aerodynamic forces. The charts are likely to be less reliable for wings with zero taper ratio than for wings with other taper ratios, and less reliable when the component of the Mach number perpendicular to the leading edge is transonic than when this component is either subsonic or supersonic. Wings with large discontinuities in the spanwise distribution of the bending or torsional stiffnesses cannot be analyzed directly by use of the charts, but a means of making approximate calculations for such wings has been presented. No charts have been presented for inertia effects but a method of estimating these effects has been outlined.

In addition to facilitating the calculation of various static aeroelastic phenomena, the charts serve to simplify design procedure in many instances, because they can be used at the preliminary design stage to estimate the amount of additional material required to stiffen a wing which is strong enough and because they indicate that the best way of distributing this additional material is to locate most of it near the wing tip.

Also, the charts facilitate the achievement of aeroisoclinic conditions, inasmuch as they serve to define a simple relation between the elastic-axis location and the wing stiffness ratio which is required to obtain this condition for a given plan form. Finally, the charts indicate that a wing which is strong enough is most likely to be affected by aeroelastic phenomena if it is to operate at high dynamic pressures, if it is thin, if it has a large angle of sweep, if it is designed for a low

wing loading, if it has an elastic-axis location relatively far back on the chord, and if it is to operate at transonic or high supersonic Mach numbers.

Langley Aeronautical Laboratory
National Advisory Committee for Aeronautics
Langley Field, Va., September 13, 1951

APPENDIX A

METHODS OF CALCULATIONS ON WHICH CHARTS ARE BASED

The Aeroelastic Equations

The methods of calculating aeroelastic phenomena used in preparing the charts of this paper are based on the following assumptions:

(1) Aerodynamic induction is taken into account by applying an over-all correction to strip theory and, when matrix integrations are used, by rounding off the resulting load distribution at the tip.

(2) Aerodynamic and elastic forces are based upon the assumption of small deflections.

(3) The wing is clamped at the root perpendicular to a straight elastic axis (see fig. 1), and all deformations are considered to be given by the elementary theories of bending and torsion about the elastic axis.

In keeping with assumptions (1) and (2), the force per unit width on a wing section perpendicular to the elastic axis is

$$l = \frac{qc}{144}\left(C_{l_\alpha}\alpha_g + C_{l_{\alpha_e}}\alpha_s\right) \tag{A1}$$

where α_s and α_g are, respectively, the angle of attack due to structural deformations and the rigid-wing angle of attack, in planes parallel to the plane of symmetry. (The geometrical angle of attack is considered to be constant along the span in equation (A1); in the case of linear twist the coefficient $C_{l_{\alpha_e}}$ is used instead of C_{l_α}.) The torque of this force about the elastic axis is le_1c for uncambered sections.

The integral equations for the accumulated torque and the bending moment are

$$T = \int_s^{s_t} le_1c\, ds \tag{A2}$$

$$M = \int_s^{s_t} \int_s^{s_t} l \, ds \, ds \tag{A3}$$

and, insofar as assumption (3) holds, the angles of structural twist and bending referred to axes parallel or perpendicular to the elastic axis are

$$\varphi = \int_0^s \frac{1}{GJ} T \, ds \tag{A4}$$

$$\Gamma = \int_0^s \frac{1}{EI} M \, ds \tag{A5}$$

The angle of attack due to structural deformations is related to φ and Γ by the equation

$$\alpha_s = \varphi \cos \Lambda - \Gamma \sin \Lambda \tag{A6}$$

Combining equations (A1) to (A6) gives two simultaneous differential equations:

$$\frac{d}{ds}\left(GJ \frac{d\varphi}{ds}\right) = \frac{-qe_l c^2}{144}\left[C_{L_\alpha} \alpha_g + C_{L_{\alpha_e}} (\varphi \cos \Lambda - \Gamma \sin \Lambda)\right] \tag{A7}$$

$$\frac{d^2}{ds^2}\left(EI \frac{d\Gamma}{ds}\right) = \frac{qc}{144}\left[C_{L_\alpha} \alpha_g + C_{L_{\alpha_e}} (\varphi \cos \Lambda - \Gamma \sin \Lambda)\right] \tag{A8}$$

These equations are subject to the following boundary conditions:

Zero twist and bending at the root,

$$\varphi(0) = 0 \tag{A9a}$$

$$\Gamma(0) = 0 \tag{A9b}$$

Zero torque, moment, and shear at the tip,

$$\left(GJ \frac{d\varphi}{ds}\right)_{s=s_t} = 0 \tag{A10a}$$

$$\left(EI \frac{d\Gamma}{ds}\right)_{s=s_t} = 0 \tag{A10b}$$

$$\left(EI \frac{d^2\Gamma}{ds^2}\right)_{s=s_t} = 0 \tag{A10c}$$

In the following sections, equations (A7) and (A8) are solved explicitly for an untapered wing with constant stiffness along its span and by matrix integration for a wing with any arbitrary stiffness and chord variation.

Solutions for Uniform Wings

Arbitrary geometric angle of attack.- If the torsional stiffness, the bending stiffness, and the chord of the wing have constant values $(GJ)_r$, $(EI)_r$, and c_r, respectively, along the wing span, equations (A7) and (A8) become

$$\varphi'' \cos \Lambda = -q^* \left[\frac{1}{\kappa} \alpha_g + (\varphi \cos \Lambda - \Gamma \sin \Lambda)\right] \tag{A11}$$

$$\Gamma''' \sin \Lambda = -\bar{q} \left[\frac{1}{\kappa} \alpha_g + (\varphi \cos \Lambda - \Gamma \sin \Lambda)\right] \tag{A12}$$

where the differentiation denoted by the primes is with respect to $\xi \equiv 1 - \frac{s}{s_t}$ and the dimensionless parameters q^* and $\bar{q}$ are defined by

$$q^* = \frac{C_{l_{\alpha_e}} q e_1 c_r^2 s_t^2 \cos \Lambda}{144(GJ)_r} \tag{A13}$$

$$\bar{q} = \frac{C_{l_{\alpha_e}} q c_r s_t^3 \sin \Lambda}{144(EI)_r} \tag{A14}$$

Differentiating equation (A11) once with respect to ξ and combining it with equation (A12) yields the single differential equation

$$\alpha_s''' + q^*\alpha_s' - \bar{q}\alpha_s = -q^* \frac{\alpha_g'}{\kappa} + \bar{q} \frac{\alpha_g}{\kappa} \tag{A15}$$

(The factor $\frac{1}{\kappa}$ is used with α_g for the sake of consistency, despite the fact that a geometrical angle of attack which is constant over the span does not have a spanwise derivative.) Equation (A15) is subject to the following boundary conditions:

From equations (A9a) and (A9b)

$$\alpha_s(1) = 0 \tag{A16}$$

From equations (A10a) and (A10b)

$$\alpha_s'(0) = 0 \tag{A17}$$

From equations (A10c) and (A11)

$$\alpha_s''(0) = -q^*\left[\frac{\alpha_g(0)}{\kappa} + \alpha_s(0)\right] \tag{A18}$$

where functional notation is used, so that, for instance, $\alpha_s(1)$ means the value of α_s at $\xi = 1$.

The solution of equation (A15) can be effected very readily by means of of Laplace transforms. The complete solution of this equation is

$$\alpha_s(\xi) = \frac{H(1)}{f_3(1)} f_3(\xi) - H(\xi) \tag{A19}$$

where the integral $H(\xi)$ is defined as

$$H(\xi) \equiv \int_0^\xi \left[q^* f_4(\xi - \xi_1) - \bar{q} f_5(\xi - \xi_1)\right] \frac{\alpha_g(\xi_1)}{\kappa} d\xi_1 \tag{A20}$$

The functions f_3, f_4, and f_5 are defined by

$$f_3(\xi) \equiv C_1 e^{-2\beta\xi} + e^{\beta\xi}\left(C_2 \cos \gamma\xi + \frac{C_3}{\gamma} \sin \gamma\xi\right) \tag{A21a}$$

$$f_4(\xi) \equiv C_4 e^{-2\beta\xi} + e^{\beta\xi}\left(C_5 \cos \gamma\xi + \frac{C_6}{\gamma} \sin \gamma\xi\right) \tag{A21b}$$

$$f_5(\xi) \equiv C_7 e^{-2\beta\xi} + e^{\beta\xi}\left(C_8 \cos \gamma\xi + \frac{C_9}{\gamma} \sin \gamma\xi\right) \tag{A21c}$$

where -2β and $\beta \pm i\gamma$ are the roots of $r^3 + q^*r - \bar{q} = 0$ and

$$C_1 = \frac{4\beta^2}{9\beta^2 + \gamma^2}$$

$$C_2 = 1 - C_1$$

$$C_3 = \frac{3\beta^3 - \beta\gamma^2}{9\beta^2 + \gamma^2}$$

$$C_4 = \frac{-2\beta}{9\beta^2 + \gamma^2}$$

$$C_5 = -C_4$$

$$C_6 = \frac{3\beta^2 + \gamma^2}{9\beta^2 + \gamma^2}$$

$$C_7 = \frac{1}{9\beta^2 + \gamma^2}$$

$$C_8 = -C_7$$

$$C_9 = \frac{3\beta}{9\beta^2 + \gamma^2}$$

The condition for divergence is that α_s be finite when α_g is zero along the entire span. As can be seen from equations (A19) and (A20), divergence can occur only when

$$f_3(1) = 0 \tag{A22}$$

Thus, for a particular value of the parameter $k = \frac{\bar{q}}{q^*}$ the value of q^* (or $\bar{q}$) at divergence is the one which satisfies equation (A22).

Constant geometric angle of attack.- For the additional-type angle of attack, $\alpha_g(\xi) = \text{Constant}$:

$$H(\xi) = \left[1 - f_3(\xi)\right]\frac{\alpha_g}{\kappa} \tag{A23}$$

and

$$\frac{\kappa\alpha_s(\xi) + \alpha_g}{\alpha_g} = \frac{f_3(\xi)}{f_3(1)} \tag{A24}$$

For lift distributions based on assumption (1) given at the beginning of this appendix, the lift per unit width of span may then be written as

$$\frac{l}{l_0} = \frac{f_3(\xi)}{f_3(1)}$$

The wing lift coefficient, the wing-root bending-moment coefficient, and the wing-root twisting-moment coefficient are given in general by

$$C_{L_w} = \frac{L_w}{qS}$$

$$= C_{L_\alpha}\frac{s_t c_r}{S/2}\int_0^1 \frac{c}{c_r}\left[\kappa\alpha_s(\xi) + \alpha_g(\xi)\right]d\xi \tag{A25}$$

$$C_B = \frac{4M_r}{qSb}$$

$$= C_{L_\alpha}\frac{s_t c_r}{S/2}\frac{s_t}{b/2}\int_0^1\int_0^\xi \frac{c}{c_r}\left[\kappa\alpha_s(\xi) + \alpha_g(\xi)\right]d\xi\, d\xi \tag{A26}$$

$$C_T = \frac{2T_r}{qSc_r}$$

$$= C_{L_\alpha} \frac{s_t c_r}{S/2} e_1 \int_0^1 \left(\frac{c}{c_r}\right)^2 \left[\kappa\alpha_s(\xi) + \alpha_g(\xi)\right] d\xi \tag{A27}$$

Then, for the uniform wing,

$$\frac{C_{L_w}}{C_{L_{w_0}}} = \int_0^1 \frac{\kappa\alpha_s(\xi) + \alpha_g}{\alpha_g} d\xi$$

$$= \frac{f_4(1)}{f_3(1)} \tag{A28}$$

$$\frac{C_B}{C_{B_0}} = 2\int_0^1 \int_0^\xi \frac{\kappa\alpha_s(\xi) + \alpha_g}{\alpha_g} d\xi \, d\xi$$

$$= 2 \frac{f_5(1)}{f_3(1)} \tag{A29}$$

and

$$\frac{C_T}{C_{T_0}} = \frac{C_{L_w}}{C_{L_{w_0}}}$$

Linearly varying geometric angle of attack.- For the linear-twist-type angle of attack, $\alpha_g(\xi) = (1 - \xi)\alpha_{g_t}$, the factor κ is 1, and

$$H(\xi) = \alpha_g(\xi) - \left[f_3(\xi) - f_4(\xi)\right] \alpha_{g_t} \tag{A30}$$

so that

$$\frac{l}{l_{0_t}} = \frac{\alpha_s(\xi) + \alpha_g(\xi)}{\alpha_{g_t}}$$

$$= \frac{f_4(1)}{f_3(1)} f_3(\xi) - f_4(\xi) \tag{A31}$$

The ratios of the wing lift, wing-root twisting moment, and wing-root bending-moment coefficients to their rigid-wing values are then, on the basis of assumption (1),

$$\frac{C_{L_w}}{C_{L_{w_0}}} = 2\int_0^1 \frac{\alpha_s(\xi) + \alpha_g(\xi)}{\alpha_{g_t}}\, d\xi$$

$$= 2\left[\frac{f_4(1)}{f_3(1)}\, f_4(1) - f_5(1)\right] \tag{A32}$$

$$\frac{C_B}{C_{B_0}} = 3\int_0^1\int_0^\xi \frac{\alpha_s(\xi) + \alpha_g(\xi)}{\alpha_{g_t}}\, d\xi\, d\xi$$

$$= 3\left\{\frac{f_4(1)}{f_3(1)}\, f_5(1) - \frac{1}{q}\left[f_3(1) + q^* f_5(1) - 1\right]\right\} \tag{A33}$$

and

$$\frac{C_T}{C_{T_0}} = \frac{C_{L_w}}{C_{L_{w_0}}}$$

as in the preceding section.

Solution for Nonuniform Wings

Equation (A1) may be written in the matrix notation of reference 1 as

$$\{l\} = \frac{q}{144} C_{L_{\alpha_e}} [c] \left\{\alpha_s + \frac{\alpha_g}{\kappa}\right\} \tag{A34}$$

and equations (A2) and (A3) as

$$\{T\} = s_t [I'] \{l e_1 c\}$$

$$= \frac{q}{144} C_{L_{\alpha_e}} e_1 c_r^2 s_t [I'] \left[\left(\frac{c}{c_r}\right)^2\right] \left\{\{\alpha_s\} + \frac{1}{\kappa}\{\alpha_g\}\right\} \tag{A35}$$

$$\{M\} = s_t^2 [II'] \{l\}$$

$$= \frac{q}{144} C_{L_{\alpha_e}} c_r s_t^2 [II'] \left[\frac{c}{c_r}\right] \left\{\{\alpha_s\} + \frac{1}{\kappa}\{\alpha_g\}\right\} \tag{A36}$$

where the matrix $[I']$ performs an integration of the running torque le_1c from the tip inboard, and the matrix $[II']$ performs a double integration of the running load from the tip inboard. These matrices are derived and given in reference 1. They are based upon Simpson's rule with a modification at the tip, where the load distribution is assumed to go to zero with an infinite slope at the tip.

Equations (A4) and (A5), written in matrix notation, are

$$\{\varphi\} = \frac{s_t}{(GJ)_r}[I]''\left[\frac{(GJ)_r}{GJ}\right]\{T\} \tag{A37}$$

$$\{\Gamma\} = \frac{s_t}{(EI)_r}[I]''\left[\frac{(EI)_r}{EI}\right]\{M\} \tag{A38}$$

where the matrix $[I]''$ serves to integrate the accumulated torque or bending moment outboard from the wing root. This integrating matrix is based upon Simpson's rule without the tip modification and is given in reference 1.

The substitution of equations (A35), (A36), (A37), and (A38) in the matrix equivalent of equation (A6) yields

$$\{\alpha_s\} = q^*[A]\left\{\{\alpha_s\} + \frac{1}{k}\{\alpha_g\}\right\} \tag{A39}$$

where the aeroelastic matrix $[A]$ is defined by

$$[A] \equiv [I]''\left[\left[\frac{(GJ)_r}{GJ}\right][I']\left[\frac{c}{c_r}\right] - k\left[\frac{(EI)_r}{EI}\right][II']\right]\left[\frac{c}{c_r}\right] \tag{A40}$$

The parameters q^* and $\bar{q}$ are defined by equations (A13) and (A14), respectively, and

$$k \equiv \frac{\bar{q}}{q^*}$$

When α_g is zero along the entire span, equation (A39) becomes

$$\{\alpha_s\} = q^*[A]\{\alpha_s\} \tag{A41}$$

Consequently, for a particular value of k, the value of q^* at divergence can be found by the iteration of the aeroelastic matrix $[A]$.

Equation (A39) may be rearranged as follows:

$$\left[[1] - q^*[A]\right]\left\{\kappa\alpha_s + \alpha_g\right\} = \left\{\alpha_g\right\} \tag{A42}$$

The set of linear simultaneous equations represented by equation (A42) may then be solved for the total angle of attack $\kappa\alpha_s + \alpha_g$ in terms of the values of α_g along the span.

The integrations in equations (A25), (A26), and (A27) may be performed with the first rows of the $[I']$ and $[II']$ matrices. Thus

$$\frac{C_{L_w}}{C_{L_{w_0}}} = \frac{\left[I'\right]_1\left[\frac{c}{c_r}\right]\left\{\kappa\alpha_s + \alpha_g\right\}}{\left[I'\right]_1\left[\frac{c}{c_r}\right]\left\{\alpha_g\right\}} \tag{A43}$$

$$\frac{C_B}{C_{B_0}} = \frac{\left[II'\right]_1\left[\frac{c}{c_r}\right]\left\{\kappa\alpha_s + \alpha_g\right\}}{\left[II'\right]_1\left[\frac{c}{c_r}\right]\left\{\alpha_g\right\}} \tag{A44}$$

and

$$\frac{C_T}{C_{T_0}} = \frac{\left[I'\right]_1\left[\left(\frac{c}{c_r}\right)^2\right]\left\{\kappa\alpha_s + \alpha_g\right\}}{\left[I'\right]\left[\left(\frac{c}{c_r}\right)^2\right]\left\{\alpha_g\right\}} \tag{A45}$$

The aeroelastic characteristics of uniform wings were calculated by both the direct method of the preceding section and the matrix method given in this section. The values of the divergence parameter q^*_D, calculated by the direct method, were found to be about 5 percent greater than the corresponding values calculated by the matrix method. This discrepancy can be shown to be almost entirely due to the rounding off of the loading of the wing tip in the matrix method. The differences between corresponding values of $\frac{\alpha_s}{\alpha_g}$, $\frac{C_{L_w}}{C_{L_{w_0}}}$, $\frac{C_B}{C_{B_0}}$, and $\frac{C_T}{C_{T_0}}$ are negligible.

Combination of Results

The forms of the approximate formulas used in combining the results of the many computations indicated in the analysis were obtained by considering a highly idealized semirigid wing; that is, a wing which is rigid along its entire span but can bend and twist at the wing root subject to the restraint of a bending and a torsion spring.

If it is assumed that the two spring constants correspond to $\frac{(GJ)_r}{s_t}$ and $\frac{(EI)_r}{s_t}$, the value of q^* at divergence is given by the simple formula

$$q^*_D = \frac{K_1}{1 - K_2 k} \tag{A46}$$

where the factors K_1 and K_2 depend on the taper ratio and the spanwise variation of the stiffness. As shown in reference 2, this formula serves as a good approximation to the calculated values of q^*_D.

For the semirigid wing, the ratio of α_s to α_g is found to be proportional to $\frac{q/q_D}{1 - \frac{q}{q_D}}$. In order to adapt this expression to the flexible wings considered in the present analysis, the following approximate expression was found to provide satisfactory correlation:

$$\frac{\alpha_s}{\alpha_{g_t}} = \frac{1}{\kappa} \frac{q/q_D}{1 - \frac{q}{q_D}} (f + F \, \Delta f) \tag{A47}$$

where f and Δf are functions of the spanwise coordinate s^* and the wing-chord and stiffness variations; F is a function of the parameter k and the wing-chord and stiffness variations. The functions f, Δf, and F also depend on the type of spanwise variation of the geometrical angle of attack, the subscripts 1 and 2 being used to differentiate between the two types of interest. The accuracy of equation (A47) is illustrated in figures 16 and 17.

If equation (A25) is used for the wing lift coefficient (with ξ replaced by s^*) and equation (A47) for the angle-of-attack distribution, the wing lift coefficient may be expressed as

$$C_{L_w} = \nu \frac{\frac{q}{q_D}}{1 - \frac{q}{q_D}} C_{L_{w_0}} + C_{L_{w_0}} \tag{A48}$$

or

$$\frac{C_{L_w}}{C_{L_{w_0}}} = \frac{1 - \frac{q}{q_D}(1 - \nu)}{1 - \frac{q}{q_D}} \tag{A49}$$

where the parameter

$$\nu \equiv \frac{\int_0^{s_t} \frac{c}{c_r}(f + F\,\Delta f)\,ds^*}{\int_0^{s_t} \frac{c}{c_r}\frac{\alpha_g}{\alpha_{g_t}}\,ds^*} \tag{A50}$$

so that ν and $\frac{C_{L_w}}{C_{L_{w_0}}}$ are functions of k and of the wing-chord and stiffness variations and depend on the type of geometrical angle-of-attack distribution as well.

As indicated by equation (A47), within the approximation inherent in that equation, the shape of the spanwise distribution of α_s does not vary with dynamic pressure. Therefore, to a good approximation, the lateral center of pressure of the lift due to α_s (as well as that due to α_g) does not change its position along the elastic axis when the dynamic pressure changes. The following approximate formula for the wing-root bending-moment coefficient may therefore be deduced from equation (A48):

$$C_B = \bar{s}_s{}^* \nu \frac{\frac{q}{q_D}}{1 - \frac{q}{q_D}} C_{L_{w_0}} + \bar{s}_g{}^* C_{L_{w_0}} \tag{A51}$$

where $\bar{s}_s^*$ and $\bar{s}_g^*$ are the dimensionless moment arms about the effective wing root of the lifts due to α_s and α_g and are defined by

$$\bar{s}_s^* = \frac{M_{r_s}}{\frac{1}{2} L_{w_s} s_t}$$

and

$$\bar{s}_g^* = \frac{M_{r_g}}{\frac{1}{2} L_{w_g} s_t}$$

Then,

$$\frac{C_B}{C_{B_0}} = \frac{1 - \frac{q}{q_D}(1 - \mu\nu)}{1 - \frac{q}{q_D}} \tag{A52}$$

where μ is defined by

$$\mu \equiv \frac{\bar{s}_s^*}{\bar{s}_g^*} \tag{A53}$$

so that $\frac{C_B}{C_{B_0}}$ is a function of the parameter k, of the taper ratio, and of the stiffness distributions; it also depends on the type of geometrical angle-of-attack distribution.

An approximate formula for the wing-root twisting-moment coefficient may be deduced from equation (A48) as follows:

$$C_T = \bar{e}_{l_s} \nu \frac{\frac{q}{q_D}}{1 - \frac{q}{q_D}} C_{L_{w_0}} + \bar{e}_{l_g} C_{L_{w_0}} \tag{A54}$$

where $\bar{e}_{l_s}$ and $\bar{e}_{l_g}$ are the effective dimensionless moment arms about the elastic axis of the lifts due to α_s and α_g and are defined by

$$\bar{e}_{l_s} = \frac{T_{r_s}}{\frac{1}{2} L_{w_s} c_r}$$

and

$$\bar{e}_{l_g} = \frac{T_{r_g}}{\frac{1}{2} L_{w_g} c_r}$$

Then

$$\frac{C_T}{C_{T_O}} = \frac{1 - \frac{q}{q_D}(1 - \nu\tau)}{1 - \frac{q}{q_D}} \tag{A55}$$

where

$$\tau \equiv \frac{\bar{e}_{l_s}}{\bar{e}_{l_g}} \tag{A56}$$

so that $\frac{C_T}{C_{T_O}}$ is a function of k, the taper ratio, and the stiffness distributions and also depends on the type of geometrical angle-of-attack distribution.

The values of ν, μ, and τ are given for the two types of geometrical angle-of-attack distributions in figures 9 and 11.

Figure 18 shows the approximate formulas (A49), (A52), and (A55) to be in good agreement with more accurately computed values.

The foregoing approximate formulas for the structural angle of attack and for the lift, bending-moment, and twisting-moment coefficients are not applicable to wings with zero taper ratio. An attempt was made to combine and systematize the results calculated for such wings in the manner employed for wings with other taper ratios, but the approximate formulas obtained in this way were found to yield unreliable results. Consequently they are not presented in this paper; instead, the results calculated for the wings with zero taper ratio are presented directly in figures 6, 8, 10, and 12.

APPENDIX B

STIFFNESS DISTRIBUTION OF CONSTANT-STRESS WINGS

Outline of Constant-Stress Concept

In order to calculate aeroelastic effects, the bending and torsional stiffnesses of the wing structure, EI and GJ, have to be known. These stiffnesses enter the calculations in two ways. The root stiffnesses, as indices of the over-all bending and torsional stiffnesses, constitute primary parameters which are required for use of the charts of this paper, but were not required in the preparation of the charts. On the other hand, the stiffness distributions, that is, the ratios of the local stiffnesses along the span to the root stiffnesses, are secondary parameters which are not required for use of the charts but did have to be assumed in order to prepare them.

In calculations preliminary to the actual design of the structure, the bending and torsional stiffnesses of the structure are not known; they must be estimated on the basis of either past experience or considerations of an idealized structure. For the purpose of estimating stiffness distributions, past experience with similar structures is likely to be a useful guide in any specific case but does not lend itself to generalization and hence to the preparation of generally applicable charts. The stiffness distributions (other than those which vary as the fourth power of the chord) used to prepare the charts of this paper have been obtained from considerations of an idealized structure, as outlined in this appendix.

Basically, the method of this appendix consists in an effort to relate the stiffness of a wing to its strength and to estimate that strength on the basis of certain assumptions. The fundamental assumptions are that the bending and torsional stresses are constant along the span and that the applied loading is proportional to the local chord. The other assumptions concern the bending and torsional stresses caused by this load and their relation to their allowable values. In estimating these stresses the structure is assumed to be of the thin-skin, stringer-reinforced shell type. Certain effectiveness factors are used; for instance, the ratio of the allowable torsional stress to the allowable bending stress, or the ratio of the cross-sectional area of the effective torsion cell to the product of the chord and the wing thickness. The root stiffnesses estimated by the method of this appendix depend directly on the values of these ratios. The stiffness distributions, on the other hand, are largely independent of these ratios but imply the assumption that the ratios are approximately constant along the span. Consequently, the constant-stress concept used in this appendix is more likely to furnish useful results

for stiffness distributions than for the root stiffnesses, and, because of the type of structure assumed, the concept is not applicable to very thin wings.

Assumed Applied Loads

If the applied normal load is distributed in a manner proportional to the chord, that is, if

$$l = Kc \tag{B1}$$

the bending moment at any point on the span can be obtained by integrating the chord distribution as follows:

$$M = K\left(\frac{b'/2}{\cos \Lambda}\right)^2 \int_{s^*}^{1} \int_{s^*}^{1} c \, ds^* \, ds^*$$

where s^* is the dimensionless distance along the reference axis measured from the effective root. Similarly, the total normal load on one wing is given by

$$P = K \frac{b'/2}{\cos \Lambda} \int_{0}^{1} c \, ds^*$$

If the wing is linearly tapered, so that

$$c = c_r\left[1 - (1 - \lambda)s^*\right] \tag{B2}$$

where the taper ratio λ is defined by

$$\lambda = \frac{c_t}{c_r}$$

then the ratio of the bending moment at any point of the span to the product of the total normal load and the wing semispan less one-half of the fuselage width can be expressed as follows:

$$\frac{M}{P \frac{b'/2}{\cos \Lambda}} = f_6(s^*, \lambda) \tag{B3}$$

where the function f_6 of s^* and λ is defined by

$$f_6 \equiv \frac{1}{3}\left(\frac{1 + 2\lambda}{1 + \lambda} - \frac{1 - \lambda}{1 + \lambda} s^*\right)(1 - s^*)^2 \tag{B4}$$

and shown in figure 19.

Similarly, if the moment arm of the normal load applied to the wing at any station is also proportional to the chord, the constant of proportionality being e_1, the distributed torque at any station is then $e_1 c l$, and the accumulated torque is

$$T = e_1 K \frac{b'/2}{\cos \Lambda} \int_{s^*}^{1} c^2 ds^* \tag{B5}$$

which may, in turn, be expressed as

$$\frac{T}{e_1 \bar{c} P} = f_7(s^*, \lambda) \tag{B6}$$

where the function f_7 of s^* and λ is defined by

$$f_7 \equiv \frac{4}{3}\left[\frac{1 + \lambda + \lambda^2}{(1 + \lambda)^2} - \frac{(2 + \lambda)(1 - \lambda)}{(1 + \lambda)^2} s^* + \frac{(1 - \lambda)^2}{(1 + \lambda)^2} s^{*2}\right](1 - s^*) \tag{B7}$$

and the average chord $\bar{c}$ is defined by

$$\bar{c} \equiv \frac{c_r + c_t}{2} \tag{B8}$$

The function f_7 is also shown in figure 20.

The total normal load on one wing, P, can be estimated from the design gross weight and the design load factor of the airplane in the following manner:

$$P = \frac{1}{2}\left(L_w - nW_w\right) \tag{B9}$$

If the fraction of the wing lift to the total lift carried by the airplane (including that of the fuselage and tail) is designated by η_1, so that

$$\eta_1 = \frac{L_w}{L_{Total}}$$

and the fraction of the wing weight (including the amount of fuel, external stores, and so on used in the critical design condition) to the total design gross weight is designated by η_2,

$$\eta_2 = \frac{W_w}{W}$$

then equation (B9) may be written as

$$P = \frac{1}{2} \eta_3 nW \tag{B10}$$

where

$$\eta_3 = \eta_1 - \eta_2$$

With the value of P given by equation (B10), equations (B3) and (B6) serve to express the local bending and torsional moments in terms of known design parameters.

Effective Skin Thickness Required to Resist Applied Loads

The wing structure has to resist both the applied bending moments and the applied torques; in other words, the load-carrying members must resist combined axial and shear stresses. A relation commonly used in the design of wing structures loaded by compressive and shear stresses due to bending and torsion moments is

$$\frac{f_b}{F_B} + \left(\frac{f_t}{F_T}\right)^2 = 1$$

where f_b is the applied bending stress, f_t the applied shear stress, F_B the allowable (compressive) bending stress, and F_T the allowable shear stress. However, a somewhat conservative relation,

$$\frac{f_b}{F_B} + \frac{f_t}{F_T} = 1 \tag{B11}$$

is much more convenient for the present purpose and, consequently, is used as the basis of the following development. If the margin of safety is not zero, equation (B11) can be rewritten as

$$\frac{f_b}{F_B} + \frac{f_t}{F_T} = \eta_4 \tag{B12}$$

where η_4 is an effectiveness factor which can be expressed in terms of the margin of safety (M.S.) as

$$\eta_4 = \frac{1}{1 + \text{M.S.}} \tag{B13}$$

The applied bending stress is

$$f_b = \frac{Mz}{I} \tag{B14}$$

where z is the maximum ordinate on the compression side measured from and normal to the chordwise principal axis. Similarly, the applied shear stress is

$$f_t = \frac{T}{2\bar{A}t} \tag{B15}$$

where $\bar{A}$ is the cross-sectional area of the (assumed) single torsion cell, and t is the skin thickness on the compression side. Substitution of equations (B14) and (B15) into equation (B12) yields

$$\frac{Mz}{IF_B}\left(1 + \frac{T}{M}\frac{F_B}{F_T}\frac{I}{2\bar{A}tz}\right) = \eta_4 \tag{B16}$$

In order to relate the bending and torsion stiffness of the wing to the skin thickness t or to an equivalent thickness t_e which includes the material in the stringers and spar flanges, the bending stress is assumed to be carried by a box covered with sheet of an effective thickness t_e, the webs are assumed to carry no bending stress, and the torsion stress is assumed to be resisted by an equivalent single cell, the two webs of which contain all the material of the actual webs. The torsion and bending moments of inertia may then be written as

$$J = 4\frac{\bar{A}^2 t}{\bar{p}}$$

$$= 2\frac{\eta_6 \eta_7^2}{\eta_8 \eta_9} ch^2 t_e \qquad \text{(B17)}$$

and

$$I = \eta_{10} c t_e \left[\eta_5^2 \left(\frac{h}{2}\right)^2 \eta_{11}^2 + \eta_{12}\eta_{13}^2 \eta_{14}^2 \left(\frac{h}{2}\right)^2\right]$$

$$= \eta_{15} c \left(\frac{h}{2}\right)^2 t_e \qquad \text{(B18)}$$

where the effectiveness factors η_5 to η_{15} are defined in table 1. In the factor η_9, the effective perimeter $\bar{p}$ of the torsion cell is the sum of the lengths of skin around the perimeter, each weighted by the ratio of the thickness of the critically stressed element to the thickness of the given length of skin.

When the value of I given by equation (B18) is substituted into equation (B16), equation (B16) may be written as

$$t_e = \frac{Mz}{F_B \eta_4 \eta_{15} c \left(\frac{h}{2}\right)^2}\left[1 + \frac{T}{M}\frac{F_B}{F_T}\frac{\eta_{15} c \left(\frac{h}{2}\right)^2}{2\bar{A}z\eta_6}\right] \qquad \text{(B19)}$$

By making use of equations (B3), (B5), and (B10), as well as the effectiveness factors η_{16} to η_{19} defined in table 1, equation (B19) can be written as

$$t_e = \frac{\eta_3\eta_5}{\eta_4\eta_{15}} \frac{nW}{F_B} \frac{b'/2}{c^2\cos\Lambda} \frac{f_6}{h/c}\left(1 + \frac{\eta_{19}e_1}{A_\Lambda} \frac{1}{f_8}\right) \tag{B20}$$

The factor f_8 is defined in terms of the factors f_6 and f_7 given by equations (B4) and (B7) as

$$f_8 = \frac{1}{2} \frac{f_6}{f_7} \tag{B21}$$

The function f_8 is shown in figure 21.

Bending and Torsional Stiffnesses

Substitution of the value of t_e given by equation (B20) into equation (B18) yields an expression for the bending moment of inertia I or for the bending stiffness EI at any point along the span. The value of this stiffness at any point on the span may be divided by the stiffness $(EI)_r$ at the wing root. This ratio can then be expressed as

$$\frac{EI}{(EI)_r} = \frac{h}{h_r} \frac{f_6}{f_{6_r}} \frac{f_8}{f_{8_r}} \frac{f_8 + \frac{\eta_{19}e_1}{A_\Lambda}}{f_{8_r} + \frac{\eta_{19}e_1}{A_\Lambda}}$$

$$= \frac{h/c}{(h/c)_r} f_9\left(s^*, \lambda, \frac{\eta_{19}e_1}{A_\Lambda}\right) \tag{B22}$$

where

$$f_9 = \frac{c}{c_r} \frac{f_7}{f_{7r}} \frac{f_8 + \frac{\eta_{19}e_1}{A_\Lambda}}{f_{8_r} + \frac{\eta_{19}e_1}{A_\Lambda}} \tag{B23}$$

The function f_9 is plotted in figure 22. The value $(EI)_r$ may be obtained from equations (B18) and (B20) as

$$(EI)_r = \eta_{20} \frac{E}{F_B} \frac{nW}{S} c_r{}^4 A_\Lambda{}^2 \left(\frac{h}{c}\right)_r F_r\left(\lambda, \frac{\eta_{19} e_1}{A_\Lambda}\right) \tag{B24}$$

where

$$F_r = \frac{(1+\lambda)^3}{64} \frac{f_{6_r}}{f_{8_r}} \left(f_{8_r} + \frac{\eta_{19} e_1}{A_\Lambda}\right) \tag{B25}$$

The function F_r is shown in figure 3 as a function of λ, with $\frac{\eta_{19} e_1}{A_\Lambda}$ as the parameter.

Similarly the torsional stiffness GJ may be obtained by substituting the value of t_e given by equation (B20) into equation (B17). However, from equations (B17) and (B18) the ratio of the torsional stiffness to the bending stiffness may be obtained in the form

$$\frac{GJ}{EI} = 8 \frac{G}{E} \frac{\eta_6 \eta_7{}^2}{\eta_8 \eta_9 \eta_{15}} \tag{B26}$$

This equation shows that the ratio GJ/EI is constant along the span within the framework of the constant-stress concept. Equation (B26) may, therefore, be interpreted as an expression for the value GJ/EI at the wing root, that is, for the value $(GJ)_r/(EI)_r$. The torsional stiffness at any other point on the span can then be obtained from equation (B22), since

$$\frac{GJ}{(GJ)_r} = \frac{EI}{(EI)_r} \tag{B27}$$

because GJ/EI is constant over the span.

The stiffness ratios $GJ/(GJ)_r$ and $EI/(EI)_r$ can be obtained directly from figure 22 when the thickness ratio h/c of the wing is constant along the span; if the thickness ratio is not constant the factor f_9 obtained from figure 22 must be multiplied by the ratio $\frac{h/c}{(h/c)_r}$ at any station to obtain the stiffness ratio at that station. As may be seen from figure 22, the function f_9 does not vary much with the parameter $\frac{\eta_{19} e_1}{A_\Lambda}$; this parameter represents the additional amount of

skin thickness required to carry the torque (see equations (B19) and (B20)), and this additional thickness is small for most conventional wing structures. Consequently, an average value of $\frac{\eta_{19} e_1}{A_\Lambda} = 0.03$ was used to obtain the stiffness distributions used in the aeroelastic calculations on which the charts of this paper are based.

Equation (B22) shows that, once a value has been assumed for the term $\frac{\eta_{19} e_1}{A_\Lambda}$, the stiffness ratios $EI/(EI)_r$ and $GJ/(GJ)_r$ are independent of the effectiveness factors used in this analysis. Therefore, specific values of these parameters need not be known in order to estimate the stiffness distributions, but one of the assumptions on which equation (B22) is based is that whatever values the effectiveness factors have are nearly constant along the span. In order to estimate the value of $(EI)_r$, however, these factors must be known, since they enter directly into equation (B24). The estimate of $(EI)_r$ obtained in this manner is, therefore, subject to all the limitations imposed by the approximations of the constant-stress concept. Hence, some judgement must be exercised in using this estimate, and, if possible, it should be modified in the light of experience.

Structural Weight Associated with the Stiffness Distribution

The increase in structural weight associated with a given increase in stiffness can be estimated on the basis of assumptions similar to those made in relating the stiffness and the strength. For the purpose of this analysis the various components of the wing structure, exclusive of the carry-through structure within the fuselage, are classified in two groups, one which contains the elements that take the bending and torsional loads due to the assumed loading and one which contains all other components. In the first group are:

(1) The amount of top and bottom skin that is used in the estimation of the thicknesses required to withstand the bending and torsional loads, including stringers and spar flanges included in the equivalent skin

(2) Webs, including any web stiffeners

In the second group are:

(1) Skin, stiffeners, false spars, and so on, which are not considered in the estimation of the equivalent thicknesses

(2) Ribs, bulkheads, and posts designed to raise the buckling strength of the cover sheets

(3) Control surfaces and their supports, attachments, and actuating mechanisms

(4) The supports of internal stores

This analysis is concerned only with the first group and, more specifically, with the relative increase in the weight of this group occasioned by an increase in stiffness of the main structure. Means of estimating the actual magnitude of the weights involved and of estimating the weights of the items in the second group as well are given in references 7 and 8.

The weight per unit length of the structural elements of the first group can be written as

$$w_s = 2\eta_8\eta_{21}\gamma_s c t_e \qquad \text{(B28)}$$

where γ_s is the density of the material of the primary structure (or an equivalent density in the case of sandwich construction), η_{21} is the ratio of an equivalent perimeter $\bar{\bar{p}}$ to the actual perimeter of the cell, and $\bar{\bar{p}}$ is the sum of all the lengths which constitute the perimeter, each multiplied by the ratio of its equivalent thickness to the equivalent thickness t_e of the upper cover sheet.

In view of the assumption made concerning the combination of bending and torsional stresses, the thickness t_e required in equation (B28) can be obtained from equation (B18) as

$$t_e = \frac{4I}{\eta_{15} c h^2}$$

so that

$$w_s = 8\gamma_s \frac{\eta_8\eta_{21}}{\eta_{15}} \frac{I}{h^2}$$

or

$$\frac{w_s}{w_{s_r}} = \frac{I/I_r}{(h/h_r)^2} \qquad \text{(B29)}$$

Consequently, the total weight (for both wings) of the structural elements of the first group can be estimated from the relation

$$\frac{W_s/2}{w_{s_r}\frac{b'/2}{\cos\Lambda}} = \int_0^1 \frac{I/I_r}{(h/h_r)^2}\,ds^* \tag{B30}$$

Equation (B30) serves to estimate relative changes in the weight of the first group of structural elements. For instance, with a given distribution of I and h, that weight is directly proportional to I_r and inversely proportional to h_r^2. Similarly, given two different distributions of I_r and h_r with the same values at the root, the ratio of the weights is equal to the ratio of the two values obtained by using the respective distributions of I and h in the integral of equation (B30).

Although the actual value of W_s is not relevant to this discussion, it may be estimated by substituting the previously calculated stiffness distributions into equation (B30), and the result is given here as a matter of general interest:

$$W_s = 2\,\frac{\eta_3\eta_5\eta_8\eta_{21}}{\eta_4\eta_{15}\eta_{18}}\,\frac{\gamma_s}{F_B}\,\frac{nW}{\frac{h_r}{c_r}}\,A_\Lambda\,\frac{b'/2}{\cos\Lambda}\,F_w \tag{B31}$$

where

$$F_w = \frac{32}{(1+\lambda)^2}\,F_r\int_0^1 \frac{I/I_r}{(h/h_r)^2}\,ds^* \tag{B32}$$

According to equation (B31), the structural weight is directly proportional to the design gross weight, load factor, swept-span aspect ratio, span, and density of the material of the primary structure and inversely proportional to the allowable stress and the wing thickness ratio. The dependence of the weight on the taper ratio (all other parameters, notably the aspect ratio and span, are the same) is illustrated in figure 14 by a plot of the function F_w against taper ratio for several values of the parameter $\frac{\eta_{19}e_1}{A_\Lambda}$ and of the ratio of the wing thickness ratios at the tip and at the root.

REFERENCES

1. Diederich, Franklin W.: Calculation of the Aerodynamic Loading of Swept and Unswept Flexible Wings of Arbitrary Stiffness. NACA Rep. 1000, 1950.

2. Diederich, Franklin W., and Budiansky, Bernard: Divergence of Swept Wings. NACA TN 1680, 1948.

3. Diederich, Franklin W.: A Plan-Form Parameter for Correlating Certain Aerodynamic Characteristics of Swept Wings. NACA TN 2335, 1951.

4. Zender, George, and Libove, Charles: Stress and Distortion Measurements in a 45° Swept Box Beam Subjected to Bending and to Torsion. NACA TN 1525, 1948.

5. Heldenfels, Richard R., Zender, George W., and Libove, Charles: Stress and Distortion Analysis of a Swept Box Beam Having Bulkheads Perpendicular to the Spars. NACA TN 2232, 1950.

6. Weissinger, J.: The Lift Distribution of Swept-Back Wings. NACA TM 1120, 1947.

7. Micks, W. R.: Structural Weight Analysis. Wing Weight Equations. U. S. Air Force Project RAND Rep. R-198, The RAND Corp., Dec. 1950.

8. Solvey, J.: Structural Efficiency of Wings. Rep. ACA-44, Aero. Res. Consultative Committee, Dept. Supply, Commonwealth of Australia, March 1949.

TABLE 1

DEFINITIONS OF THE FACTORS η_1 TO η_{21}

$\eta_1 = \dfrac{L_w}{L_{Total}}$

$\eta_2 = \dfrac{W_w}{W}$

$\eta_3 = \eta_1 - \eta_2$

$\eta_4 = \dfrac{1}{1 + \text{Margin of safety}}$

$\eta_5 = \dfrac{\text{Ordinate of most highly stressed element}}{\text{One-half of wing thickness}}$

$\eta_6 = \dfrac{\text{Actual skin thickness of most highly stressed element}}{\text{Equivalent skin thickness of most highly stressed element}}$

$\eta_7 = \dfrac{\text{Cross-sectional area of torsion cell}}{\text{Chord} \times \text{Wing thickness}}$

$\eta_8 = \dfrac{\text{Perimeter of torsion cell}}{\text{Twice the chord}}$

$\eta_9 = \dfrac{\text{Effective perimeter } \bar{p} \text{ of torsion cell}}{\text{Actual perimeter of torsion cell}}$

$\eta_{10} = \dfrac{\text{Width of equivalent sheet}}{\text{Chord}}$

$\eta_{11} = \dfrac{\text{Average ordinate of upper skin}}{\text{Maximum ordinate of upper skin}}$

$\eta_{12} = \dfrac{\text{Equivalent thickness of lower skin}}{\text{Equivalent thickness of upper skin}}$

$\eta_{13} = \dfrac{\text{Maximum ordinate of lower skin}}{\text{One-half of wing thickness}}$

$\eta_{14} = \dfrac{\text{Average ordinate of lower skin}}{\text{Maximum ordinate of lower skin}}$

$\eta_{15} = \eta_{10}\left(\eta_5^2\eta_{11}^2 + \eta_{12}\eta_{13}^2\eta_{14}^2\right)$

$\eta_{16} = \dfrac{\text{Allowable torsion stress}}{\text{Allowable bending stress}}$

$\eta_{17} = \dfrac{\bar{c}b'}{S \cos \Lambda}$

$\eta_{18} = \eta_{17}\left(\dfrac{b}{b'}\right)^2$

$\eta_{19} = \dfrac{1}{4}\dfrac{\eta_{15}\eta_{18}}{\eta_5\eta_6\eta_7\eta_{16}}$

$\eta_{20} = \dfrac{\eta_3\eta_5}{\eta_4\eta_{17}\eta_{18}^2}$

$\eta_{21} = \dfrac{\text{Equivalent perimeter } \bar{\bar{p}} \text{ of torsion cell}}{\text{Actual perimeter of torsion cell}}$

TABLE 2

VALUES OF THE COEFFICIENTS K_1 AND K_2

Taper ratio λ	GJ and EI	$\frac{(h/c)_t}{(h/c)_r}$	K_1		K_2	
			By matrix integration	By analytic integration (reference 2)	By matrix integration	By analytic integration (reference 2)
1.0	Vary as c^4	1.0	2.58	2.47	0.381	0.390
.5		1.0	2.83	2.74	.480	.497
.2		1.0	2.92	2.81	.590	.614
0		1.0	1.45	2.25	.620	-----
1.0	Given by constant-stress criterion	1.0	.795	----	.252	-----
.5		1.0	1.287	----	.357	-----
.2		1.0	1.830	----	.480	-----
0		1.0	1.440	----	.626	-----
.5		.5	.928	----	.310	-----
.5	Increased beyond values required by constant-stress criterion	1.0	1.700	----	.398	-----

TABLE 3.- PARAMETERS OF WING USED IN ILLUSTRATIVE EXAMPLE

Geometrical parameters	
A	4
Λ, deg	37.5
S, sq in.	37,498
b, in.	387.4
w/2, in.	20.0
b'/2, in.	173.7
c_r, in.	102.8
c_t, in.	54.2
λ	0.527
c_{MAC}, in.	100.4

Structural parameters	
e	0.444
$(GJ)_r$, lb/sq in.	8.94×10^9
$(EI)_r$, lb/sq in.	9.56×10^9
$GJ/(GJ)_r$	$\approx (c/c_r)^4$
$EI/(EI)_r$	$\approx (c/c_r)^4$
Δs^{Φ}, in.	0
Δs^{Γ}, in.	-5.6
Δs, in.	-3.0
$s_t \left(= \frac{b'/2}{\cos \Lambda} + \Delta s\right)$, in.	215.9

Aerodynamic parameters		
	Subsonic (M < 0.65)	Supersonic (M = 1.5)
a	0.25	0.425
e_1	0.194	0.019
$C_{l_{\alpha_e}}$	2.78	4.92
κ	0.78	1.00

Aeroelastic parameters		
	Subsonic (M < 0.65)	Supersonic (M = 1.5)
k	7.76	79.0
K_1	2.82	2.82
K_2	0.474	0.474
q^*_D	-1.053	-0.0774
q_D, lb/sq ft	-6400	-2700
f_1	Fig. 5(c)	Fig. 5(c)
Δf_1	Fig. 5(c)	Fig. 5(c)
F_1	-0.27	-0.02
ν_1	0.655	0.662
μ_1	1.303	1.333
$\frac{C_{l_w}}{C_{l_{w_0}}}$	$\frac{1 - 0.345\frac{q}{q_D}}{1 - \frac{q}{q_D}}$	$\frac{1 - 0.338\frac{q}{q_D}}{1 - \frac{q}{q_D}}$
$\frac{\bar{s}}{\bar{s}_0}$	$\frac{1 - 0.146\frac{q}{q_D}}{1 - 0.345\frac{q}{q_D}}$	$\frac{1 - 0.118\frac{q}{q_D}}{1 - 0.338\frac{q}{q_D}}$

NACA

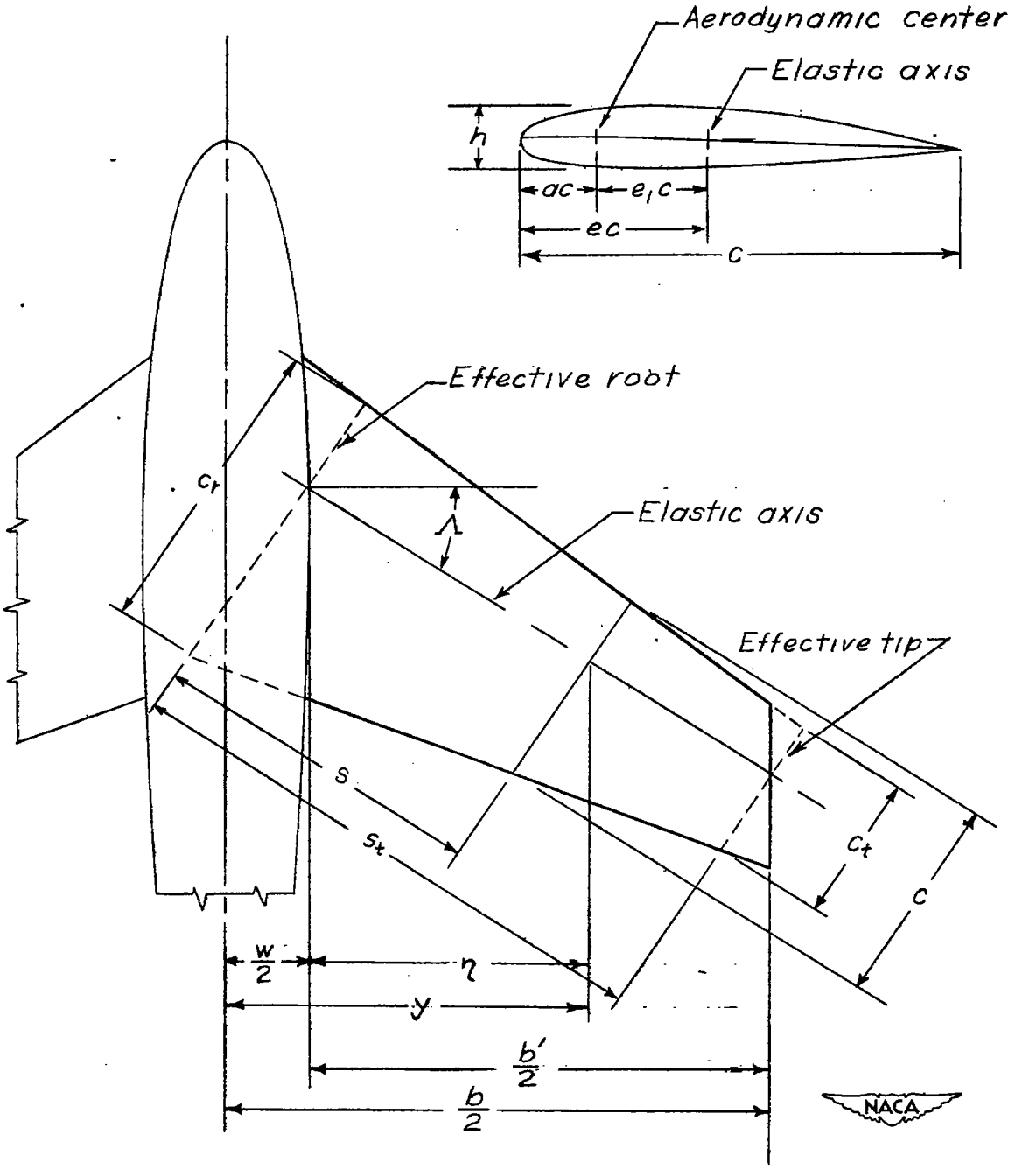

Figure 1.- Definitions of geometric parameters.

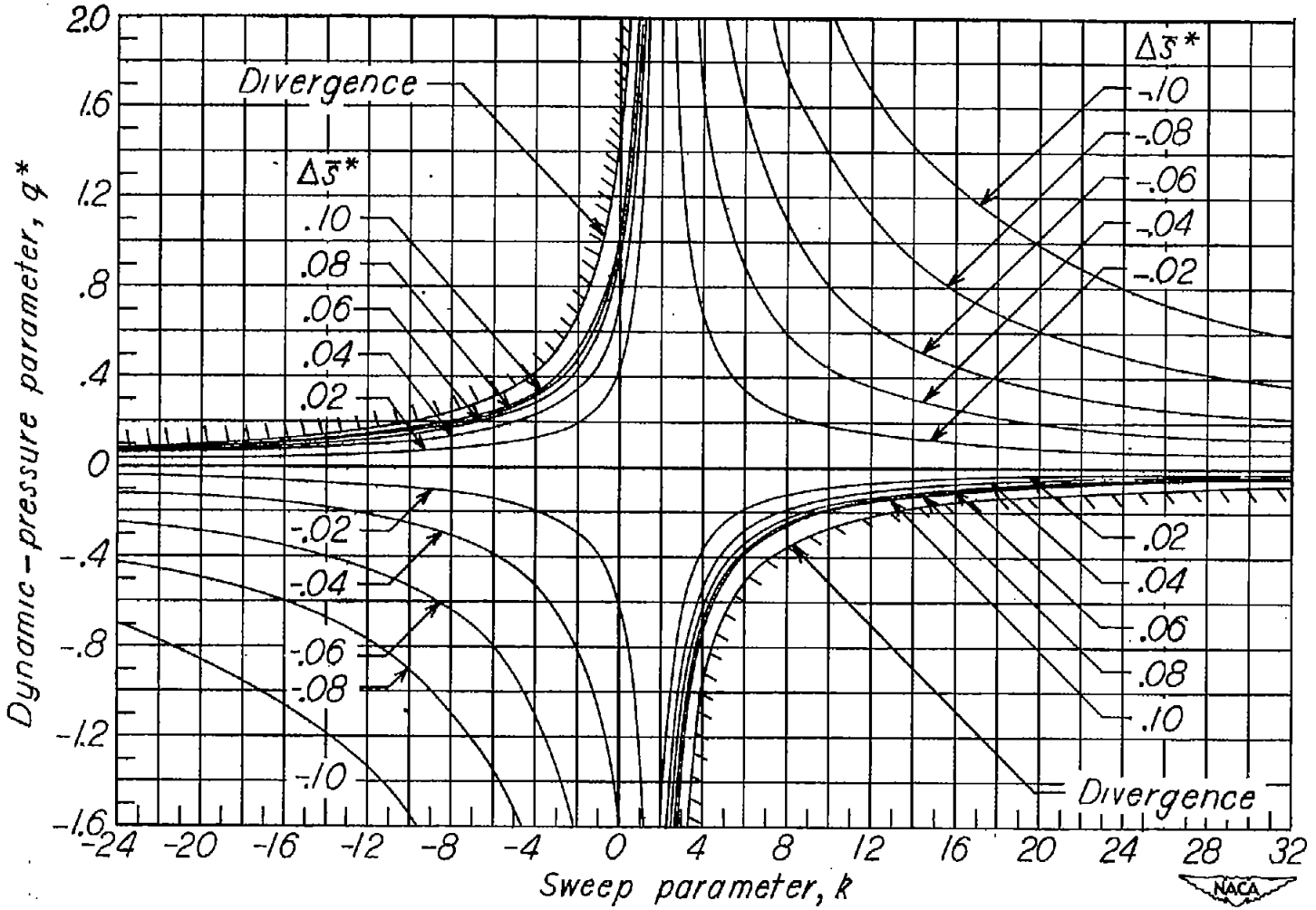

(a) Wings of taper ratio 0.

Figure 2.- Charts for a preliminary survey of aeroelastic phenomena.

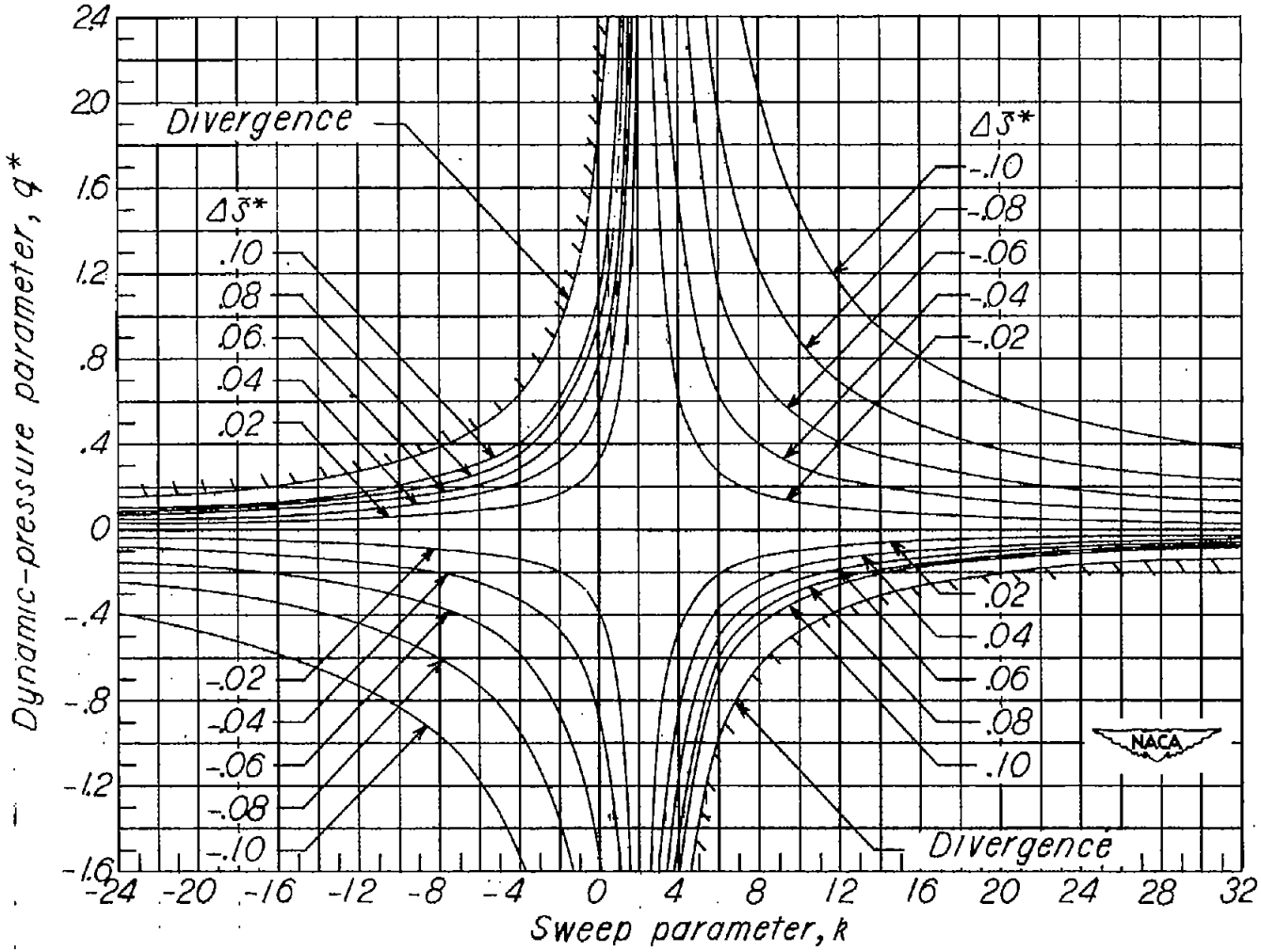

(b) Wings of taper ratio 0.2.

Figure 2.- Continued.

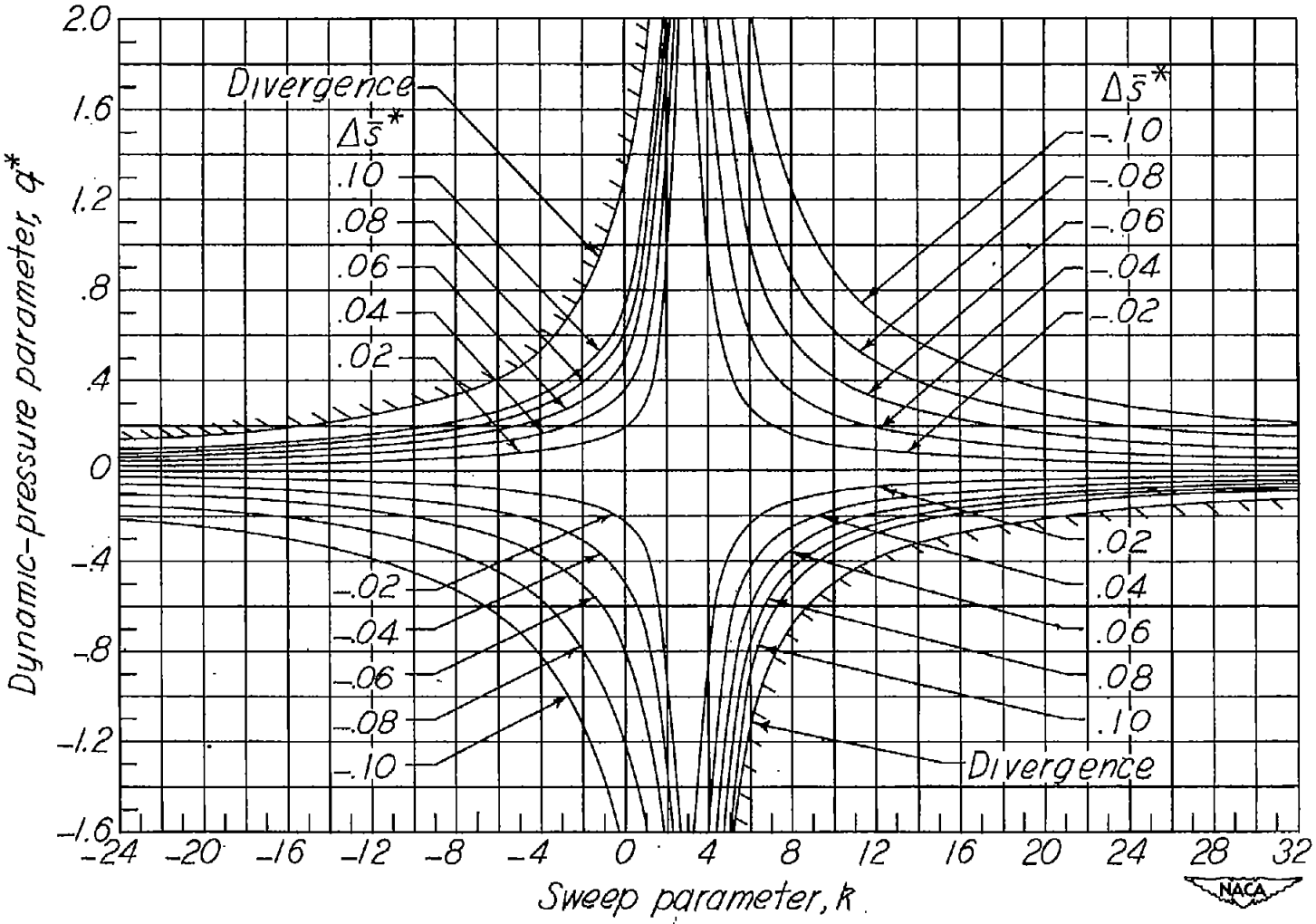

(c) Wings of taper ratio 0.5.

Figure 2.- Continued.

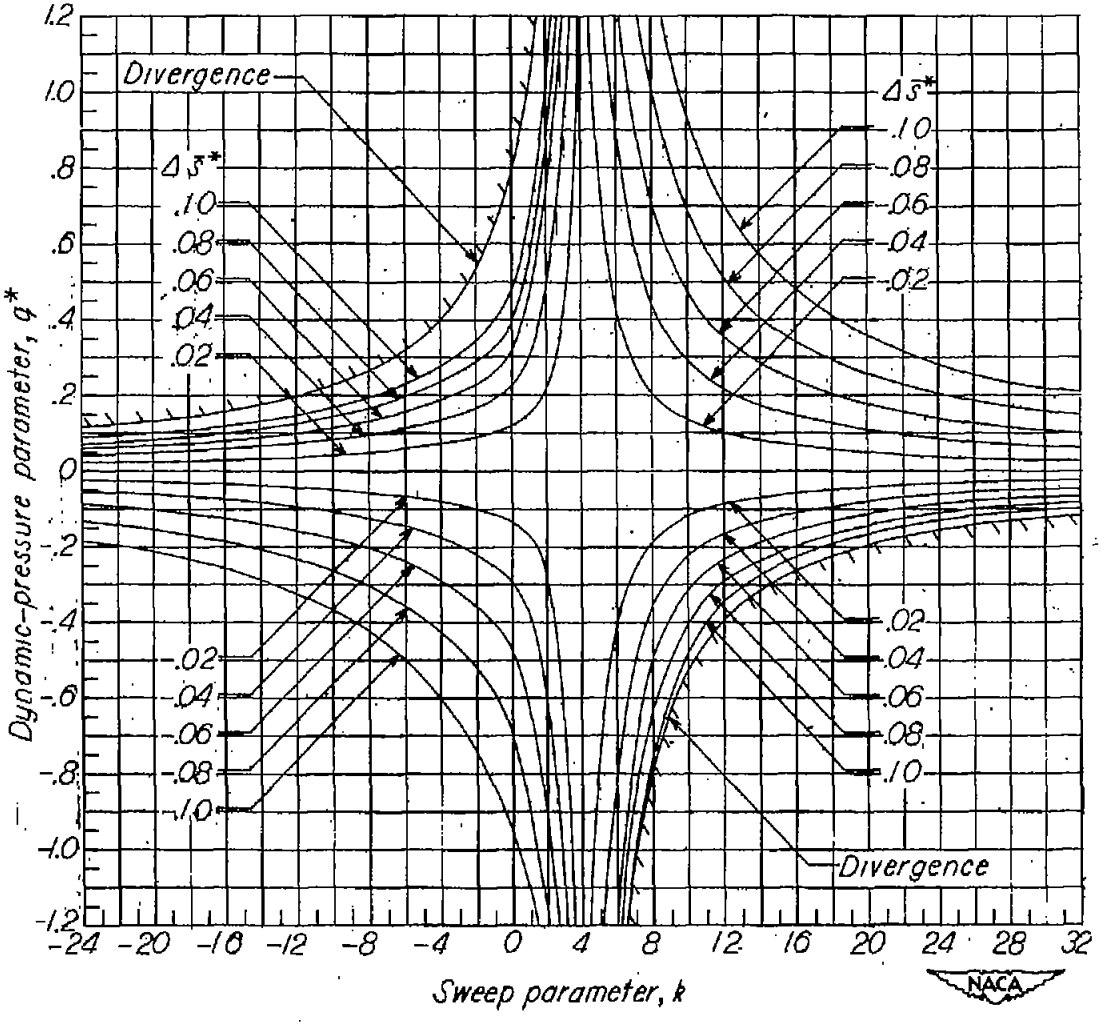

(d) Wings of taper ratio 1.0.

Figure 2.- Continued.

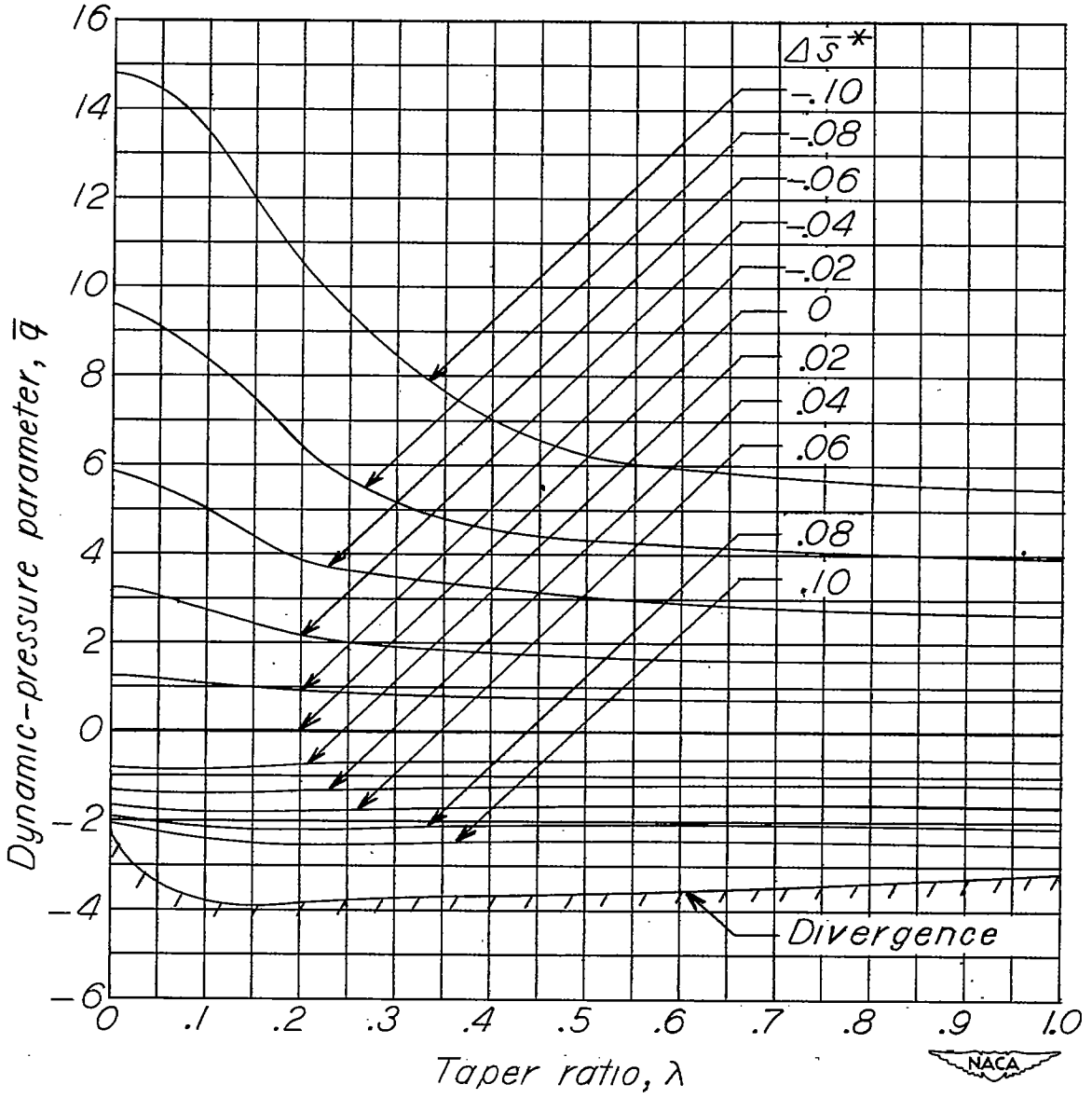

(e) Wings with moment arm $e_1 = 0$ (or $|k| > 25$).

Figure 2.- Concluded.

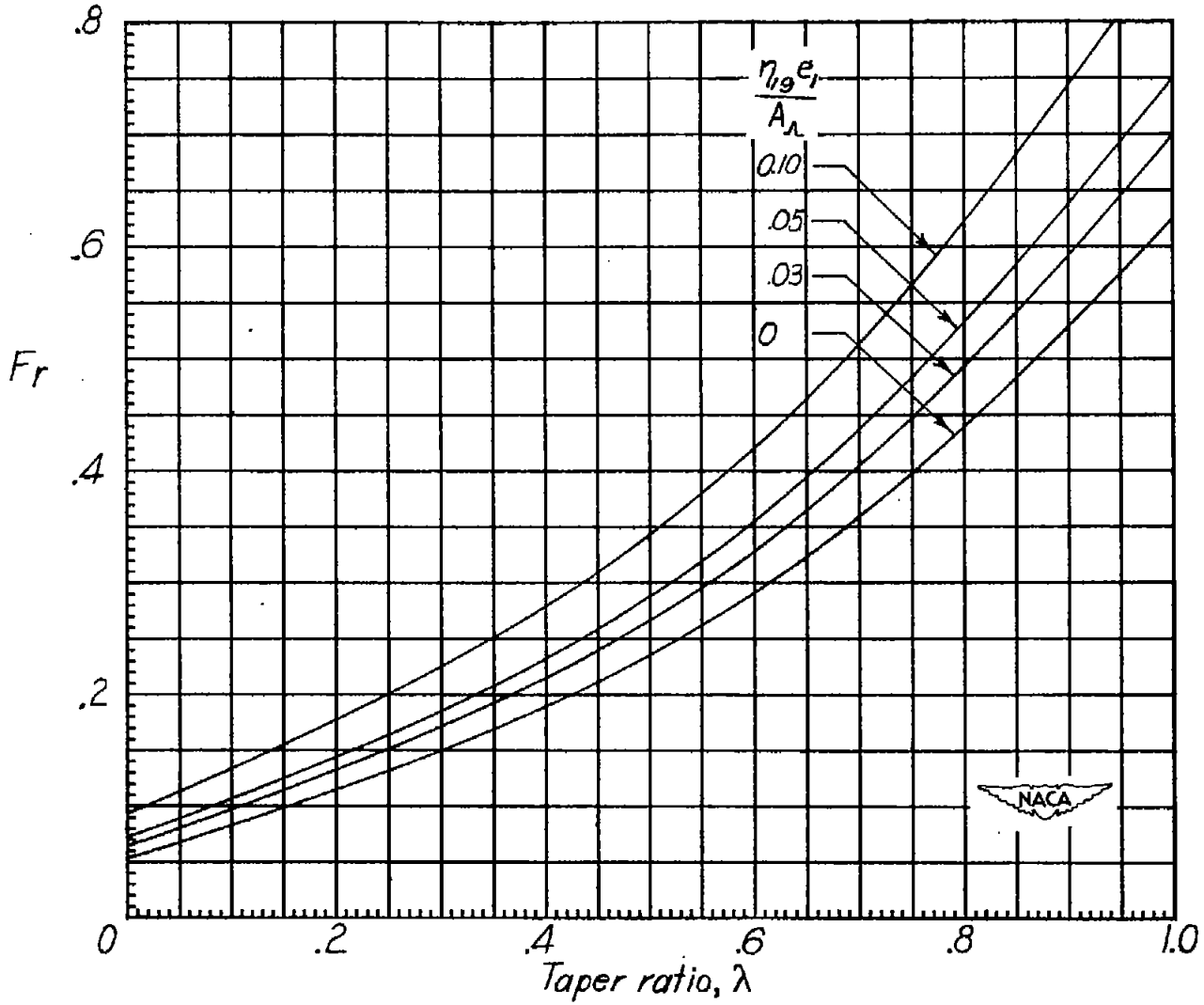

Figure 3.- The root-stiffness function F_r.

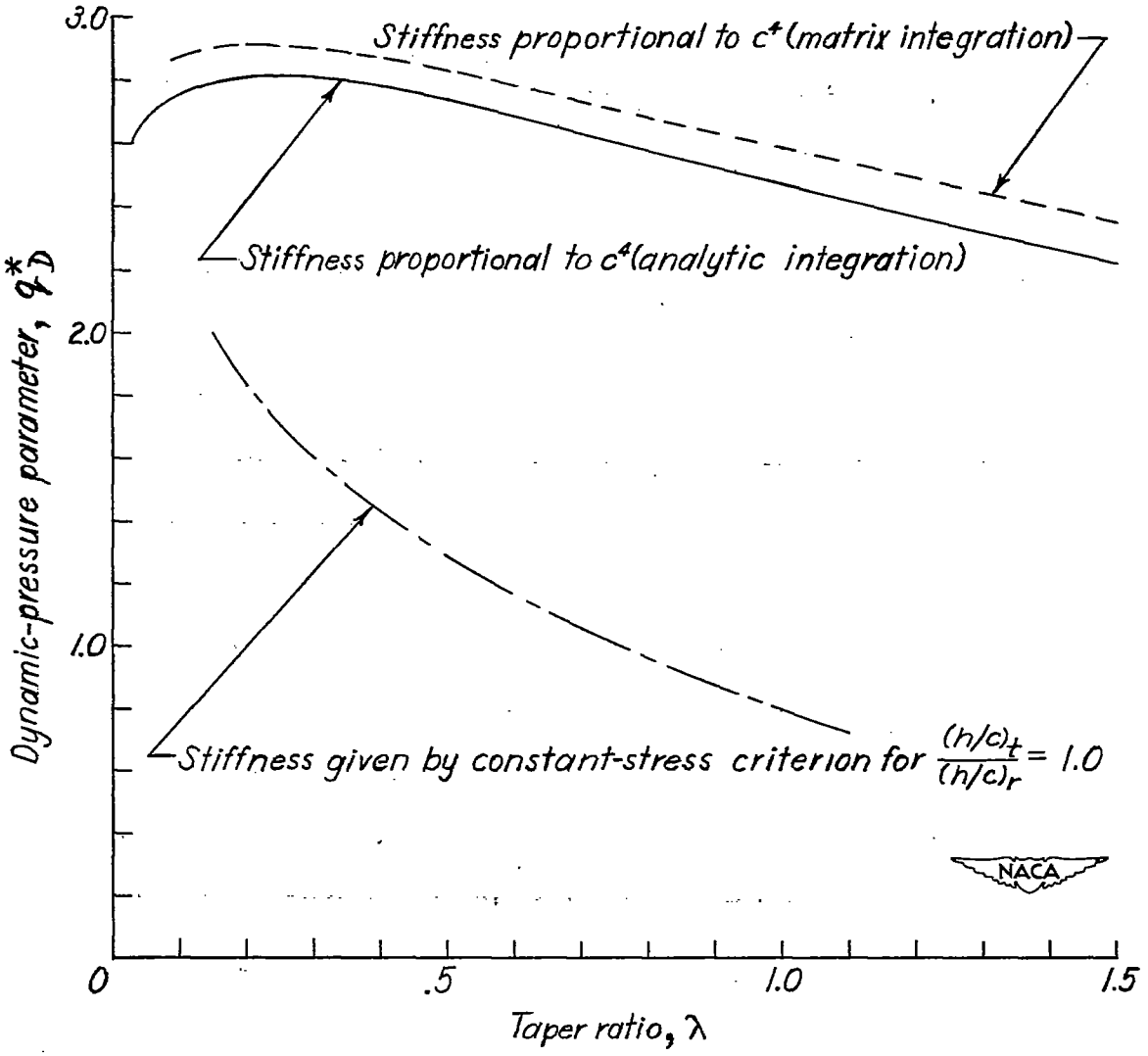

(a) Effect of taper ratio on q^*_D for unswept wings. ($q^*_D = K_1$ in this case.)

Figure 4.- Effect of taper ratio on the dynamic pressure at divergence.

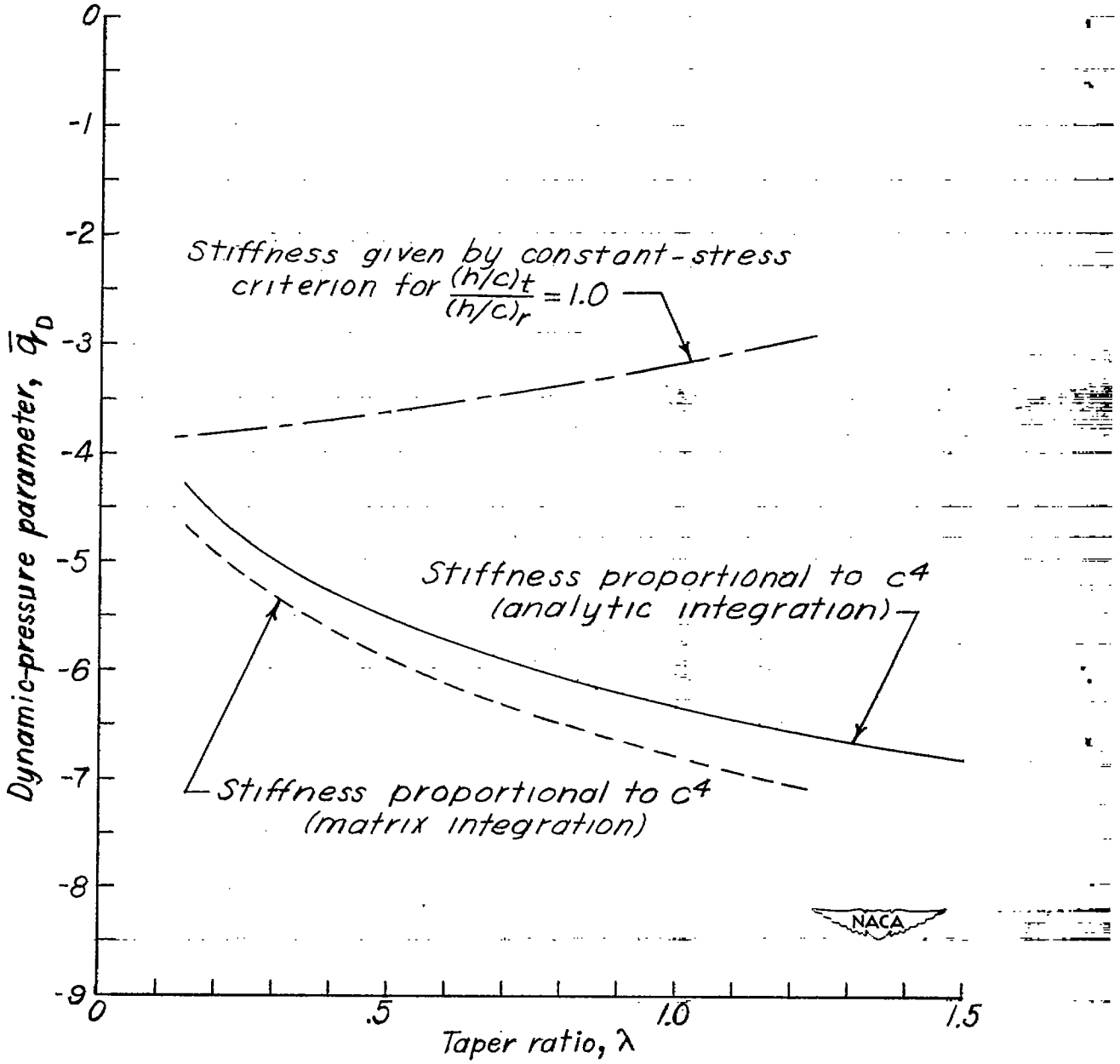

(b) Effect of taper ratio on $\bar{q}_D$ for $e_1 = 0$. $\left(\bar{q}_D = -\frac{K_1}{K_2} \text{ in this case.}\right)$

Figure 4.- Concluded.

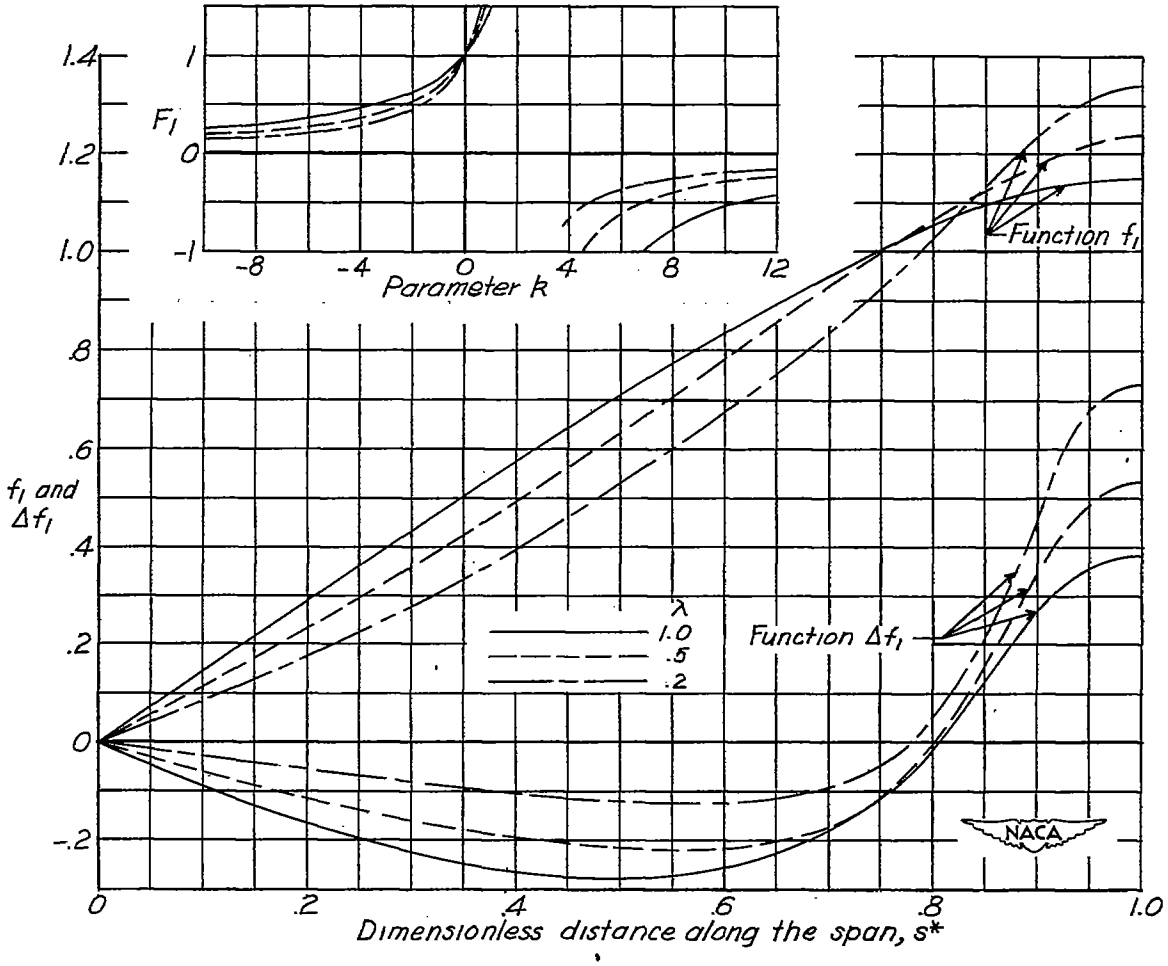

(a) Stiffnesses given by constant-stress criterion for $\frac{(h/c)_t}{(h/c)_r} = 1.0$.

Figure 5.- The angle-of-attack distribution functions f_1, Δf_1, and F_1 for constant geometric angles of attack.

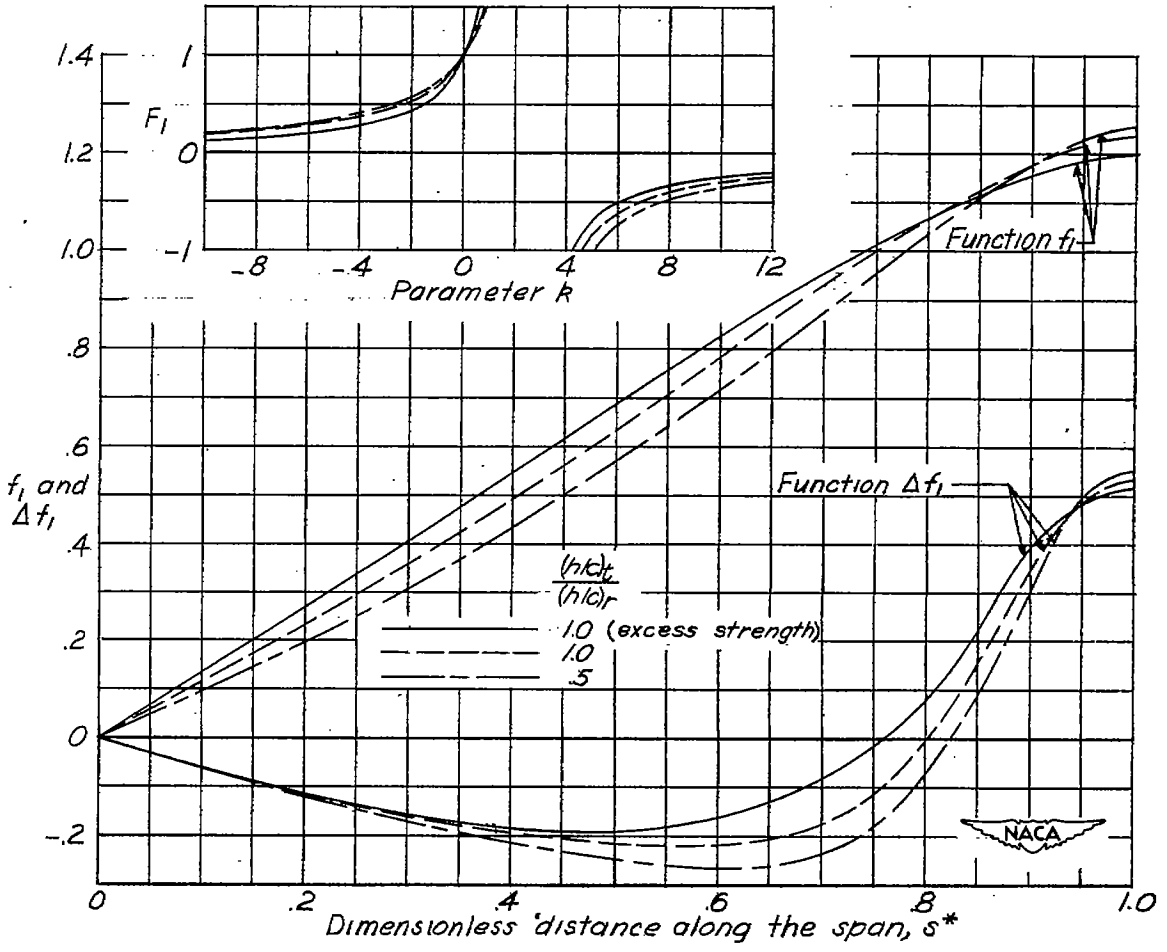

(b) Stiffnesses related to those given by constant-stress criterion for wings with taper ratio 0.5.

Figure 5.- Continued.

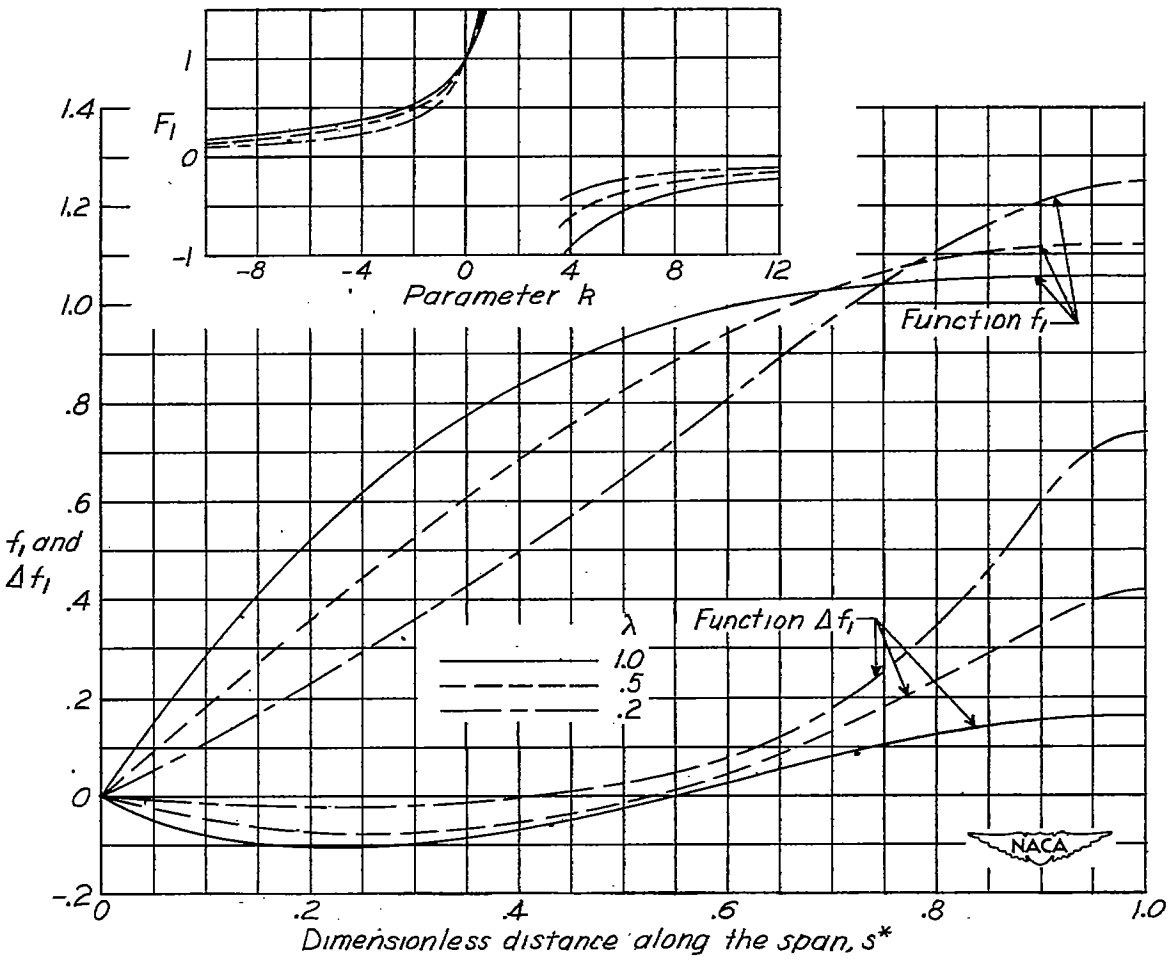

(c) Stiffnesses proportional to c^4.

Figure 5.- Concluded.

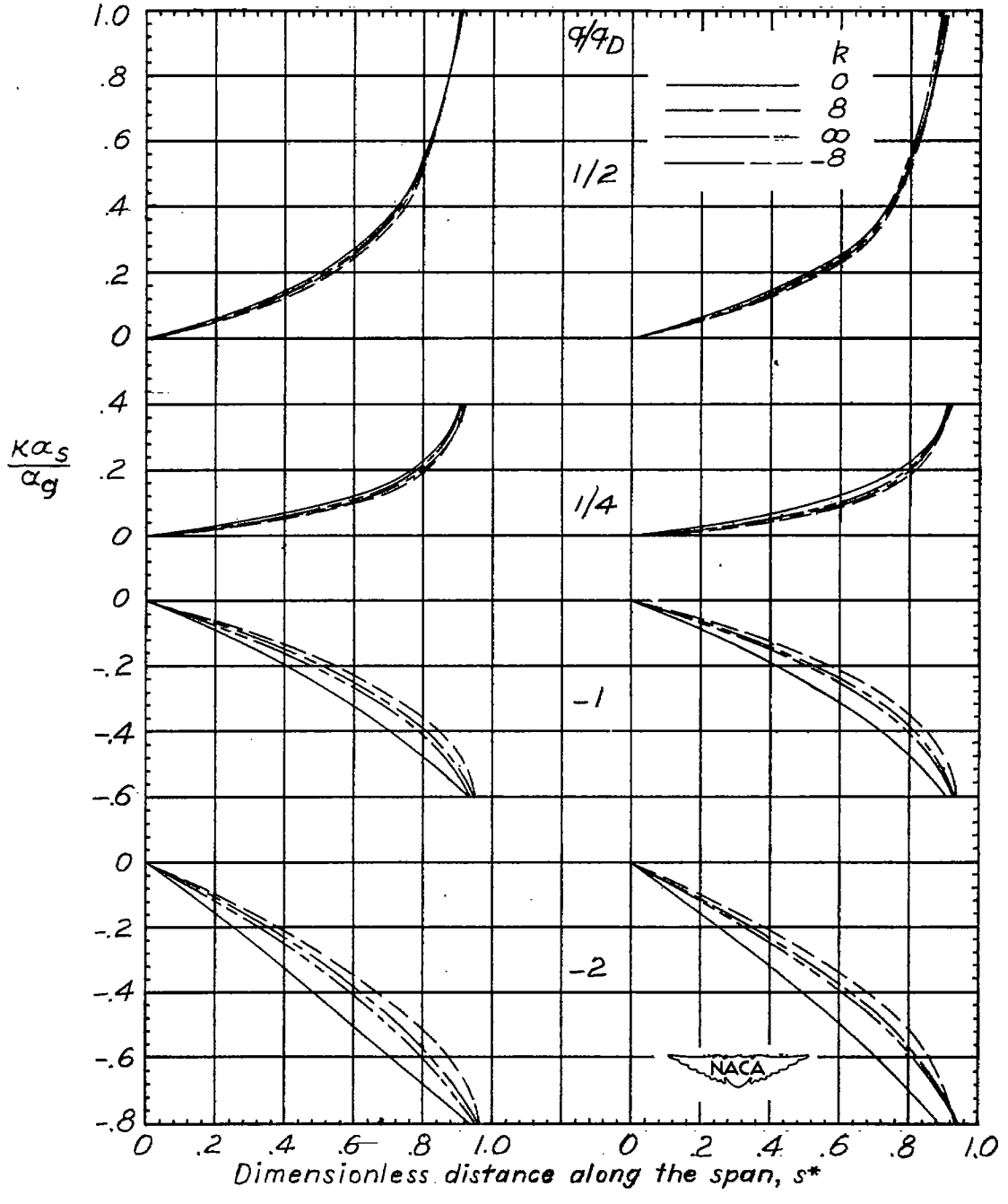

(a) Stiffnesses proportional to c^4.

(b) Stiffnesses given by constant-stress criterion.

Figure 6.- The angle-of-attack distributions for constant geometric angles of attack for wings of taper ratio 0.

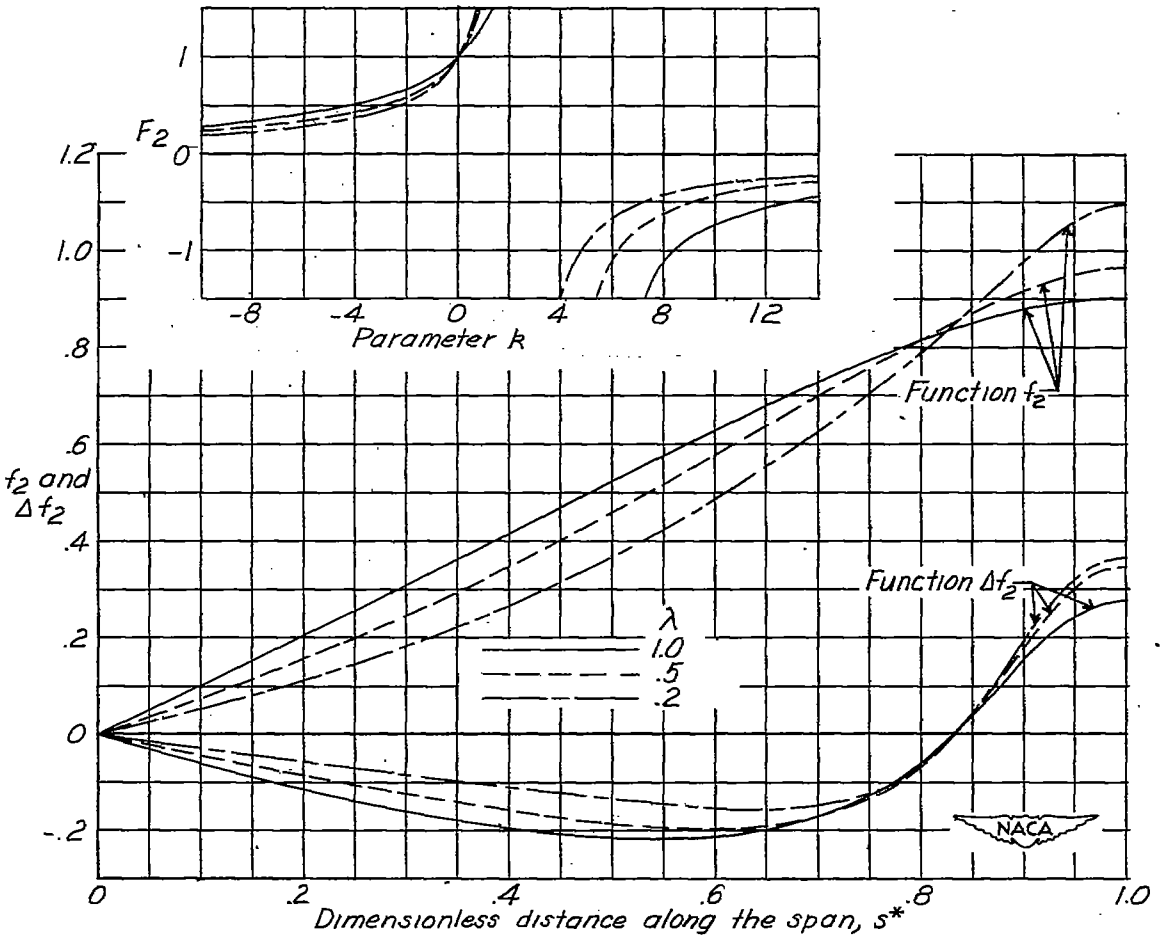

(a) Stiffnesses given by constant-stress criterion for $\frac{(h/c)_t}{(h/c)_r} = 1.0$.

Figure 7.- The angle-of-attack distribution functions f_2, Δf_2, and F_2 for linearly varying geometric angles of attack.

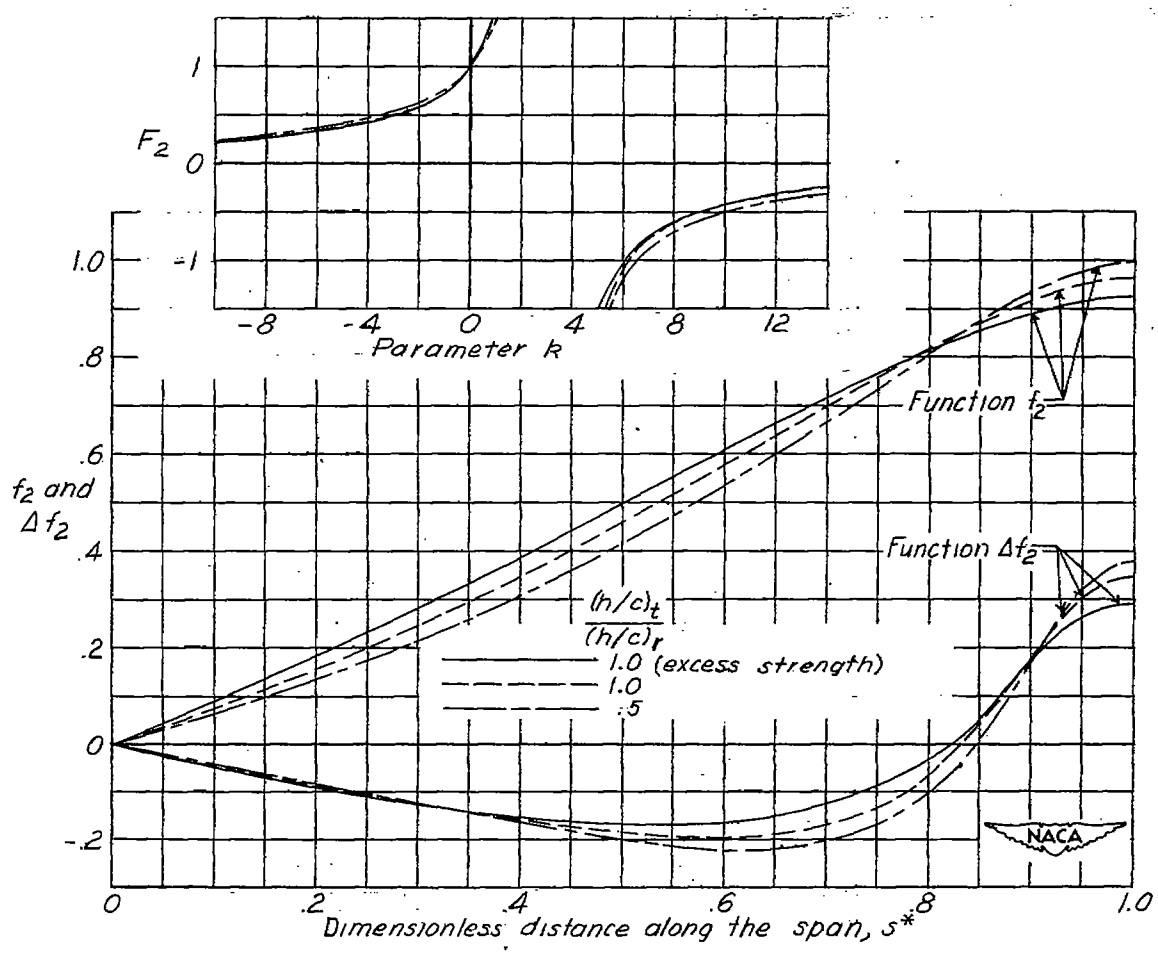

(b) Stiffnesses related to those given by constant-stress criterion for wings with taper ratio 0.5.

Figure 7.- Continued.

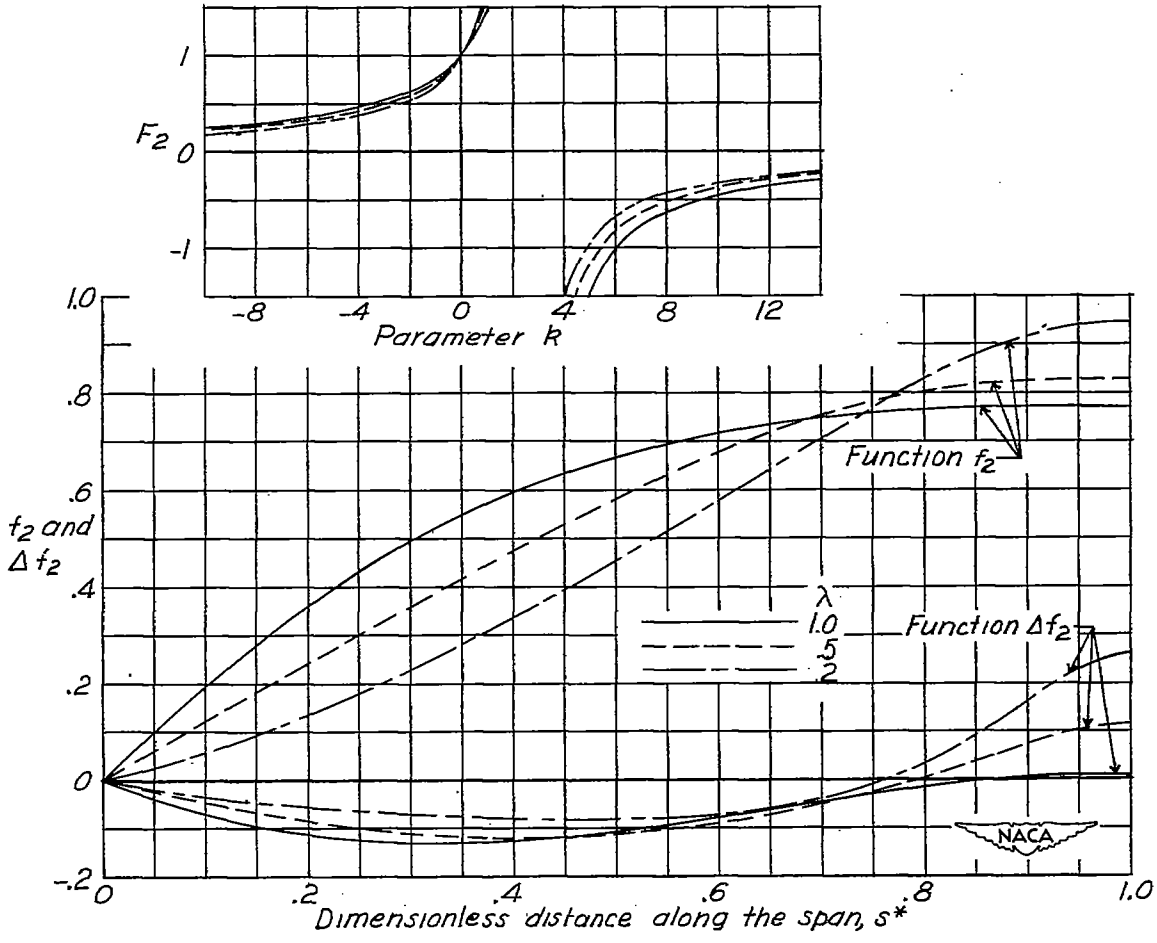

(c) Stiffnesses proportional to c^4.

Figure 7.- Concluded.

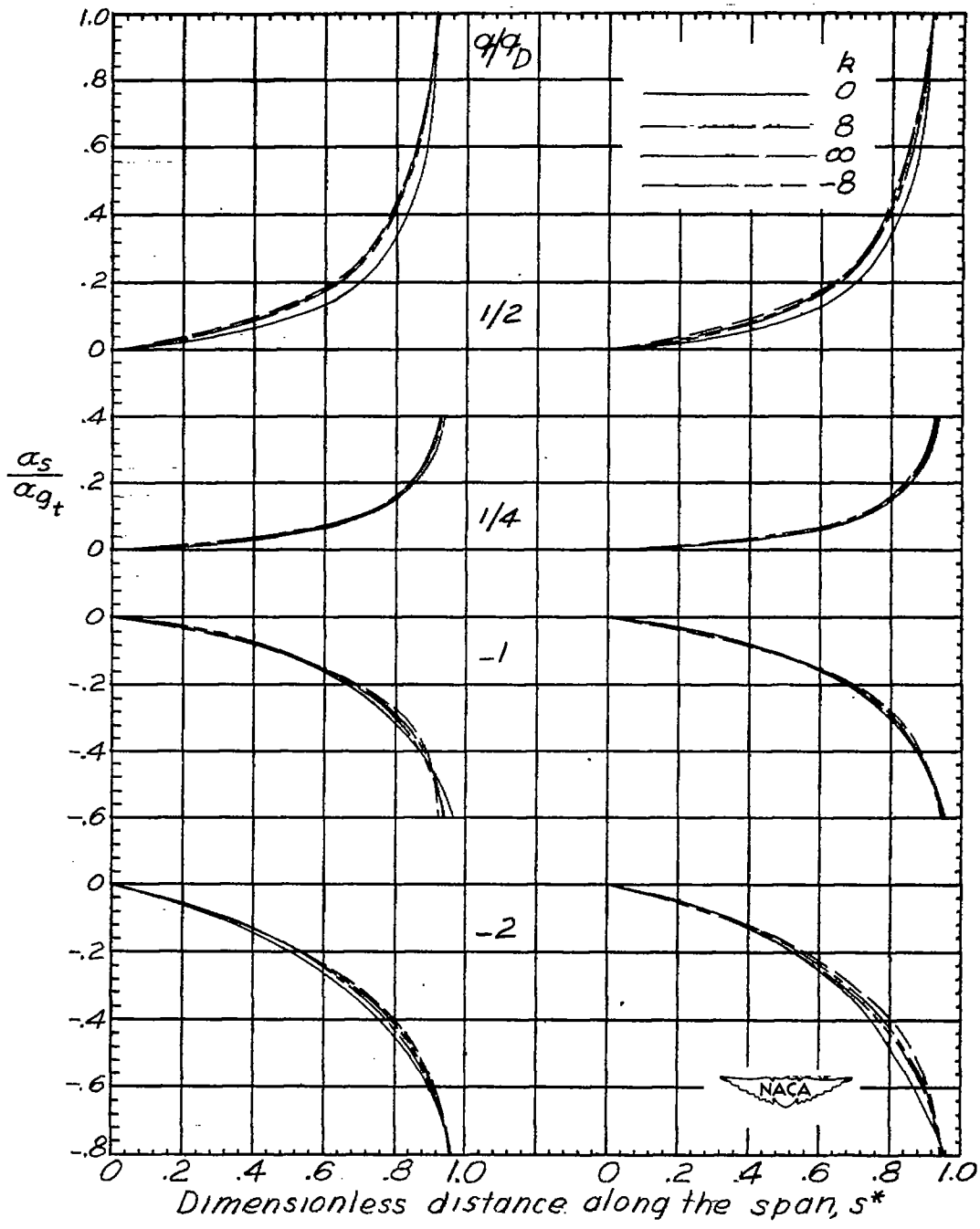

(a) Stiffnesses proportional to c^4.

(b) Stiffnesses given by constant-stress criterion.

Figure 8.- The angle-of-attack distributions for linearly varying angles of attack for wings of taper ratio 0.

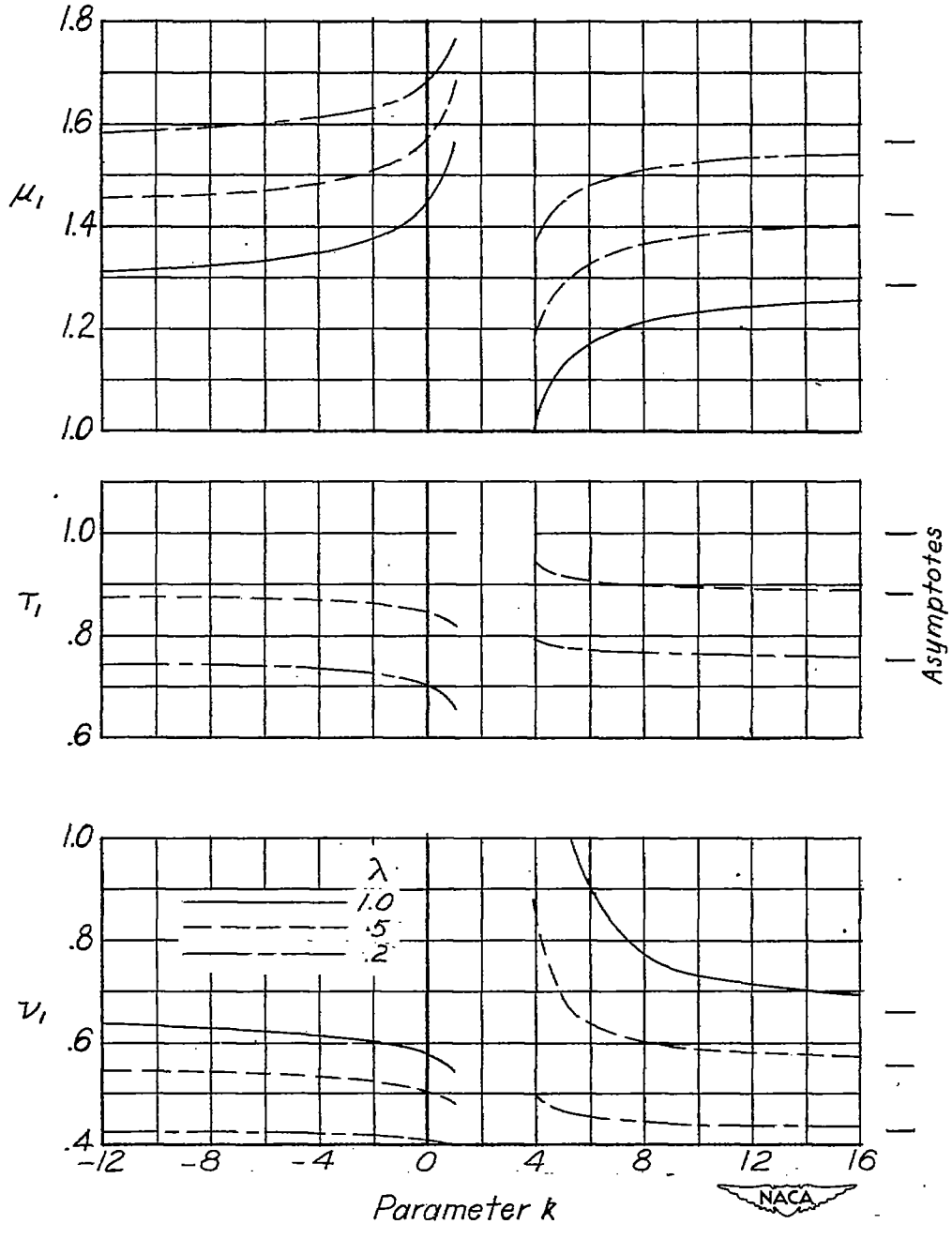

(a) Stiffnesses given by constant-stress criterion for $\frac{(h/c)_t}{(h/c)_r} = 1.0$

Figure 9.- The lift- and moment-coefficient parameters μ_1, ν_1, and τ_1 for constant geometric angles of attack.

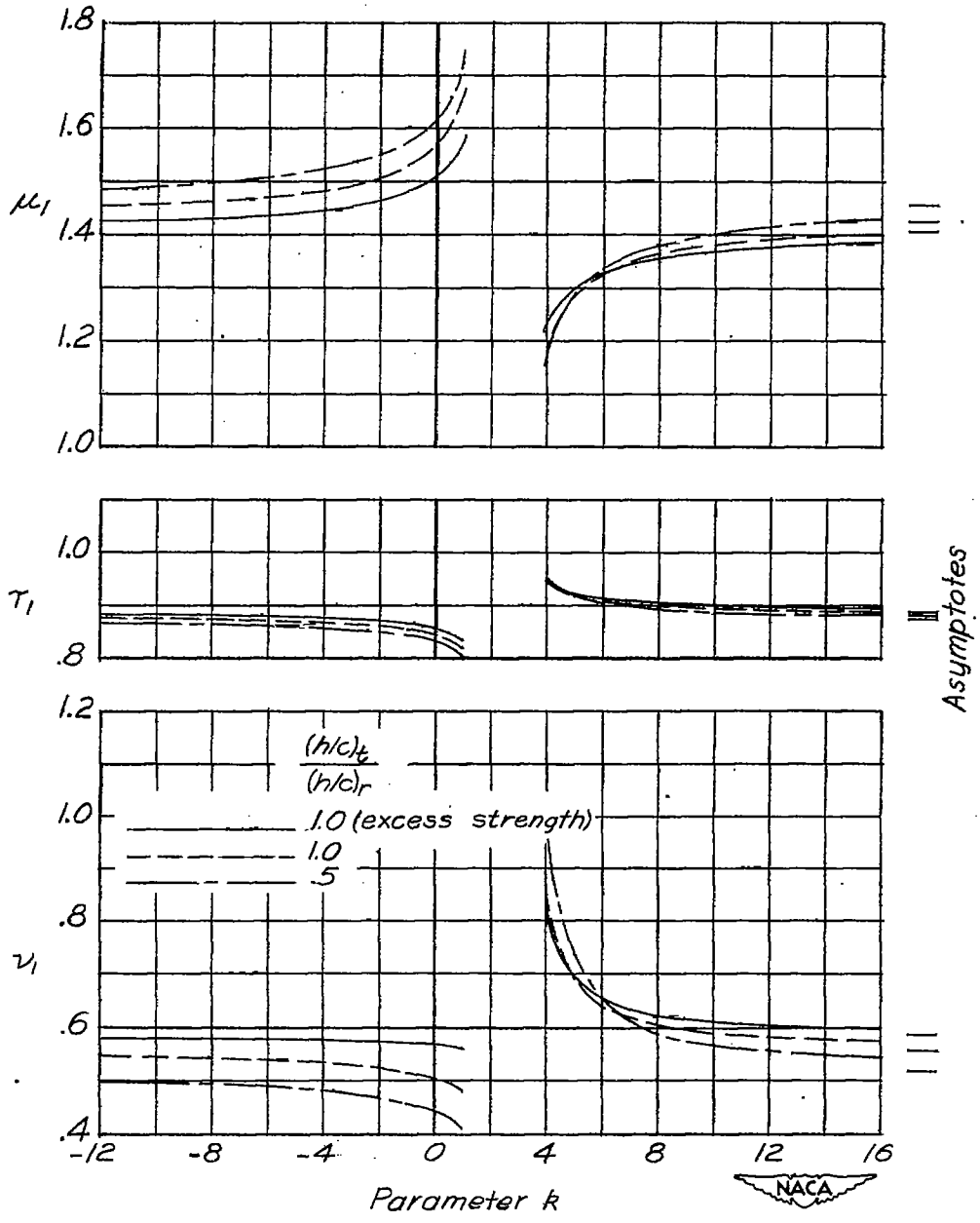

(b) Stiffnesses related to those given by constant-stress criterion for wings with taper ratio 0.5.

Figure 9.- Continued.

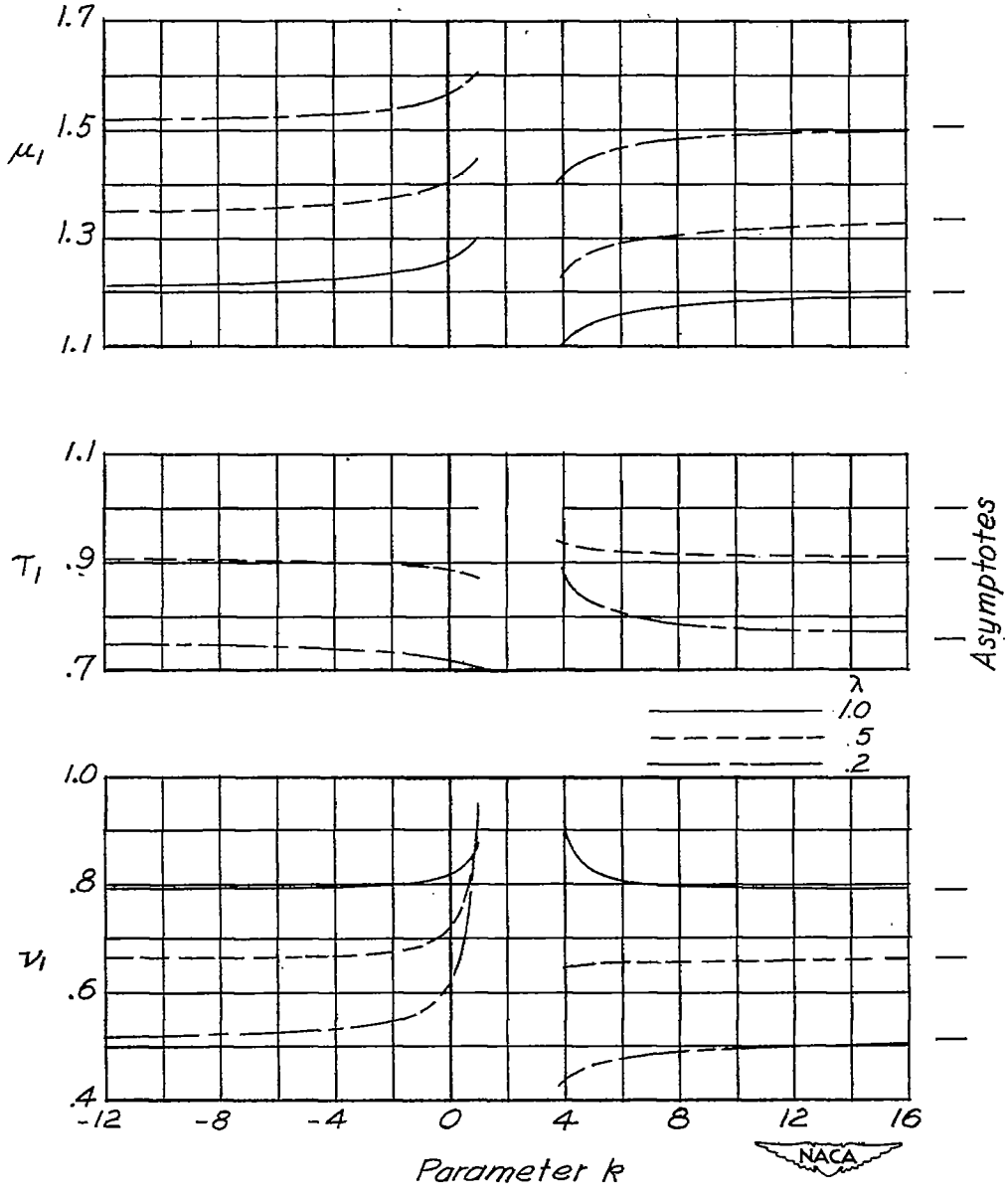

(c) Stiffnesses proportional to c^4.

Figure 9.- Concluded.

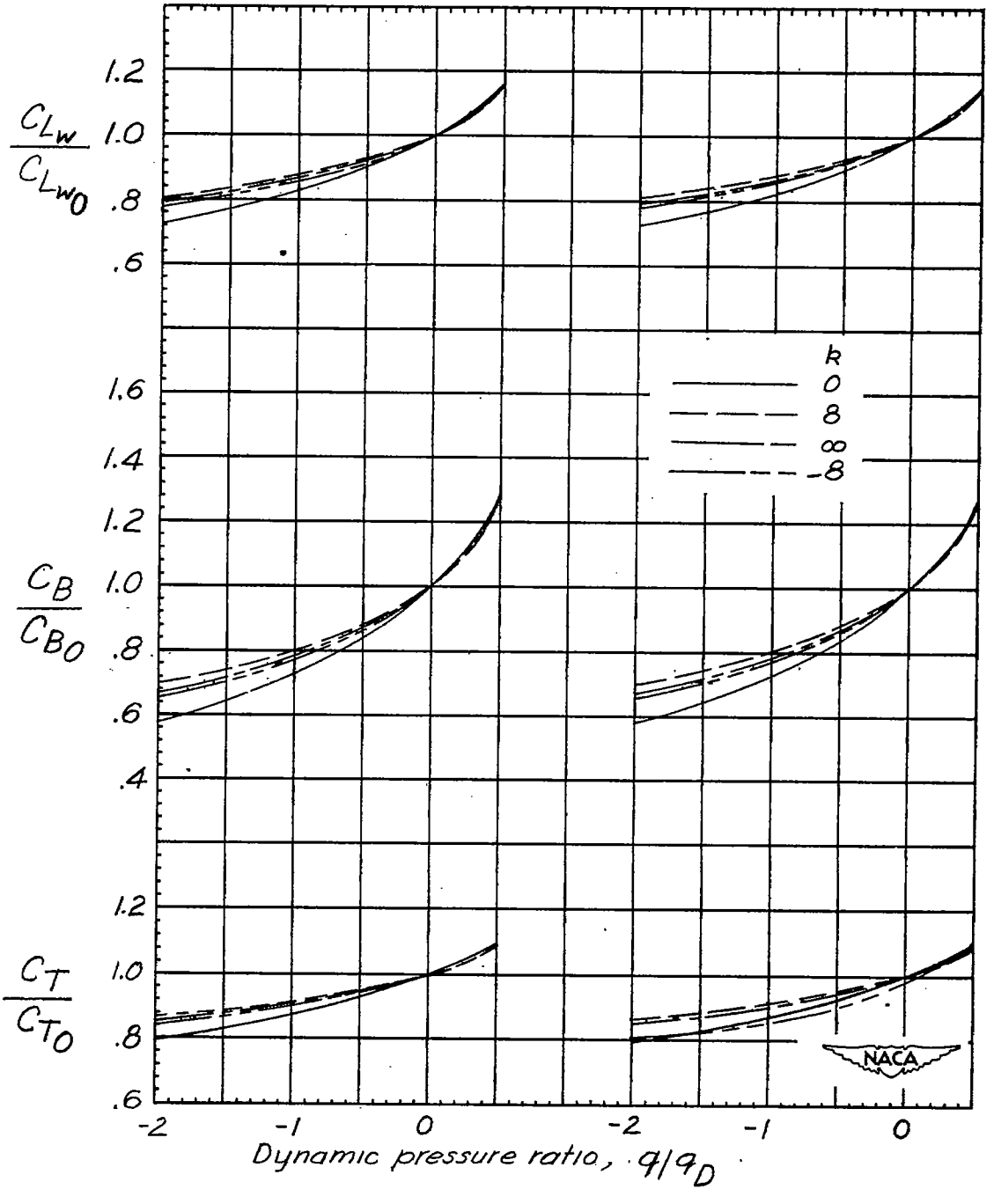

(a) Stiffnesses proportional to c^4.

(b) Stiffnesses given by constant-stress criterion.

Figure 10.- The lift- and moment-coefficient ratios for constant geometric angles of attack for wings of taper ratio 0.

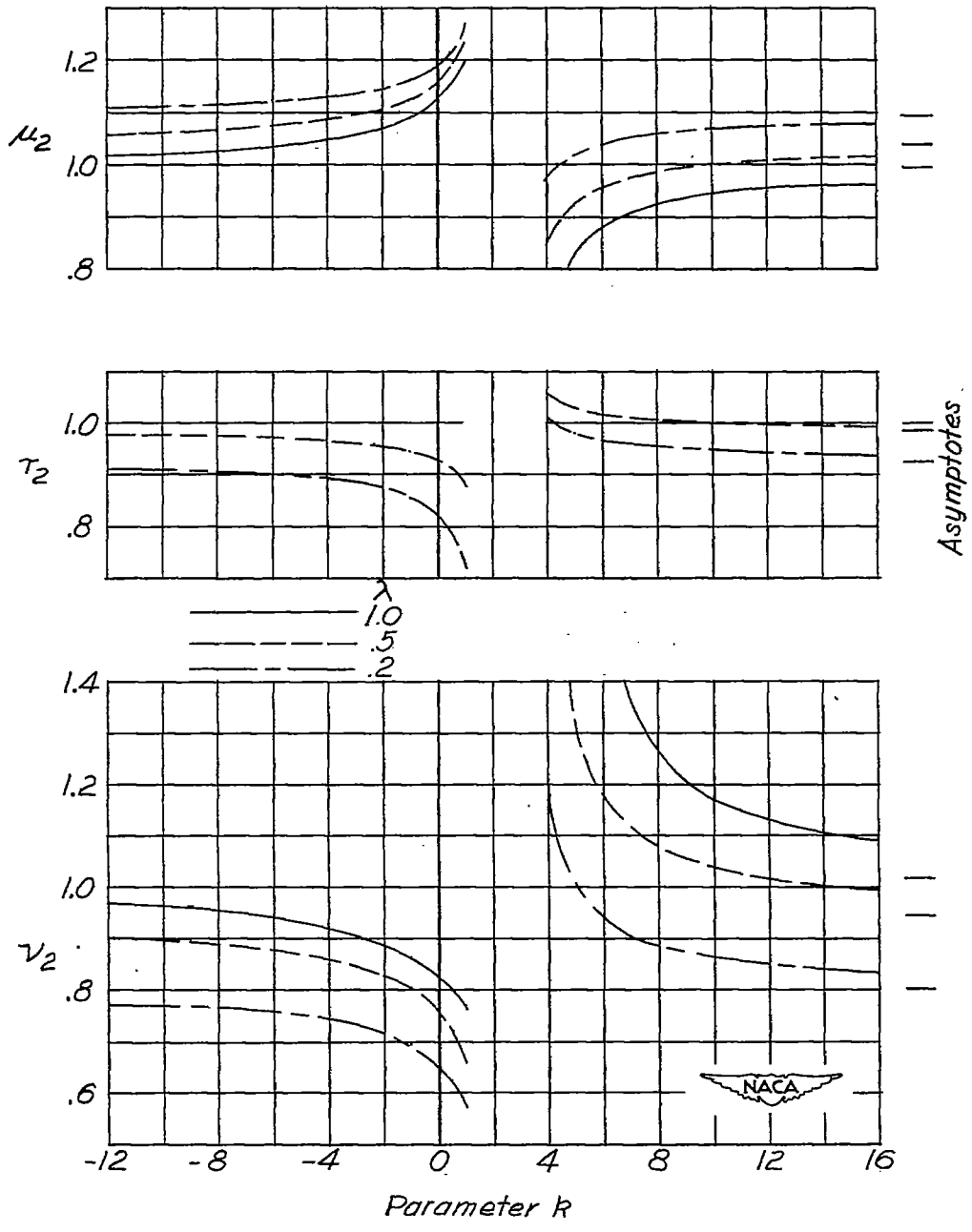

(a) Stiffnesses given by constant-stress criterion for $\frac{(h/c)_t}{(h/c)_r} = 1.0$.

Figure 11.- The lift- and moment-coefficient parameters μ_2, ν_2, and τ_2 for linearly varying geometric angles of attack.

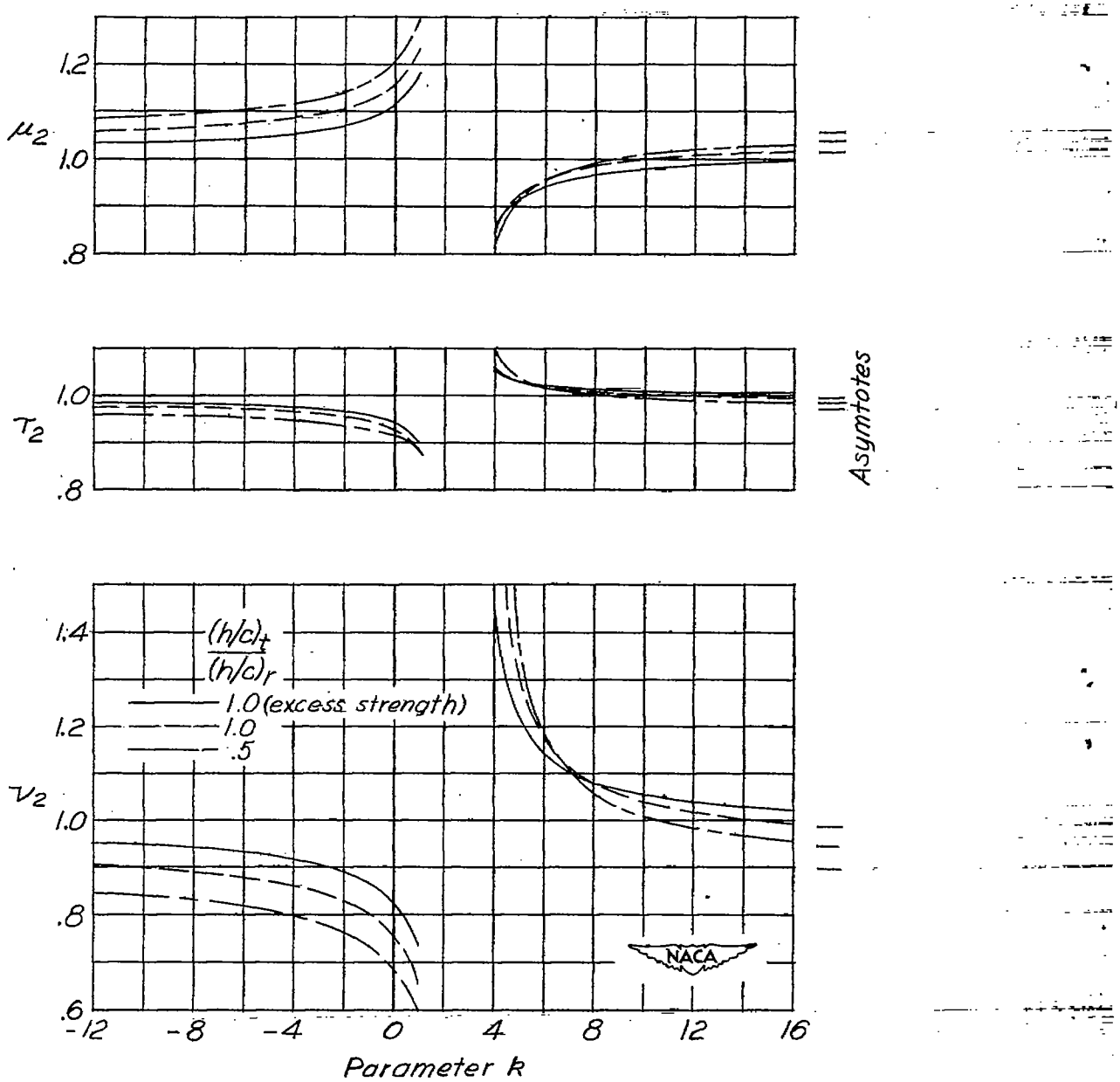

(b) Stiffnesses related to those given by constant-stress criterion for wings with taper ratio 0.5.

Figure 11.- Continued.

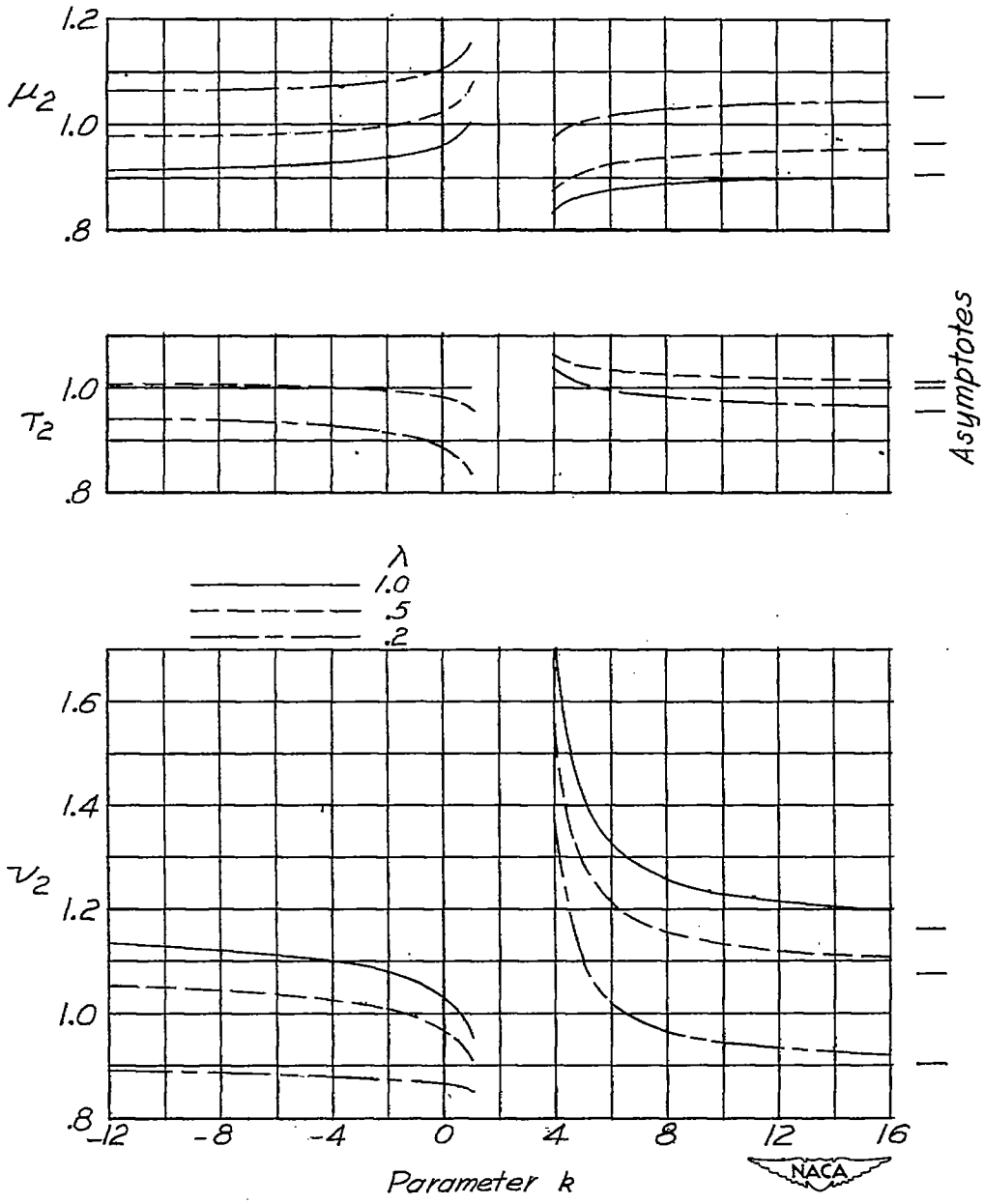

(c) Stiffnesses proportional to c^4.

Figure 11.- Concluded.

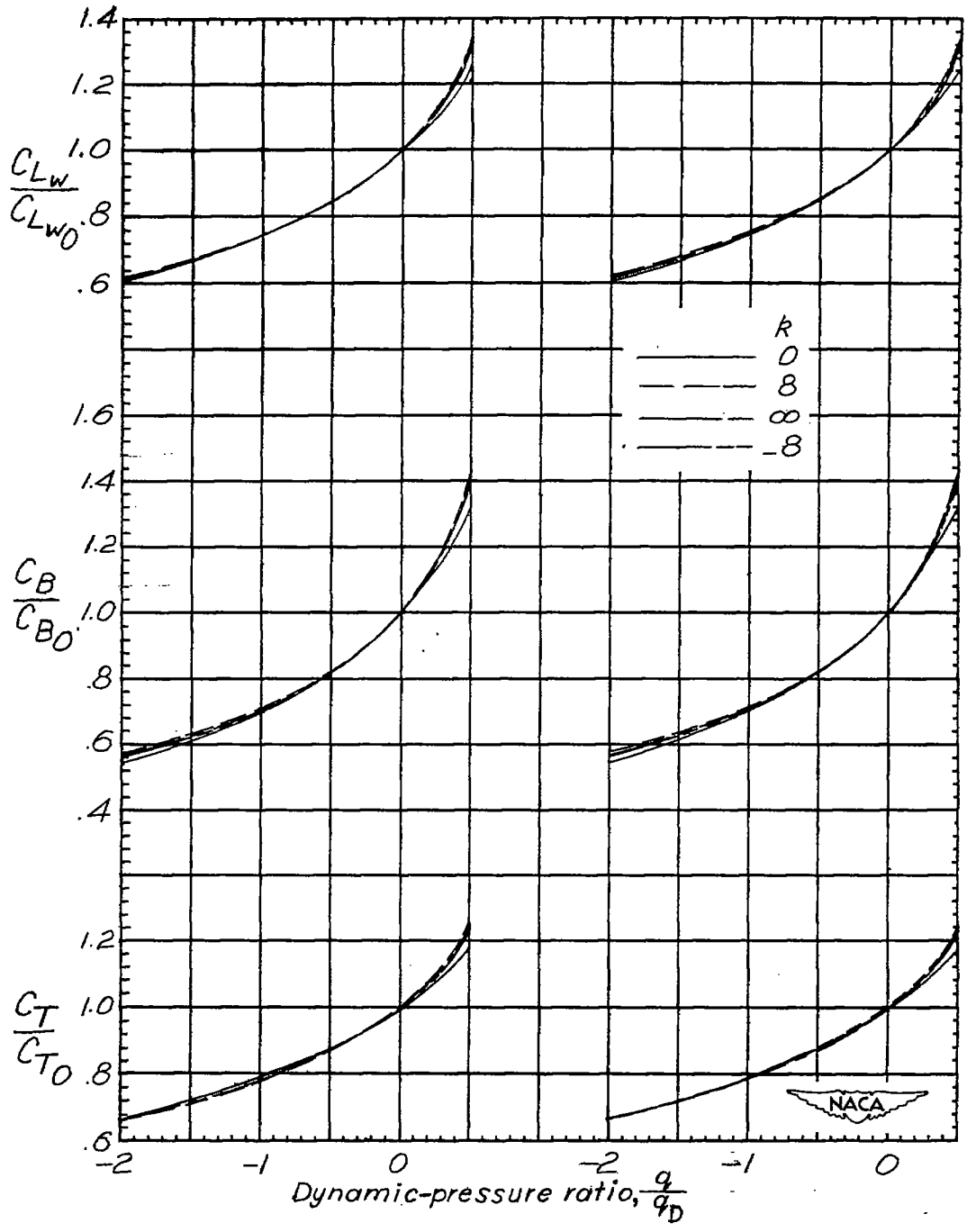

(a) Stiffnesses proportional to c^4.

(b) Stiffnesses given by constant-stress criterion.

Figure 12.- The lift- and moment-coefficient ratios for linearly varying geometric angles of attack for wings of taper ratio 0.

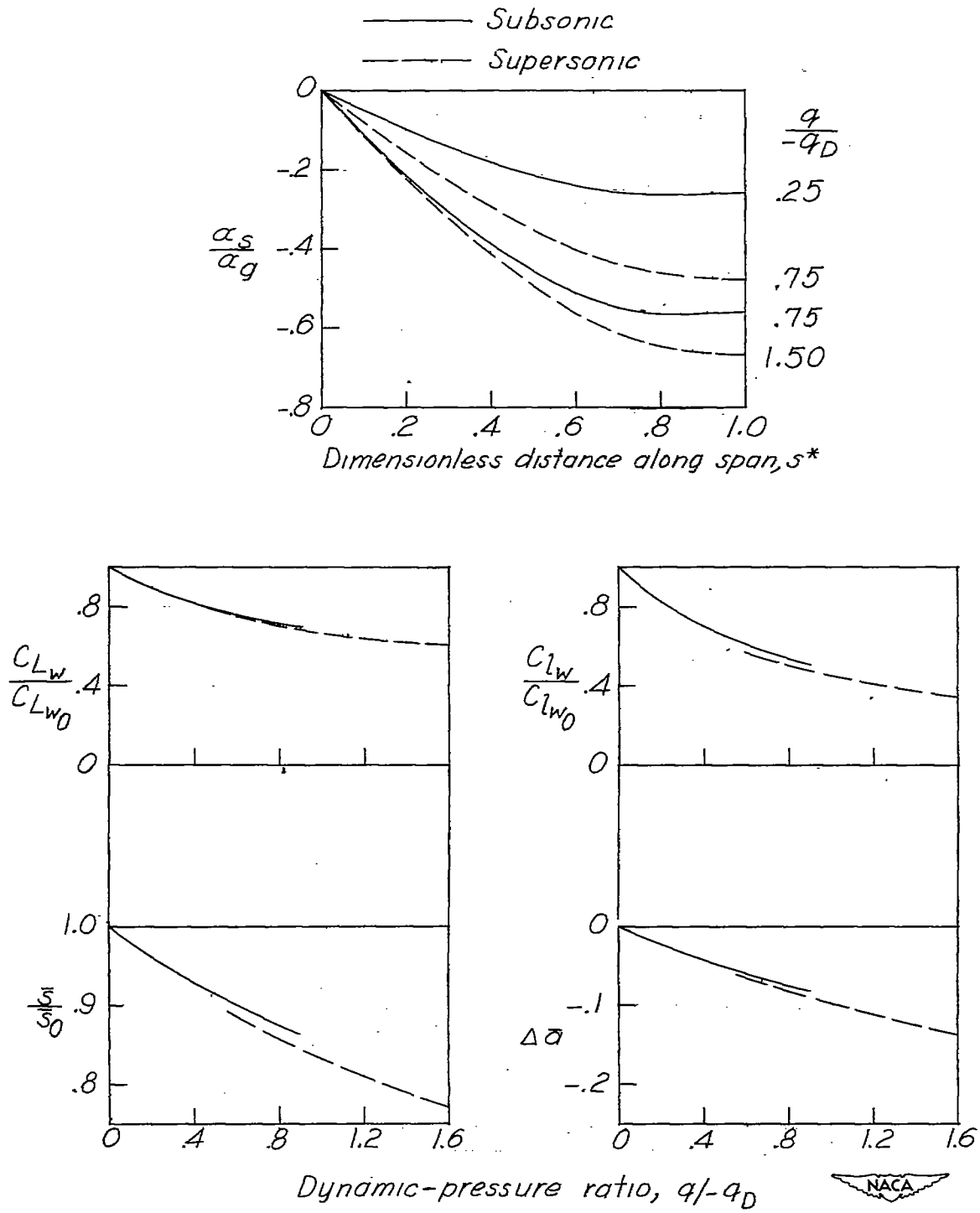

Figure 13.- Effect of aeroelastic action on some aerodynamic properties of the wing used in illustrative example.

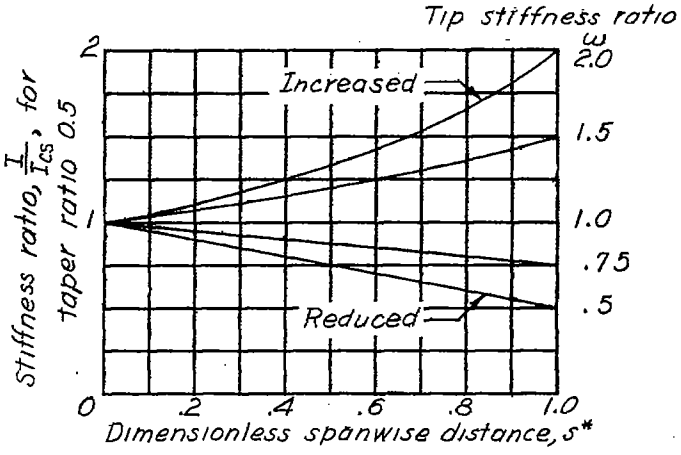

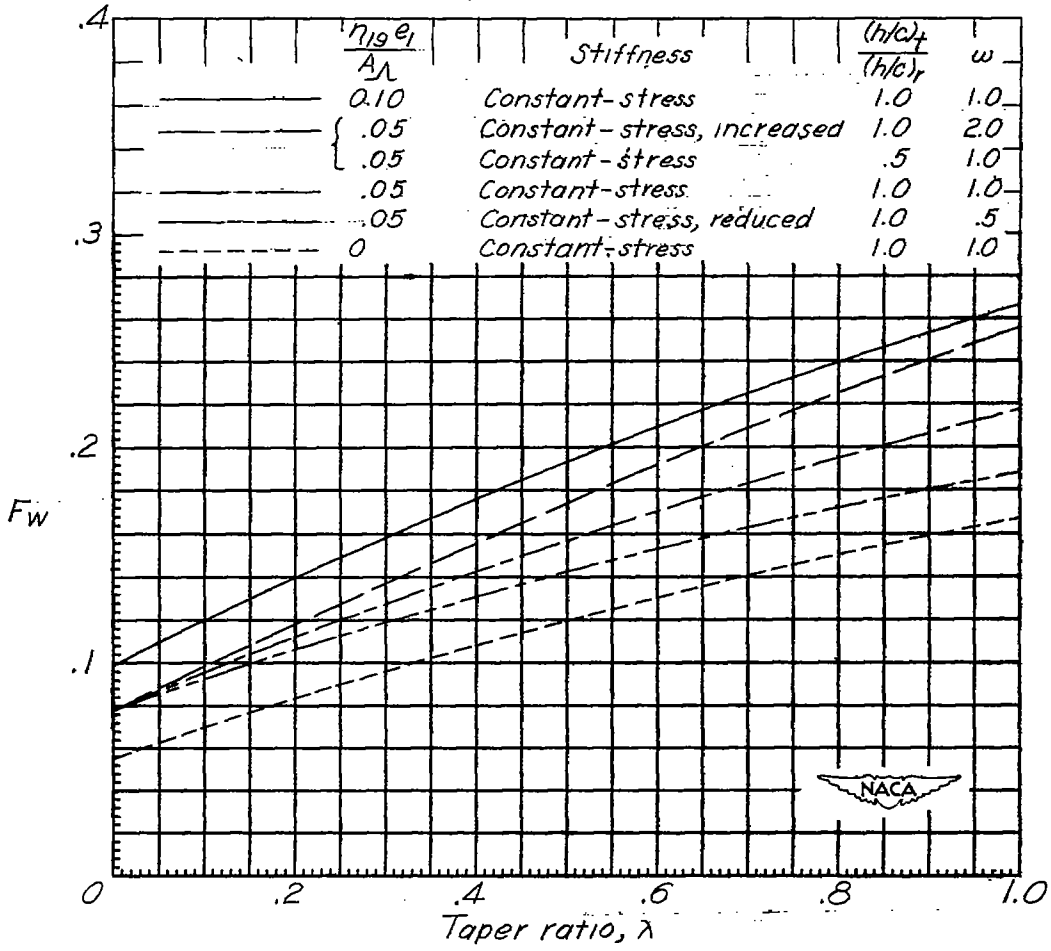

Figure 14.- The structural weight function F_w.

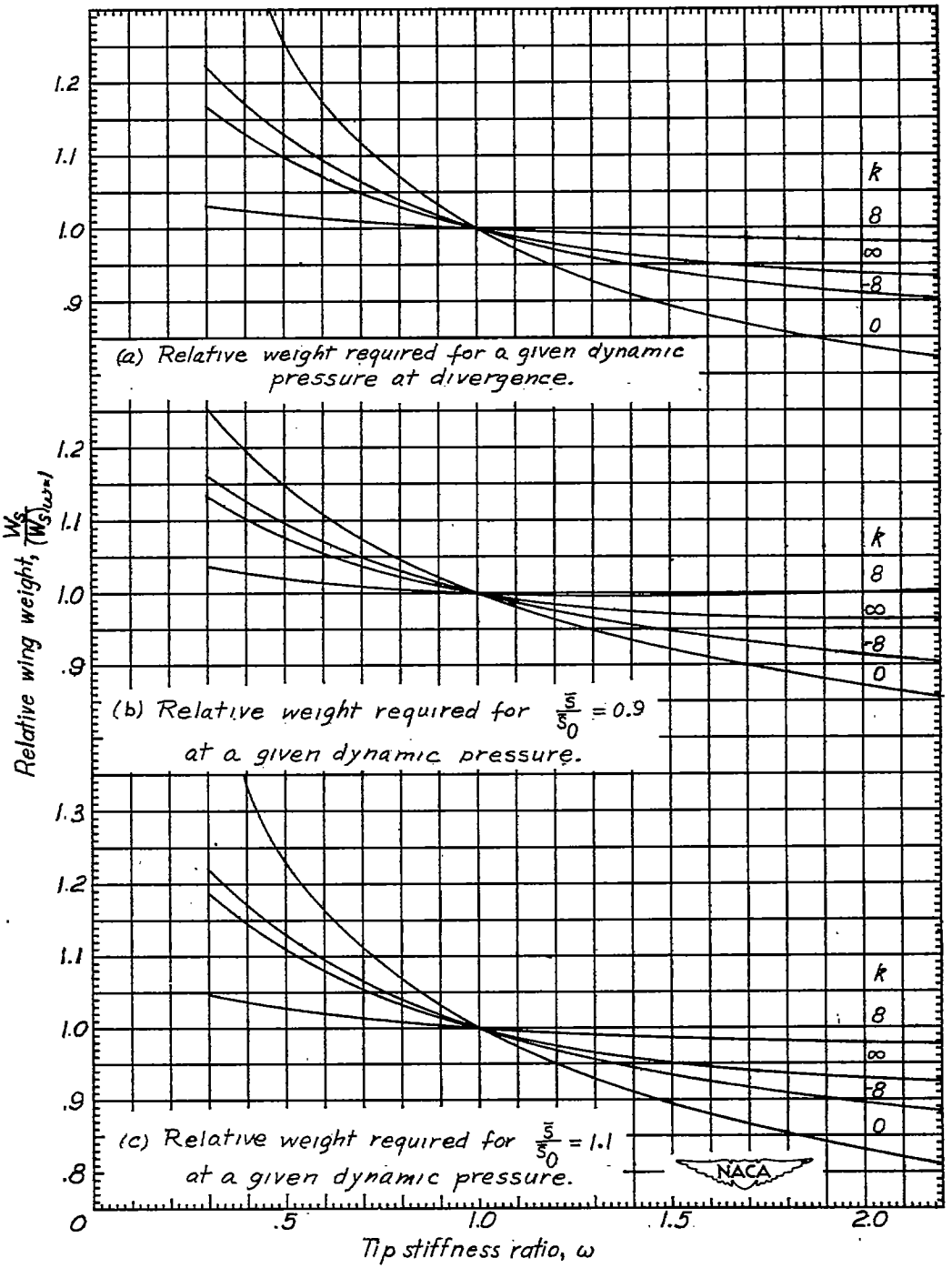

Figure 15.- The effect of the tip stiffness ratio on the structural weight required for a given divergence dynamic pressure or given shifts in the spanwise center of pressure of wings with taper ratio 0.5.

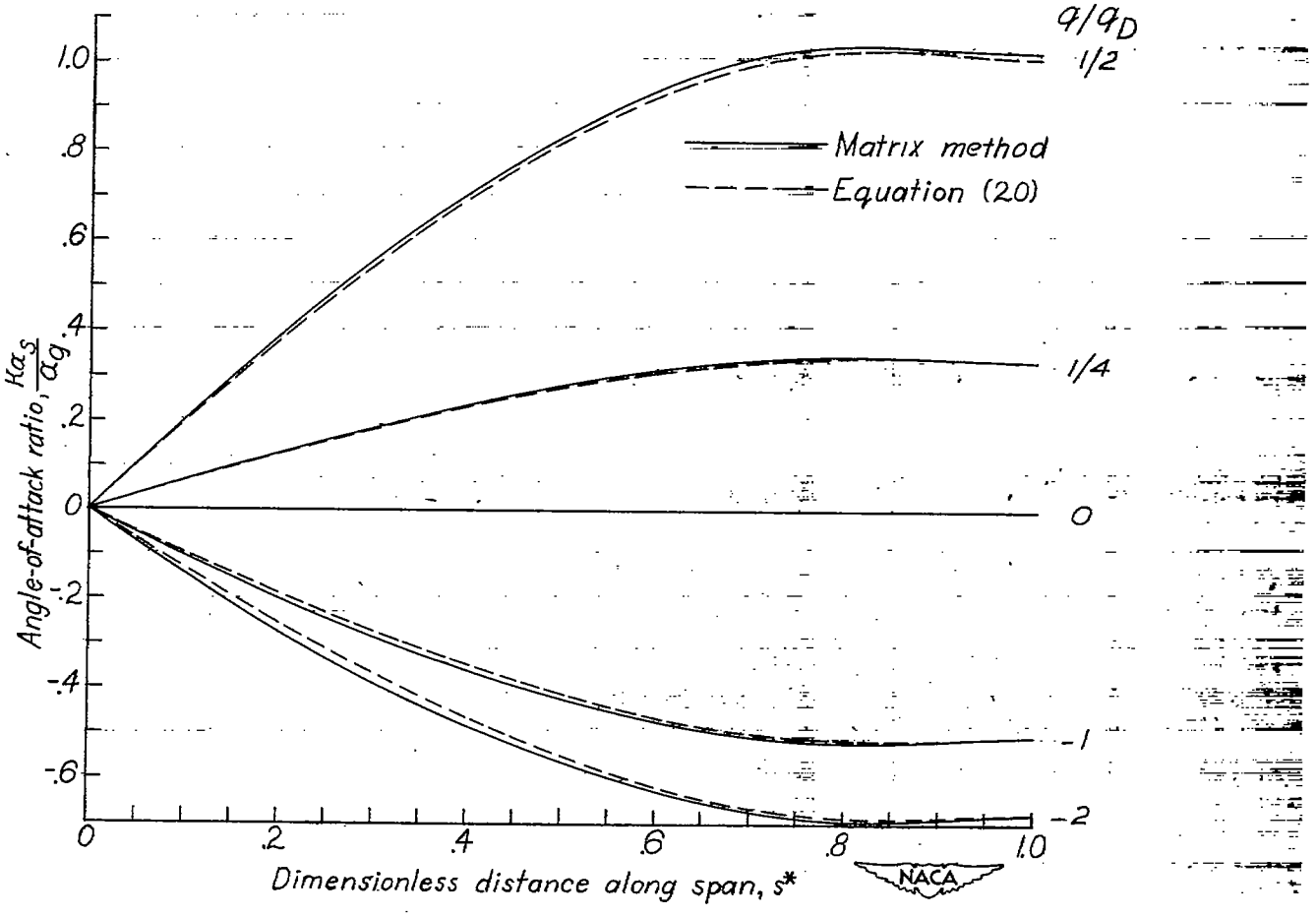

Figure 16.- Comparison of angle-of-attack ratios calculated by the matrix method of appendix A with those calculated from equation (20) for constant geometric angles of attack at various dynamic-pressure ratios. $\lambda = 0.5$, $k = 8$, stiffnesses proportional to c^4.

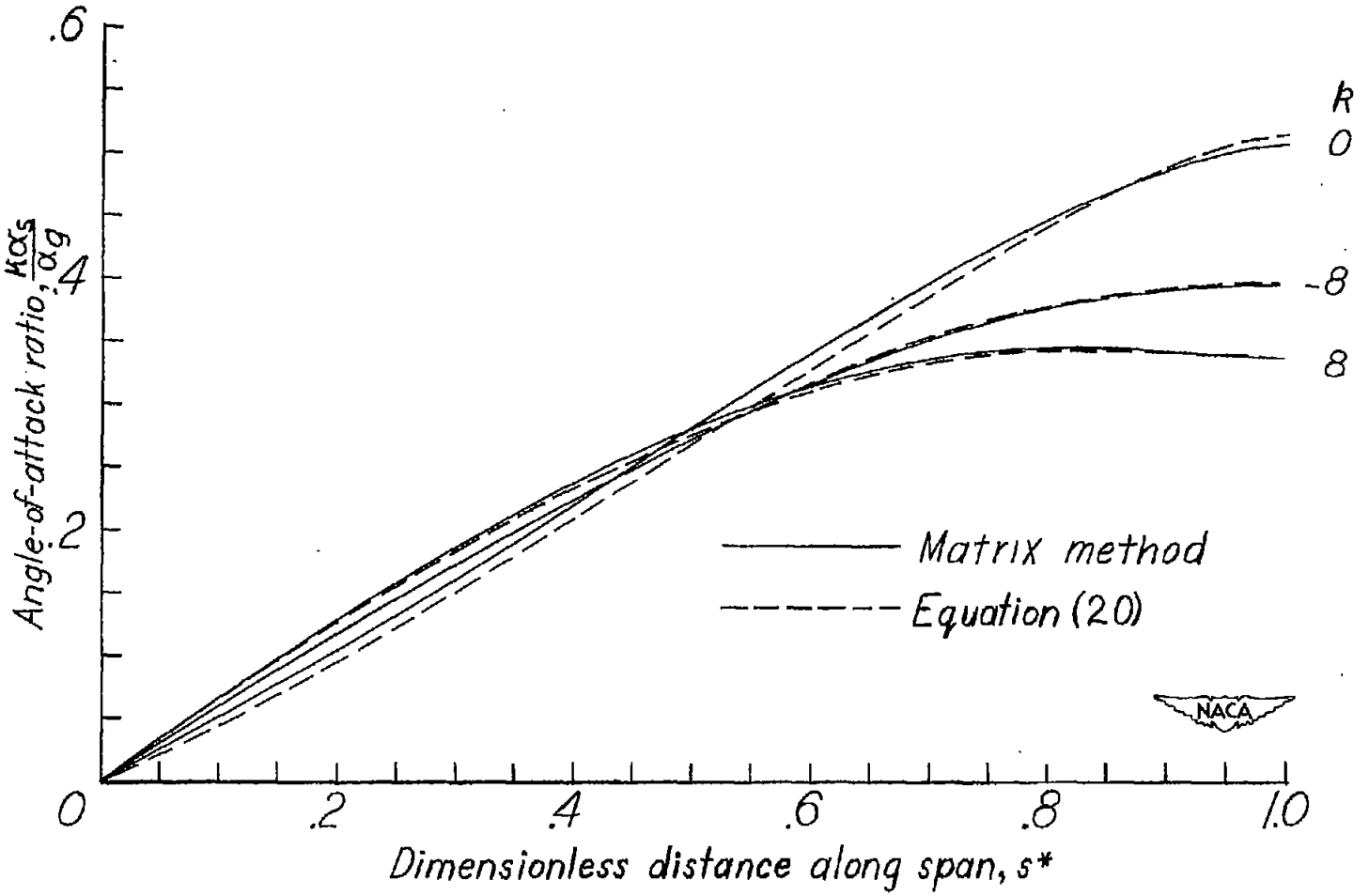

Figure 17.- Comparison of angle-of-attack ratios calculated by the matrix method of appendix A with those calculated from equation (20) for constant geometric angles of attack and for various values of the parameter k. $\lambda = 0.5$, $\frac{q}{q_D} = \frac{1}{4}$, stiffnesses proportional to c^4.

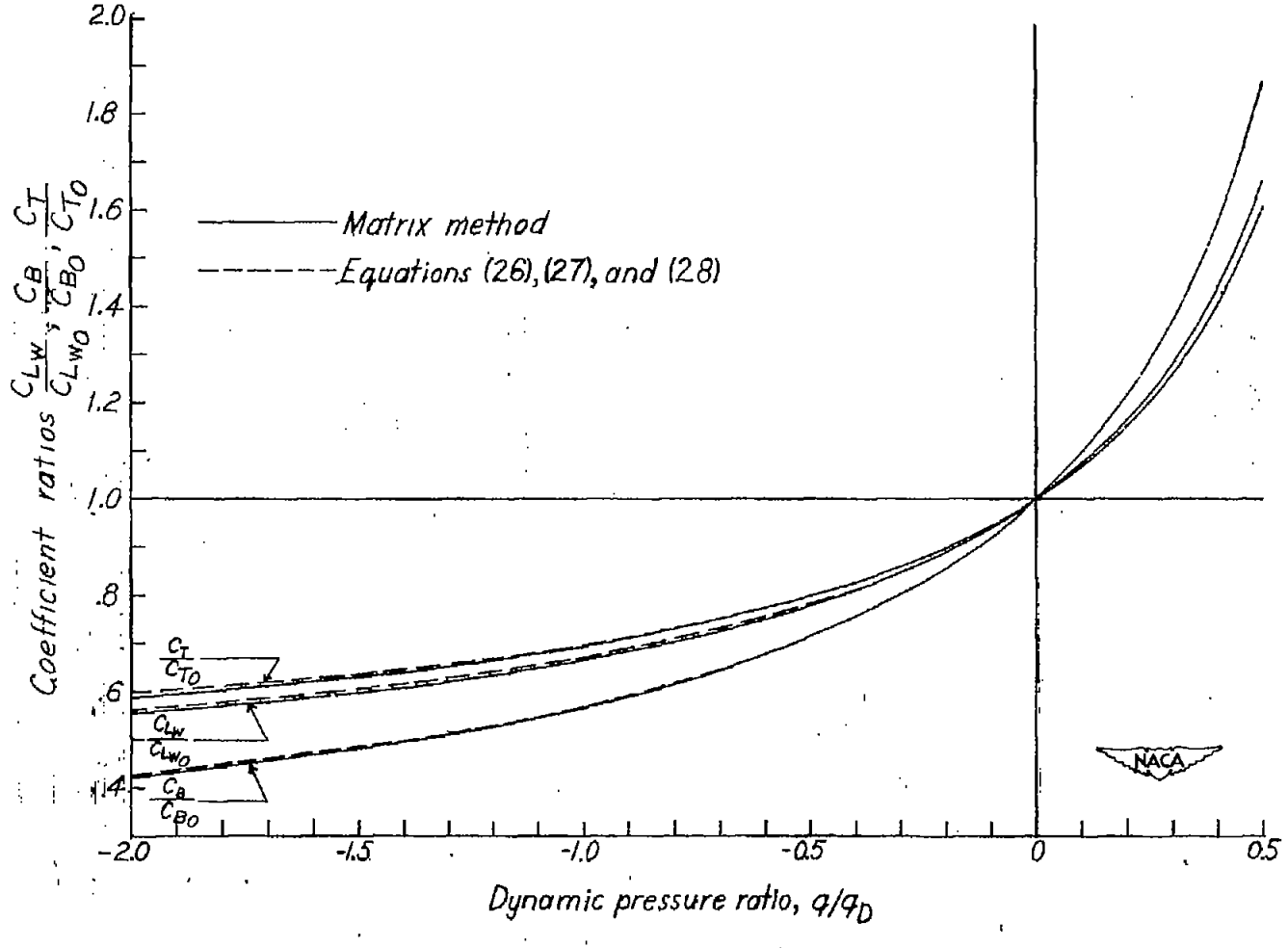

Figure 18.- Comparison of lift- and moment-coefficient ratios for constant geometric angles of attack calculated by the matrix method of appendix A with those calculated from equations (26), (27), and (28). $\lambda = 0.5$, $k = 8$, stiffnesses proportional to c^4.

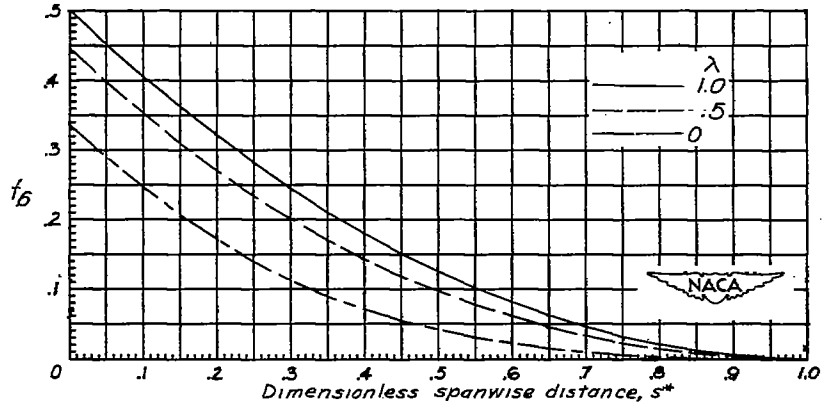

Figure 19.- The bending-moment function f_6.

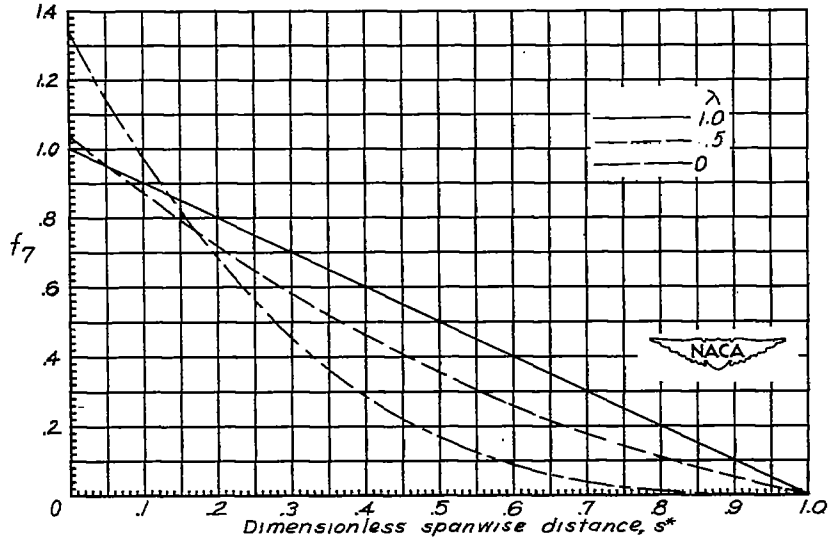

Figure 20.- The twisting-moment function f_7.

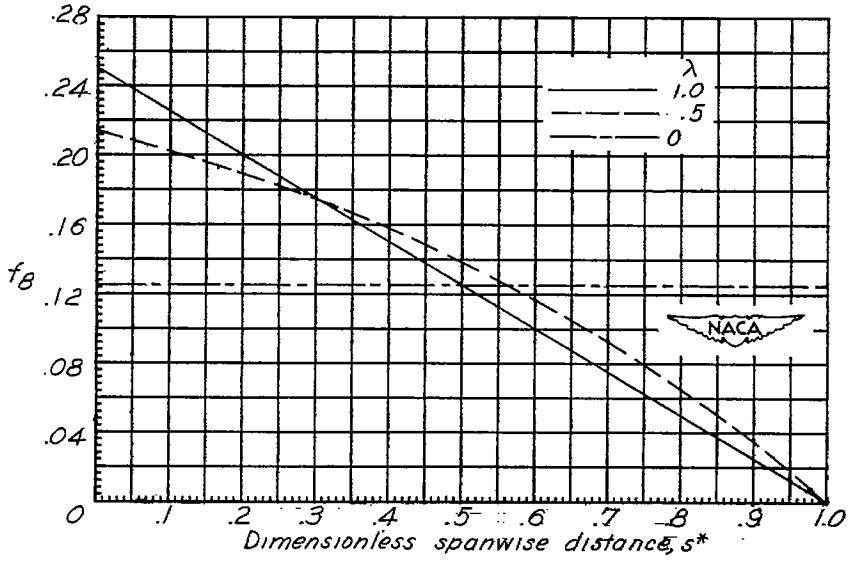

Figure 21.- The moment-ratio function f_8.

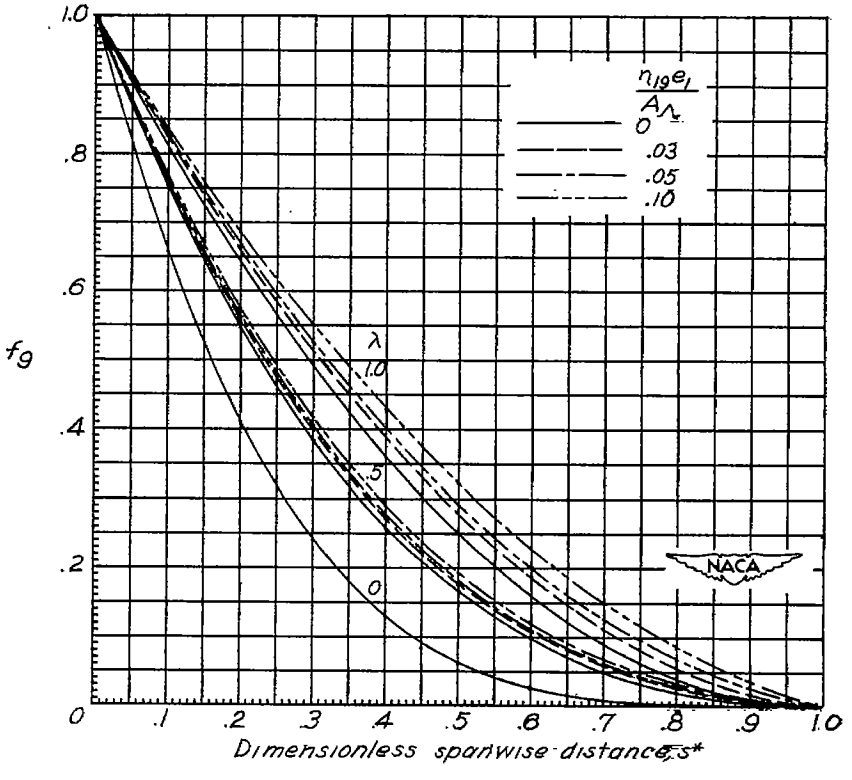

Figure 22.- The stiffness-distribution function f_9.